Ionosphere Modelling for Galileo Single Frequency Users

Benoît Bidaine

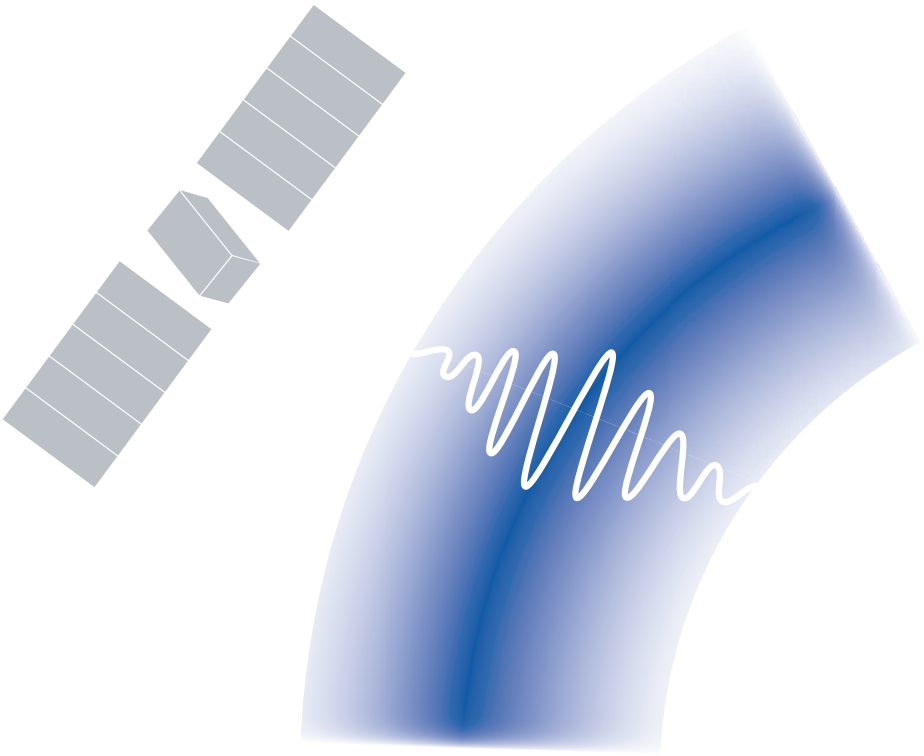

Ionosphere Modelling for Galileo Single Frequency Users

A thesis submitted in partial fulfilment
of the requirements for the academic degree of

Philosophiæ Doctor in Sciences
at the University of Liège (College of Geography)

by

Benoît Bidaine
Physics engineer of the University of Liège

October 2012

The present thesis has been supervised by the promoter

Prof. Dr. René Warnant.

Jury members:

Dr. Ir. Bertram Arbesser-Rastburg	European Space Agency (ESA)
Prof. Dr. Roland Billen	University of Liège, president
Dr. Ir. Ljiljana R. Cander	Rutherford Appleton Laboratory
Prof. Dr. Jean-Claude Gérard	University of Liège
Dr. Ir. Jean-Claude Jodogne	Royal Meterological Institute of Belgium
Prof. Dr. René Warnant	University of Liège, promoter

The research described in this thesis was supported by the Fund for Scientific Research - FNRS (www.fnrs.be). It was conducted within the Geomatics Unit of the University of Liège (www.geo.ulg.ac.be).

Front cover figure by Benoît Bidaine
Back cover figure by Olivier Dupont

Abstract

Nowadays the ionosphere constitutes one of the most often modelled natural media. Indeed each GPS receiver among nearly two million units sold daily throughout the world runs a model to mitigate the ionospheric effect affecting the signal propagation from the satellites. This propagation is delayed by the free electrons in the atmosphere so that the navigation signals appear to travel distances larger than actual ones by $7m$ on average. Hence this delayed propagation deteriorates the positioning accuracy deemed on a $10 - m$ level for mass-market applications mainly involving single frequency users.

Tomorrow the European navigation system Galileo will offer a new mitigation strategy to single frequency users. This strategy will rely on the NeQuick ionospheric model and associated broadcast information. To be properly implemented, it must be extensively described to future Galileo users. These users will also wonder about its effectiveness in accounting for the ionospheric delay.

The PhD research covered by the present thesis has built on Belgian expertise in ionosphere monitoring to investigate the NeQuick model and its use for Galileo. It began with the collection and handling of ionosphere measurements including GPS data. It analysed various situations at different places in the world encompassing a whole year (2002).

This PhD thesis provides the ins and outs of the Galileo Single Frequency Ionospheric Correction Algorithm. It gathers an algorithm description, a performance evaluation and a variant investigation. In the shape of a paper collection, it discloses many figures as visual entry-points into the juxtaposed text and includes many references allowing to dig into the details.

The algorithm performances are usefully characterised both in terms of delay mitigation and positioning accuracy. On the one hand, the residual ionospheric delay reaches 31% for the chosen sites and year. On the other hand, the positioning accuracy amounts to $6m$ horizontally and $9.3m$ vertically.

The performance evaluation allowed to emphasise several aspects of the Galileo ionospheric correction. This correction depends largely on the modelling of the topside, the upper part of the ionosphere, which hosts more complex physical processes. It owes its good performances to data ingestion, the model adaptation technique to actual measurements underlying the Galileo algorithm. It does not necessarily provide highly correlated correction levels in terms of delay on the one hand and positioning on the other. It enables the definition of alternative regional procedures following a compatible design but coping with its weaknesses.

The present thesis paves the way for future work related to ionosphere modelling for Galileo single frequency users. It supplies comparative information for the algorithm assessment in the framework of successive phases of Galileo deployment. It establishes a conceptual basis for an Assisted Ionospheric Correction Algorithm (A-ICA) disseminating more flexible ionospheric information thanks to the integration of Global Navigation Satellite Systems and telecommunications.

Keywords ionosphere, satellite navigation, GNSS, Galileo, single frequency, absolute positioning, point positioning, ionospheric delay, ionospheric correction, mitigation, positioning accuracy, total electron content (TEC), ionosonde, ionosphere modelling, NeQuick model, electron density model, topside, data ingestion, effective ionisation level, multiple ingestion, variance-driven ingestion, adaptative effective ionisation level, parametrised ingestion, TEC map ingestion

Résumé

De nos jours, l'ionosphère constitue l'un des milieux naturels les plus souvent modélisés. En effet chaque récepteur GPS parmi presque deux millions d'unités vendues quotidiennement dans le monde utilise un modèle afin de corriger l'effet ionosphérique qui affecte la propagation du signal depuis les satellites. Cette propagation est retardée par les électrons libres dans l'atmosphère de sorte que les signaux de navigation semblent parcourir des distances plus grandes de 7 m en moyenne que les distances réelles. Par conséquent cette propagation retardée détériore la précision de positionnement réputée de l'ordre de 10 m pour les applications grand public impliquant principalement des utilisateurs simple fréquence.

Demain, le système européen de navigation Galileo offrira une nouvelle stratégie de correction pour les utilisateurs simple fréquence. Cette stratégie s'appuiera sur le modèle ionosphérique NeQuick et des informations émises associées. Pour être correctement mise en oeuvre, elle doit être décrite en détails aux futurs utilisateurs Galileo. Ces utilisateurs s'interrogeront également sur son efficacité à prendre en compte le délai ionosphérique.

La recherche doctorale couverte par la présente thèse s'est appuyée sur l'expertise belge en observation de l'ionosphère pour investiguer le modèle NeQuick et son utilisation pour Galileo. Elle a commencé par la collecte et la prise en main de mesures ionosphériques y compris des données GPS. Elle a analysé différentes situations à différents endroits dans le monde englobant une année entière (2002).

Cette thèse de doctorat présente les tenants et les aboutissants de l'algorithme de correction ionosphérique simple fréquence de Galileo. Elle rassemble une description de l'algorithme, une évaluation des performances et une investigation de variantes. Sous forme d'un recueil d'articles, elle arbore de nombreuses figures comme autant de points d'entrée dans le texte juxtaposé et comprend de nombreuses références permettant d'approfondir les détails.

Les performances de l'algorithme sont utilement caractérisées à la fois en termes de correction du délai et de précision du positionnement. D'une part, le délai ionosphérique résiduel atteint 31% pour les sites et l'année choisis. D'autre part, la précision de positionnement s'élève à $6m$ horizontalement et de $9,3m$ verticalement.

L'évaluation des performances a permis de souligner plusieurs aspects de la correction ionosphérique Galileo. Cette correction dépend en grande partie de la modélisation du *topside*, la partie supérieure de l'ionosphère, qui abrite des processus physiques plus complexes. Elle doit ses bonnes performances à l'ingestion de données, la technique d'adaptation du modèle à des mesures réelles, qui sous-tend l'algorithme de Galileo. Elle ne fournit pas nécessairement des niveaux de correction fortement corrélés en termes de délai d'une part et de positionnement de l'autre. Elle permet de définir des procédures alternatives régionales suivant une conception compatible mais neutralisant ses faiblesses.

La présente thèse ouvre la voie pour de futurs travaux liés à la modélisation de l'ionosphère pour les utilisateurs Galileo simple fréquence. Elle fournit des informations comparatives pour l'évaluation de l'algorithme dans le cadre des phases successives de déploiement de Galileo. Elle établit une base conceptuelle pour un algorithme assisté de correction ionosphérique diffusant des informations ionosphériques plus flexibles grâce à l'intégration des systèmes globaux de navigation par satellites et des télécommunications.

Mots-clés ionosphère, navigation par satellites, GNSS, Galileo, simple fréquence, positionnement absolu, positionnement ponctuel, délai ionosphérique, correction ionosphérique, précision du positionnement, contenu électronique total (TEC), ionosonde, modélisation de l'ionosphère, modèle NeQuick, modèle de densité électronique, *topside*, ingestion de données, niveau d'ionisation effectif, ingestion multiple, ingestion conduite par la variance, niveau d'ionisation effectif adaptatif, ingestion paramétrée, ingestion de cartes de TEC

Galileo is about to be a part of our daily lives

Vice-President of the European Commission Antonio Tajani
October 21^{st}, 2011
Launch of the first two operational Galileo satellites

Acknowledgements

For a fruitful and enjoyable PhD, take

a fertile research environment including a faithful promoter, a helpful committee and a kindly jury, thanks to the University of Liège (ULg), the Belgian Fund for Scientific Research (F.R.S.-FNRS), the Royal Meteorological Institute of Belgium (RMI), the European Space Agency (ESA), the European Cooperation in Science and Technology (COST) framework, the Abdus Salam International Centre for Theoretical Physics (ICTP), the International GNSS Service (IGS), the European Reference Frame (EUREF) Permanent Network, the Continuously Operating Reference Station (CORS) network and many other organisms;

a stimulating team of enthusiastic colleagues at the Geomatics Unit;

enriching networking and sharing experiences as well as mutual aid through the Réseau des Doctorants among others;

chance encounters, key opportunities and unique, memorable moments;

loving, understanding and supportive family, wife and son.

Contents

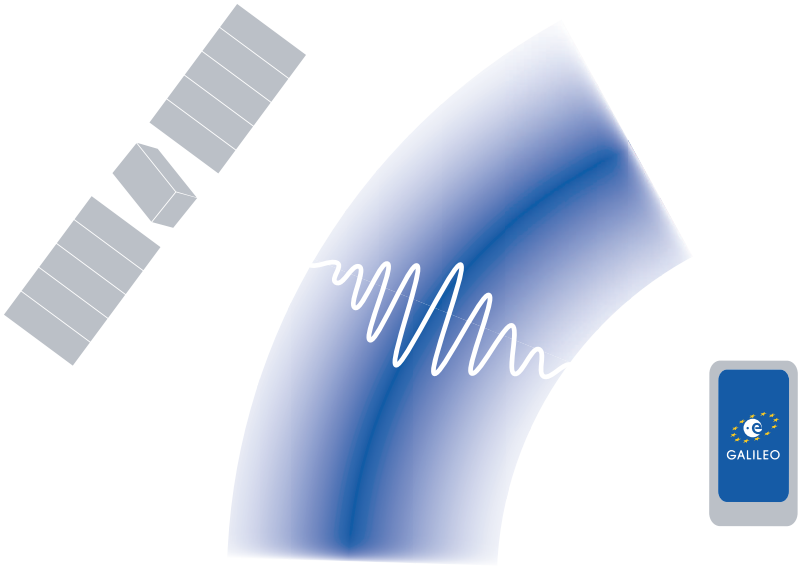

Figure 1.1: The ionospheric effect on GNSS. The ionospheric delay will affect Galileo single frequency users, not unlike any transatmospheric radiowave consumer.

1

Introduction

Most people think of a GPS as an electronic device placed on a car dashboard and talking the way to follow in a nice voice. They do not expect the bunch of science and technology behind the Global Positioning System (GPS) or more generally Global Navigation Satellite Systems (GNSS). They count among the users of these remarkable ground and space infrastructures. They will probably not associate GNSS only to car navigation any more in the near future. Besides the road market, GNSS will indeed grant access to a range of location-based services through smartphones. These smartphones will constitute the majority of the new GNSS-enabled devices which should reach a billion additional units annually in the next five years (GSA, 2012).

Mass-market GNSS receivers decode navigation signals from a bandwidth around a single carrier frequency in order to compute their position. They are referred to as *single frequency users*. On the contrary, multiple frequency users extract data from several frequencies. GNSS data are indeed broadcast on two and, soon, even three frequencies with the Galileo and modernised GPS satellites. These data enable more accurate, yet more specific applications requiring more expensive material.

Single frequency users face *positioning errors due to signal radiopropagation through* the atmosphere and *the ionosphere* in particular. The ionosphere covers regions of the atmosphere concentrating enough free electrons to disturb passing electromagnetic waves (Davies, 1990). It slows down navigation signals, inducing delays in their transmission (Fig. 1.1). These delays mainly depend on the Total Electron Content (TEC) i.e. the amount of free electrons met by the signals during their travel from a given satellite to the receiver. Like TEC, they are mainly driven by solar activity as free electrons are actually produced by solar ionisation.

Single frequency users model the ionosphere to mitigate its effects. They rely on empirical models and associated update information broadcast by navigation systems. In particular, GPS receivers run the Klobuchar model together with eight broadcast coefficients (GPS Wing, 2010). This model also referred to as Ionospheric Correction Algorithm (ICA) provides a vertical delay subsequently converted to the slant path considered, through a dedicated obliquity factor. In contrast, *Galileo receivers will operate the NeQuick model* in combi-

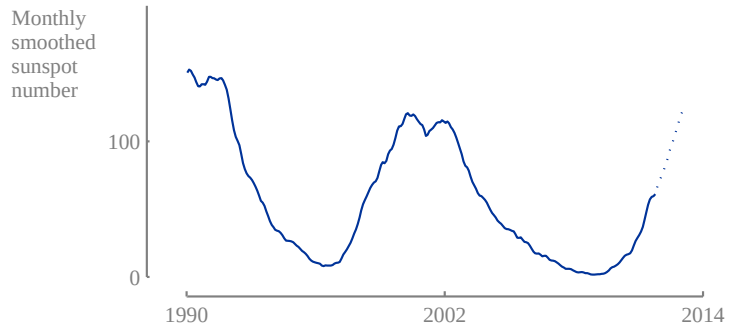

Figure 1.2: The temporal evolution of the solar activity. The solar activity reached its last maximum in 2002. It should again have risen to a high level by 2014, when Galileo will become operational. It is commonly characterised by the monthly smoothed sunspot number for which provisional values (dotted line) are provided by the Solar Influences Data analysis Center of the Royal Observatory of Belgium (`http://www.sidc.be`).

nation with three broadcast coefficients (European Union, 2010). This model predicts the electron density at any point in the ionosphere, integrated along the satellite-to-receiver path to derive TEC. It is expected to supply a 70% correction of the ionospheric delay vs. 50% for the Klobuchar model.

The novel mitigation technique developed for Galileo *required extensive validation*. This technique is built on NeQuick, originally a climatological model providing monthly median vertical electron density profiles. NeQuick itself models TEC with a certain degree of accuracy which needed to be quantified. In the framework of Galileo, the model will be updated with broadcast information computed on the basis of measurements. Indeed NeQuick is mainly driven by its solar activity input, an effective value of which can be determined in order to fit a set of measurements. This optimisation procedure called data ingestion improves TEC accuracy but may yield undesirable effects. For Galileo, it should enable single frequency users to enhance their positioning accuracy. However the positioning accuracy improvement does not necessarily reach the same order of magnitude as the expected TEC correction level (70%).

Successive operation modes of the NeQuick model have been assessed *at globally distributed locations and under high solar activity* in the framework of the PhD research reported in the present thesis. The first operation mode has been investigated in the following of an internship at the European Space Agency (ESA) (Bidaine, 2006). It has benefited from the access to complimentary data recorded at the Geophysical Centre of the Royal Meterological Institute of Belgium, an original research partner. These data have been collected during the year 2002. The same year was chosen for subsequent analyses. Indeed it experienced a solar activity level similar to the one foreseen for Galileo initial operations in 2014 (Fig. 1.2).

The present thesis proposes a *practical insight in the Galileo Single Frequency Ionospheric Correction Algorithm*.

- First it provides *fundamentals* about the algorithm (Chapter 2). These fundamentals should enable the reader to fully appreciate the research questions subsequently defined. The reader will also get familiarised with the data exploited to address the research questions.

- Second it exposes the evaluation of the algorithm *performances* (Chapter 3). This evaluation covers NeQuick intrinsic formulation, TEC modelling through data ingestion and positioning accuracy obtained from simulated ionospheric corrections.

- Finally it introduces potential *variants* for the algorithm (Chapter 4). These variants elude the discrepancies stated through the performance evaluation. They could yield regional procedures for single frequency ionospheric correction.

Algorithm

2

Designed at ESA, the Galileo Single Frequency Ionospheric Correction Algorithm was born from long-standing European research. Its core element, the NeQuick model, has been developed at the Abdus Salam International Centre for Theoretical Physics (ICTP) in Trieste (Italy) and the University of Graz (Austria) since the eighties (Radicella, 2009). It has been maturing during successive actions of the European Cooperation in Science and Technology (COST) framework (Bradley, 1995; Hanbaba, 1999; Zolesi & Cander, 2004; Bourdillon et al., 2009) and is recommended by the Internation Telecommunication Union (ITU) as a suitable prediction method for the design of satellite services and systems (ITU, 2009a).

Besides its adoption for Galileo, NeQuick has met satellite navigation at several occasions. It has contributed to the definition of the specifications of the European Geostationary Navigation Overlay Service (EGNOS), the European Satellite-Based Augmentation System (SBAS) supplementing GPS over Europe since 2009 (Ventura-Traveset & Flament, 2006). It has been included in a simulation toolkit developed in Australia to quantify the performance improvements of the future multi-GNSS infrastructure over the Asia Pacific region (Seynat et al., 2004). It serves as background for the Global Ionospheric Scintillation Model (GISM) estimating the intensity and phase fluctuations affecting navigation signals during their propagation through the ionosphere (Béniguel & Hamel, 2011).

Giving a glimpse of the reasons for this success, this chapter covers the context of the present thesis. First it introduces *state-of-the-art* elements about ionosphere modelling for GNSS. Second it defines the *questions* underlying the reported research driven by model validation. Third it presents the adopted *methodology* emphasising the data employed.

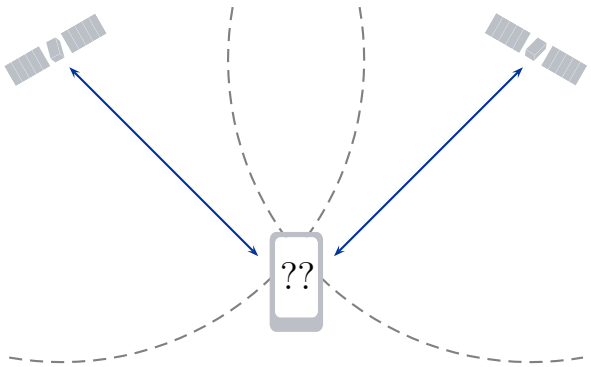

Figure 2.1: The trilateration principle. In this two-dimensional simplication, the user determines its two unknown coordinates from two distance measurements towards satellites at known locations. In practice, he is not confronted to an ambiguity between several geometrical solutions as he needs an a priori approximation of his position to proceed with the adjustment (Eq. 2.6).

2.1 Background

The Galileo ionospheric correction has been designed thanks to experts primarily interested in the ionosphere for professionals concerned with the mitigation of its effects. Reading this section, the first will get more acquainted with the principles of *satellite positioning*[1] and the second with the origin of the *ionospheric delay*. Aiming at a common goal, both will finally deepen their understanding of the *Galileo correction*.

2.1.1 Satellite positioning

Conceptually satellite positioning is based on *trilateration*. It enables a GNSS user to determine his position from the simultaneous observation of several satellites (Hofmann-Wellenhof et al., 2008). These satellites constitute beacons broadcasting their own position consequently known to the user who decodes the navigation message[2]. Hence the user deduces his location from the distance separating him from the observed satellites. In a flat frozen world, he would need two distance measurements to determine two unknowns, finding the intersection of two circles centred about two satellites (Fig. 2.1). With an additional dimension, he would solve for the third unknown collecting an extra range.

To obtain the distance from a given satellite, the receiver measures the signal time of arrival from this satellite. Unfortunately this time measurement is not consistent with the time of emission provided in the navigation message as the receiver is usually not equipped with a clock as accurate as the satellite atomic oscillator. Hence the receiver achieves synchronisation considering its clock error as a fourth unknown. Moreover it must compensate various propagation delays which are however not considered as unknowns of the problem.

As the basic observable, the *pseudorange* P_p^i derived by the receiver p from the signal received from satellite i formalises the difference between the (unknown) geometric range D_r^i and the actual measurement[3]. It results from time

[1] The distinction between satellite *navigation* and *positioning* depends on the context. The first designation surely refers to the maritime origin of the field and compares with celestial, radio or inertial navigation. Nevertheless it involves the computation of successive positions most of the time but implies a real-time, less accurate notion due to motion. The second designation originates in the geodesy and surveying worlds. Therefore it is sometimes associated to static problems solved in post-processing up to high accuracies. It is preferred here for its more evident link with the parameters handled such as positioning accuracy. On the other hand, *navigation* is associated to technical concepts such as signals or message.

[2] The content of the navigation message is fully described in Interface Control Documents (ICD), e.g. (GPS Wing, 2010) for GPS and (European Union, 2010) for Galileo.

[3] In the framework of the most common Code Division Multiple Access (CDMA) technique, this measurement proceeds from the correlation of the received signal and time-shifted replicas of Pseudo-Random Noise (PRN) codes. These so-called ranging codes justify the

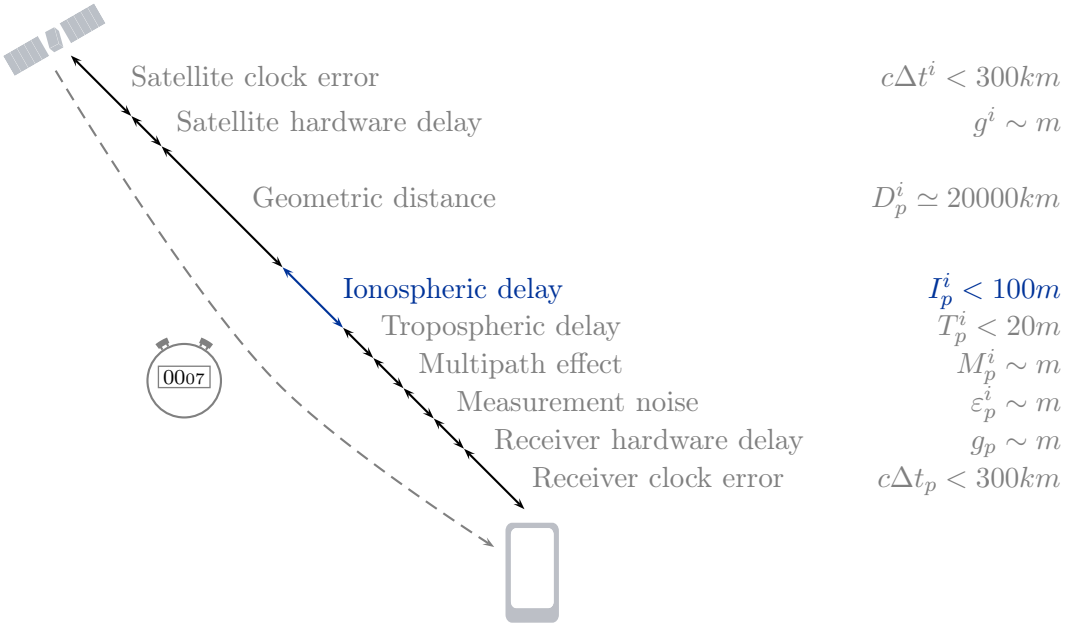

Figure 2.2: The pseudorange and its constitutive terms. The basic pseudorange observable corresponds to the time of flight of navigation signals between the satellite and the receiver. As navigation satellites are inserted in a Medium Earth Orbit (MEO) at about $20000km$ altitude, these signals reach the surface in about $\frac{2\ 10^7}{3\ 10^8} \simeq 0.07s$. For positoning purposes, this duration is superseded by its equivalent distance called pseudorange. This distance differs from the geometric range due to a number of delays abusively quantified in m. Among others, these delays include the ionospheric delay (Section 2.1.2). (Hernandez-Pajares et al. (2008) inspired this figure.)

information expressed in time scales more or less synchronised with the reference GPS time. It consists in the difference between the time of arrival $t_p(t)$ as measured by the receiver and the time of emission $t^i(t_e)$ recorded by the satellite, converted to a distance to avoid very small values (Eq. 2.1). As both times are affected by errors $\Delta t_p(t)$ and $\Delta t^i(t_e)$ induced by clock drifts and the signal does not cross the atmosphere (and the electronics) at the speed of light c in a straight line, the pseudorange breaks up into several terms (Eq. 2.2, Fig. 2.2).

$$P_p^i = c\left(t_p(t) - t^i(t_e)\right) \tag{2.1}$$

$$= D_p^i + c\left(\Delta t^i(t_e) - \Delta t_p(t)\right) + T_p^i + I_p^i + M_p^i - g^i + g_p + \varepsilon_p^i \tag{2.2}$$

The constitutive terms of the pseudorange equation are sorted out between unknowns, systematic and random errors depending on the positioning technique. For single frequency *absolute positioning*, the above-mentioned four unknowns appear in the geometric distance and the receiver hardware delay g_p grouped to the receiver clock error. Systematic errors include the satellite clock error, the tropospheric or neutrospheric delay T_p^i, the ionospheric delay I_p^i and the satellite hardware delay[4] g^i. These errors are modelled mainly from information provided in the navigation message. Nevertheless they leave residual contributions considered as random errors. These random errors also incorporate the effect of interfering signals from reflections on surrounding objects called multipath M_p^i and the measurement noise ε_p^i.

Practically the positioning problem is solved through a *least-squares adjustment* schematised in three steps[5].

1. The adjustment requires an a priori approximation $\mathbf{x}_0$ of the unknown position $\mathbf{r}$ and common bias b gathering the receiver clock error and its hardware delay[6].

2. It is fed by observations consisting in the differences $\mathbf{\Delta P}$ between the measured pseudoranges[7] to the n satellites in view of the receiver and the corresponding predictions based on the a priori approximation and modelled effects (Eq. 2.3).

$$\Delta P^i = P^i - \left(||\mathbf{r}^i - \mathbf{r}_0|| + c\Delta t_{mod}^i + T_{mod}^i + I_{mod}^i\right) \tag{2.3}$$

3. It extracts the updates $\hat{\mathbf{\Delta x}}$ to the approximation from the corresponding system of equations. This system results from the linearisation of the

designation *code pseudorange* denoting basically a time measurement.

[4] Only a differential value is actually calculated together with the clock error. Hence g^i does not appear explicitly any more in Eq. 2.3.

[5] van Diggelen (2009) inspired the following discussion.

[6] b is usually initialised at 0 and actually comprises any delay common to all satellites.

[7] In the following, the subscript p is omitted as a single receiver is considered.

receiver-to-satellite distances and is characterised by the design matrix A containing the unit vectors $\mathbf{u}^i$ ($i = 1$ to n) in the receiver-to-satellite directions. It is usually overdetermined ($n \geq 4$) and admits a solution in the least-squares sense (Eq. 2.6).

$$A\ \mathbf{\Delta x} = \mathbf{\Delta P} + \boldsymbol{\nu} \tag{2.4}$$

$$A = \begin{pmatrix} -\mathbf{u}^1 & 1 \\ \vdots & \vdots \\ -\mathbf{u}^n & 1 \end{pmatrix}, \mathbf{\Delta x} = \begin{pmatrix} \mathbf{\Delta r} \\ \Delta b \end{pmatrix}, \mathbf{\Delta P} = \begin{pmatrix} \Delta P^1 \\ \vdots \\ \Delta P^n \end{pmatrix} \tag{2.5}$$

$$\hat{\mathbf{\Delta x}} = \arg\min \boldsymbol{\nu}^T \boldsymbol{\nu} = \left(A^T A\right)^{-1} A^T\ \mathbf{\Delta P} \tag{2.6}$$

$$\begin{pmatrix} \hat{\mathbf{r}} \\ \hat{\Delta} b \end{pmatrix} = \mathbf{x}_0 + \hat{\mathbf{\Delta x}} \tag{2.7}$$

The adjustment solution yields the final position $\hat{\mathbf{r}}$. This position depends on the observation accuracy and the validity of the adjustment hypotheses. These hypotheses include the assimilation of the (residual) errors – among which the ionospheric delay I – to random variables.

2.1.2 Ionospheric delay

The *ionospheric delay* originates in the interaction of navigation signals with the atmospheric plasma characterised by its electron density Ne. It is equivalent to the time-of-flight difference τ between signal propagation in the ionosphere[8] and in free space (Eq. 2.8). This propagation is determined by the refractive index n representing the ratio between the speed of light c and the actual speed of propagation v (Eq. 2.9).

$$\tau = \int_{sat.}^{rec.} \frac{ds'}{v} - \int_{sat.}^{rec.} \frac{ds}{c} \simeq \frac{1}{c} \int_{sat.}^{rec.} (n-1) ds \tag{2.8}$$

$$n = \frac{c}{v} \simeq 1 + \frac{1}{2} \left(\frac{f_p}{f}\right)^2 \simeq 1 + 40.3\ \frac{Ne}{f^2} \tag{2.9}$$

This index obtained solving Maxwell's equations of wave propagation (Davies, 1990) simplifies for large signal frequencies f such as those employed for navigation ($f \simeq 1.5GHz$): it remains only affected by free electron oscillations induced by the passing wave at the so-called plasma frequency f_p. Much smaller than the signal frequency ($f_p \simeq 10MHz$), the plasma frequency depends on the electron density which consequently influences the refractive index and the ionospheric delay.

[8] Admittedly, a high-frequency signal reaching the receiver from an elevation angle larger than 10° has travelled in straight line from the satellite like in free space. This assumption allows to merge the integrals in τ formula.

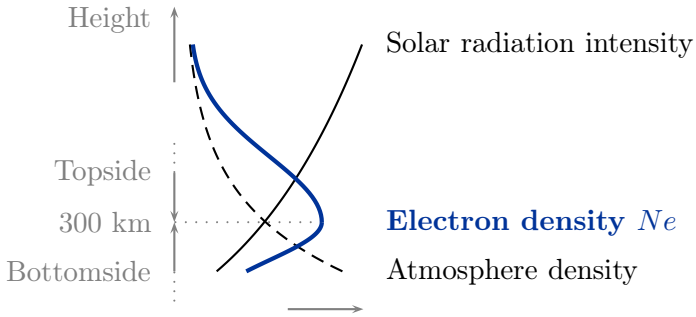

Figure 2.3: The electron density vertical profile. The electron density Ne (thick line) is produced by the combination of the atmospheric density (dashed line) and the solar radiation intensity (continuous line). The electron density profile exhibits a peak around $300km$, at the lower end of the International Space Station orbital heights, distinguishing the bottomside (below) and the topside (above). This peak is characterised by a density amounting to around 10^{12} free electrons per m^3. For the sake of comparison, the air density at sea level reaches around 10^{25} molecules per m^3 and decreases by 6 orders at $100km$. (Odijk (2002) inspired this figure.)

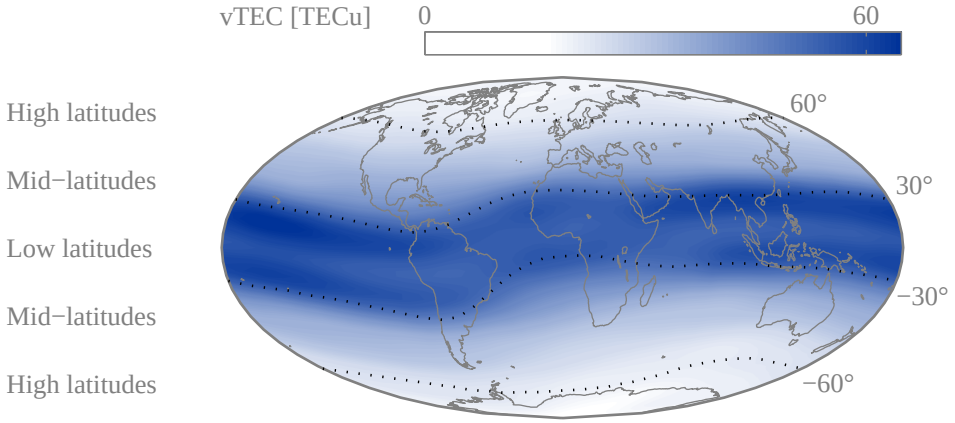

Figure 2.4: The vTEC spatial distribution. vTEC follows the geomagnetic field: it varies mainly across latitudes from the smallest values at the poles to the largest at both sides of the geomagnetic equator known as the crests of the equatorial anomaly. It is often associated to bands (left expressions) limited by specific modip values (dotted lines). In this 2002 yearly mean example, it reaches around $60TECu$ inducing a delay of $60 \cdot 0.16m \simeq 10m$ for the most common single frequency GNSS user.

This delay is actually function of the integral of the electron density along the path between the satellite and the receiver (Eq. 2.10) called the *slant Total Electron Content*[9] (sTEC). It is positive as, according to $n > 1$, the signal propagates in the ionosphere more slowly than light due to energy losses in plasma interaction.

$$I = c\tau \simeq \int_{sat.}^{rec.} (n-1)\ ds \simeq \frac{40.3}{f^2} \int_{sat.}^{rec.} Ne\ ds = \frac{40.3}{f^2} sTEC \tag{2.10}$$

The electron density is produced during atmosphere ionisation by the *solar radiation*. It participates to various physical processes involving the atmospheric constituents and the extreme ultraviolet and X solar emissions and defining several layers denoted by letters (D, E, F_1 and F_2) in different altitude regions. Hence it is vertically distributed along a so-called *profile* (Fig. 2.3) following the combination of the atmosphere density (decreasing with height) and the solar radiation intensity (increasing with altitude inversely to absorption). This combination results in a peak separating the profile in two main regions, namely the *bottomside* below the peak and the *topside* above. This peak corresponding to the maximum electron density above a certain location is rather faint but suffices to disturb radiowave propagation significantly.

The electron density distribution is constrained by the *geomagnetic field*. This field induces a recognisable pattern in the vertical TEC (vTEC), the integral of the vertical Ne profile best summarising the spatio-temporal ionospheric variability. This pattern (Fig. 2.4) exhibits larger (resp. smaller) vTEC values towards the equator (resp. the poles). However it is not aligned with geographic parallels. Like many other ionospheric characteristics, it is thus better described by means of a geomagnetic-dependent variable such as the modified dip-latitude (*modip*) μ (Eq. 2.11) based on the geomagnetic inclination I and the geographic latitude φ.

$$\tan\mu = \frac{I}{\sqrt{\cos\varphi}} \tag{2.11}$$

This variable was introduced to define a suitable system for the interpolation of ionospheric parameters (Rawer, 1963): it combines the physically-sound dependence on the geomagnetic field, especially at low latitudes, and the increasing influence of geographic latitude at higher latitudes. It is commonly used to separate the world in different regions sometimes called *modip bands* which host different ionospheric phenomena. For instance, the equatorial band referred to as low latitudes (besides mid- and high latitudes) is dominated by the equatorial anomaly consisting in a local vTEC minimum at the geomagnetic equator between two crests of increased electron density northwards and southwards.

[9] One TEC unit ($TECu$) commonly used to measure TEC equals 10^{16} electrons per m^2. Considering a navigation signal on the most common carrier ($f \simeq 1575.42MHz$ for GPS or Galileo), it implies a delay of $40.3\frac{10^{16}}{1.57542^2\ 10^18}m \simeq 0.16m$.

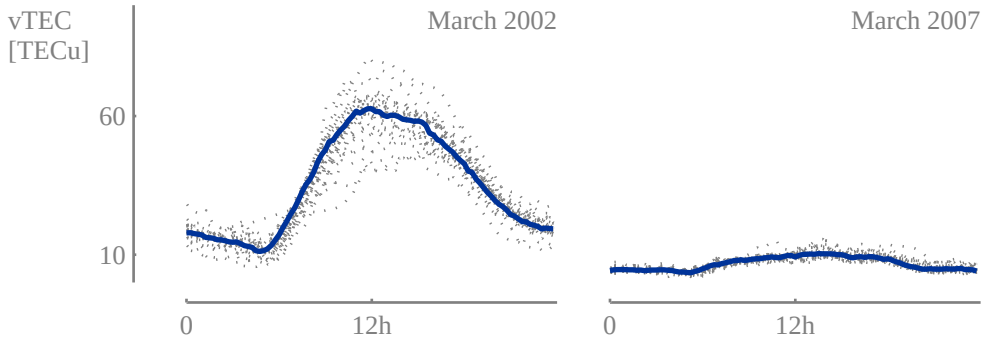

Figure 2.5: The vTEC temporal variation. vTEC local-time profiles (dotted curves, one for each day of the month) increase (resp. decrease) in the morning (resp. afternoon). They group around a monthly median curve (thick curves). Their magnitude largely depends on solar activity: it rises up to $60TECu$ (meaning $10m$ vertical delay) at Brussels in March 2002 (high level, left plot), 6 times more than in March 2007 at noon (low level, right plot).

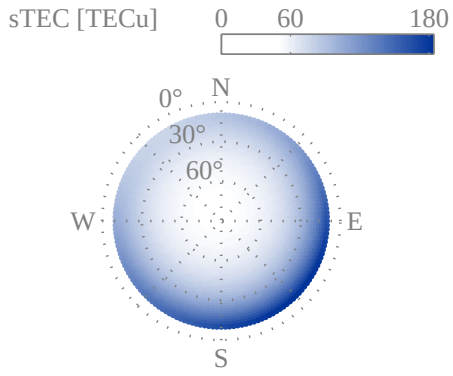

Figure 2.6: The sTEC directional variability. sTEC increases with decreasing elevation (on circles of increasing radius). At Brussels (50.8°N) on March 21^{st} at 9:00 in the morning, it attains $180TECu$ (equivalent to a $30-m$ delay) in the south-east sector, towards regions of larger electron densities (Fig. 2.4; low latitudes seen from northern mid-latitudes including Brussels). (Mohino (2008) inspired this figure.)

The effect of solar radiation varies with time. It shapes the vTEC daily profile (Fig. 2.5) with the largest (resp. smallest) values around local noon (resp. at night) when the ionisation is the most active (resp. absent)[10]. This profile oscillates around a monthly median accounting for the seasonal TEC dependence. Furthermore its overall order of magnitude is mainly influenced by the 11-year solar cycle (Warnant & Pottiaux, 2000): during low solar activity daytime, its maximum may drop below high solar activity nighttime values. Hence it is often characterised by means of *solar activity indices* such as the solar radio flux at $10.7cm$ $F10.7$, the sunspot number R or its monthly smoothed value R_{12} (Fig. 1.2).

These variations contribute to the typical *directional variability* of the sTEC and the ionospheric delay. At northern mid-latitudes for example, this delay appears larger southwards, and eastwards (resp. westwards) in the morning (resp. afternoon), apparently following sun azimuth (Fig. 2.6). More generally it lengthens at lower elevation due to the longer travel path in the atmosphere.

[10] At times, the solar radiation experiences significant disturbances implying much different vTEC profiles. These disturbances are due to heliophysical phenomena such as solar flares and reflect in the whole electromagnetic Earth environment, including the ionosphere. They are associated to so-called ionospheric storms – the most known being the Halloween storms in October 2003 – which remain not easily measured nor modelled. In particular, these storms are not specifically handled by the Galileo ionospheric correction – which situates them out of the scope of the present thesis – even if they obviously affect GNSS (Arbesser-Rastburg & Jakowski, 2007).

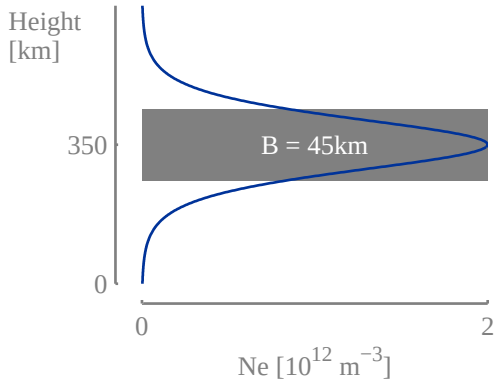

Figure 2.7: The Epstein layer employed for NeQuick electron density vertical profile. An Epstein layer is fully described by means of three parameters (sample values corresponding to the figure given in brackets): the peak amplitude N_{max} (2 10^{12} electrons m^{-3}) and height h_{max} (350km) as well as the thickness parameter B (45km). This parameter finds a useful interpretation in the function integral C: this integral is equivalent to the area of a rectangle (in gray) with N_{max} and 4B edges ($C = 4\ N_{max}\ B = 36TECu$).

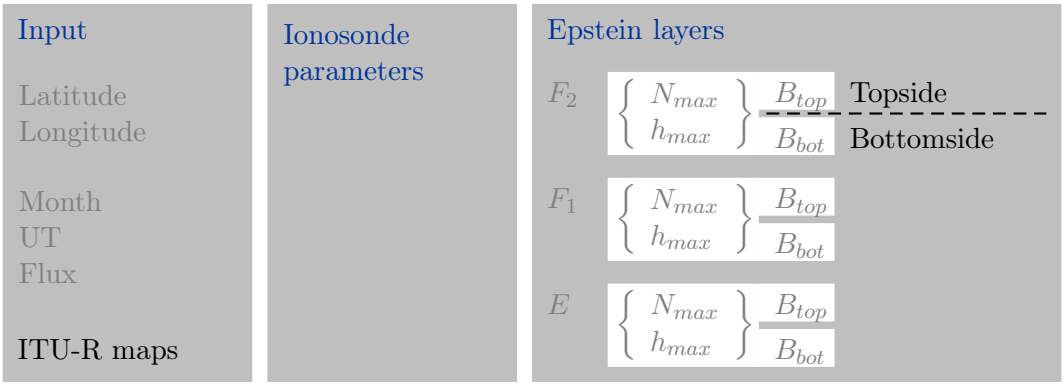

Figure 2.8: NeQuick constitutive parameters. NeQuick input data (left frame) serve to compute ionosonde parameters (centre frame). In turn, these parameters are employed to generate 6 semi-Epstein layers from 12 parameters (right frame) as peak amplitudes and heights are equal for successive layer couples.

2.1.3 Galileo correction

Galileo single frequency users will run the *NeQuick model* to mitigate the ionospheric delay. They will integrate the electron density Ne calculated by the model along every satellite-to-receiver path. To this extent, they will feed NeQuick with adequate parameters corresponding to the above-described spatio-temporal variability: location (latitude, longitude and height) varying from the receiver to the satellite, month, universal time (UT) and solar flux. In particular, the users will process information broadcast through the navigation message to compute an *effective ionisation level* Az playing the role of the solar flux (European Union, 2010).

NeQuick is an empirical electron density model called *profiler*[11]. It represents the vertical Ne profile by means of analytical functions derived by Epstein (1930). Employed to describe the permittivity[12] of a stratified medium, these functions yield an analytical solution to the wave propagation problem through this medium. Like the electron density profile (Fig. 2.3), they exhibit a peak of a predefined amplitude N_{max} at an arbitrary height h_{max} (Fig. 2.7). They are fully described with a third thickness parameter B related to the extension around the peak (Eq. 2.12).

$$Ne(h) = 4\ N_{max}\ \frac{e^{\frac{h-h_{max}}{B}}}{(1+e^{\frac{h-h_{max}}{B}})^2} \tag{2.12}$$

Six semi-Epstein functions – or layers – are combined in the NeQuick model to account for the three main ionospheric layers (E, F_1 and F_2), each layer being affected by a different thickness parameter below and above its own peak (Hochegger et al., 2000; Radicella & Leitinger, 2001; Appendix D). More precisely five functions compose the bottomside. The topside – admittedly the upper part of the F_2 layer – consists in a single sixth semi-Epstein layer with a height-dependent thickness parameter. In total, twelve parameters need being evaluated (Fig. 2.8) but are mostly conditioned by the main peak corresponding to the maximum of the F_2 layer. Hence these parameters are computed on the basis of ionosonde measurements (f_oF_2 and $M(3000)F_2$; Section 2.3.1) related to the F_2 peak (amplitude and height). For a standard use of NeQuick, these measurements are provided through files associated to the model in the shape of worldwide monthly median maps known as ITU-R (former CCIR) maps (ITU, 2009b). They are interpolated to the given location, month, UT and solar activity level.

[11] It is available for download from `http://www.itu.int/oth/R0A04000018/` and is comprehensively described in (Bidaine, 2006).

[12] The permittivity ε relates to the electron density Ne through the refractive index n: $\frac{\varepsilon}{\varepsilon_0} = n^2 \simeq 1 + 80.6\ \frac{Ne}{f^2}$.

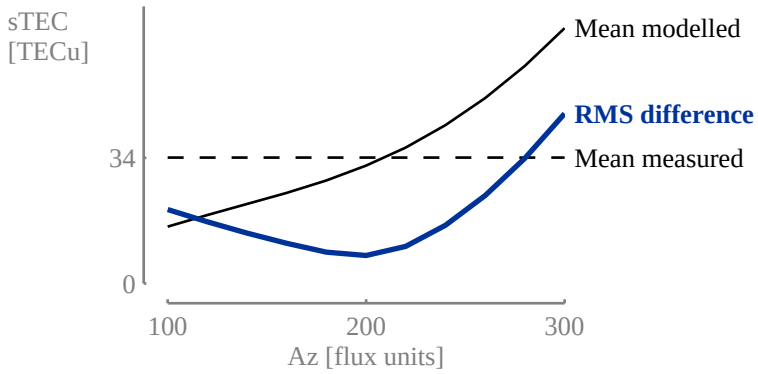

Figure 2.9: The modelled sTEC variation with the ionisation level Az. sTEC data ingestion into NeQuick minimises the RMS difference (thick line) between modelled and measured sTEC (continuous and dashed lines depicting respective mean values): it provides an effective ionisation level Az for the period covered with measurements. It is enabled by the monotonic behaviour of modelled sTEC in function of Az. In this example (Brussels, September 1^{st}, 2002), it supplies one Az for one station and a whole day.

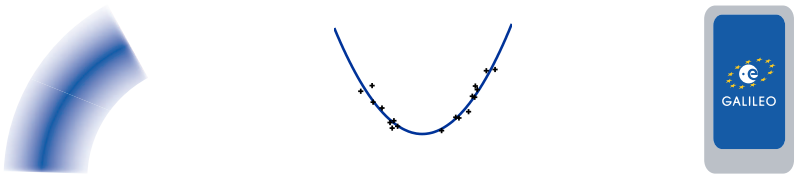

Measure
sTEC

Optimise
$Az(\mu)$

Run
NeQuick

Figure 2.10: The Galileo algorithm phases. The Galileo Single Frequency Ionospheric Correction Algorithm comprises three phases: (1) measuring sTEC at the Galileo Sensor Stations (GSS) and ingesting it into NeQuick, (2) optimising the effective ionisation level dependence in function of the GSS modip through a parabolic interpolation and (3) running NeQuick together with the Az computed from the resulting broadcast coefficients at the receiver modip.

For operational purposes, NeQuick is driven towards a specific data set thanks to *ingestion*. Combined with numerical integration, NeQuick produces sTEC values depending monotonically on its solar flux input (Fig. 2.9). Considering a set of sTEC measurements (often derived from GNSS data; Section 2.3.2), this input can be adjusted to minimise the mismodelling with respect to these measurements (Nava et al., 2006). It is then referred to as *effective ionisation level* Az as it denotes an optimised parameter suited for NeQuick and the corresponding data set instead of a solar activity proxy. Classicaly it proceeds from the minimisation of the Root Mean Square (RMS) difference between modelled and measured sTEC (Eq. 2.13 where $\langle\rangle$ denotes averaging the available differences within a given period).

$$\hat{Az} = \arg\min \mathrm{RMS}(\mathrm{Az}) = \arg\min \sqrt{\left\langle (sTEC_{mod}(Az) - sTEC_{meas})^2 \right\rangle} \quad (2.13)$$

Based on sTEC data ingestion into NeQuick and initiated within the Galileo Mission Segment (GMS), the Galileo ionospheric correction (Arbesser-Rastburg, 2006; Hofmann-Wellenhof et al., 2008) will proceed from an algorithm in three steps (Fig. 2.10).

1. Besides orbit determination, time synchronisation and integrity determination, each of the thirty to fourty Galileo Sensor Stations (GSS) will routinely measure sTEC. Each station will then compute a corresponding effective ionisation level (Eq. 2.13) from these measurements once a day.

2. Each day, the Galileo Control Centres (GCC) will synthesise the information broadcast the next day by the satellites through the navigation message. This information will consist in 3 coefficients a_i $(i = 0, 1, 2)$ obtained from a second-order interpolation of the GSS Az against corresponding modip (Eq. 2.14).

$$Az(\mu) = a_0 + a_1\mu + a_2\mu^2 \quad (2.14)$$

3. Finally the users will retrieve the Az corresponding to their own modip from the broadcast coefficients generated one day before. They will run NeQuick with this value to model the ionospheric contribution to the pseudoranges.

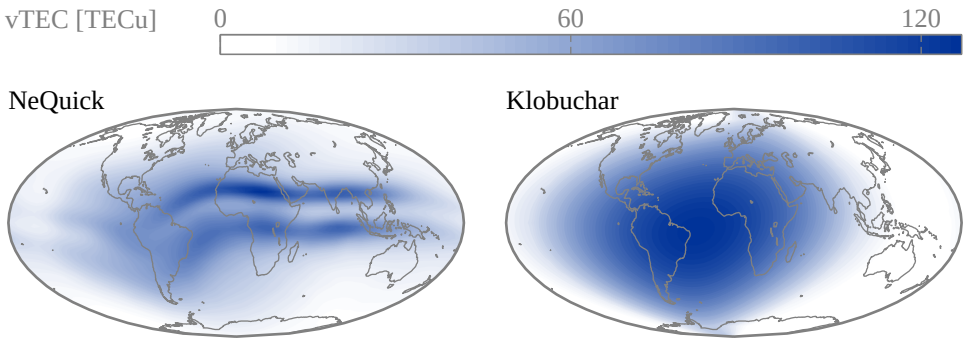

Figure 2.11: vTEC maps from NeQuick (left) and Klobuchar (right) models. NeQuick provides a finer representation of the ionosphere than the Klobuchar model used for the GPS single frequency ionospheric correction. These vTEC maps correspond to March 21^{st}, 2002 at 18:00 UT.

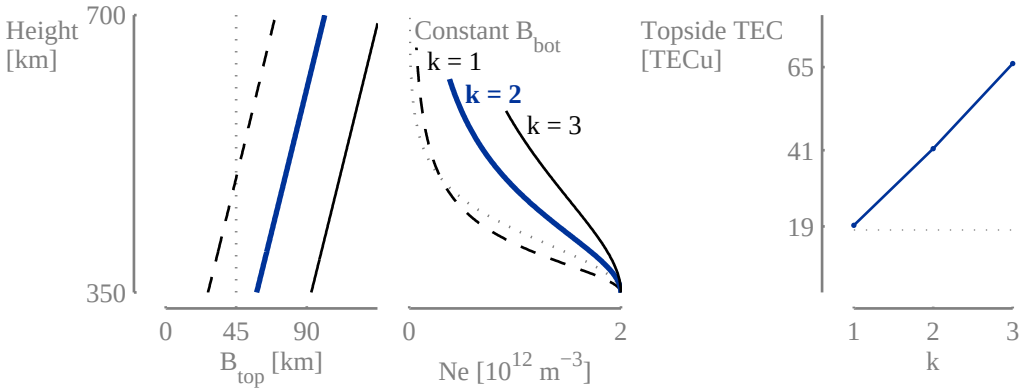

Figure 2.12: NeQuick topside parameters. NeQuick topside representation involves a height-dependent thickness parameter B_{top} (left plot) determined by the topside shape parameter k. Based on the sample Epstein layer previously exhibited (Fig. 2.7, $N_{max} = 2\ 10^{12}$ electrons m^{-3}, $h_{max} = 350km$ and $B_{bot} = 45km$ depicted by the vertical dotted line), different values of k are illustrated (dashed line for $k = 1$, thick line for $k = 2$, continuous line for $k = 3$) and compared to the use of the constant thickness parameter of the bottomside B_{bot} (dotted line). These k values lead to electron density profiles (center plot) decreasing more slowly with height than with a fixed thickness parameter at the peak and above. They correspond more or less to the ratio between the topside TEC (right plot) and the bottomside TEC (dotted horizontal line).

2.2 Research directions

Blending satellite positioning and ionosphere modelling, the research described in the present thesis was undertaken to contribute to the investigation of the *performances of the Galileo ionospheric correction*. It was driven by corresponding research questions related to *NeQuick intrinsic formulation* of the ionosphere, *sTEC data ingestion* incorporated in the Galileo algorithm to accommodate actual situations and *positioning accuracy* considered as single frequency users' final concern.

2.2.1 NeQuick intrinsic performances

Early after its initial development, NeQuick has been considered as a good candidate for *rapid global ionospheric modelling*. On the one hand, it provides a more realistic picture of the ionosphere than other models (Coisson et al., 2004) including the GPS ICA (Fig. 2.11). On the other hand, it remains computationally efficient for real-time operation at the price of a number of simplifications.

NeQuick exists in *several versions* corresponding to successive simplification revisiting. NeQuick 1 constitutes the original version recommended by the ITU-R. At first, it has been improved regarding the bottomside (Leitinger et al., 2005): unrealistic electron density horizontal gradients at low and high latitudes due to problematic transitions between layers have been overcome reformulating the parameters associated to the E and F_1 layers. These improvements have been included in two subsequent versions, the one currently considered for the final Galileo algorithm – referred to as NeQuick G in the following – and the latest NeQuick 2 (Nava et al., 2008).

The *most serious simplification* concerns the *topside*. The topside is governed by diffusive equilibrium conditions leading to a transition between 0^+ and H^+ ions among others: the lighter H^+ ions become relatively more and more abundant with increasing altitude. These conditions were not taken into account at all in the original analytical model of the electron density profile by Di Giovanni & Radicella (1990), NeQuick precursor. The improved DGR analytical model published by Radicella & Zhang (1995) introduced an asymmetry between bottomside and topside: exploiting the analytical expression of the integral of an Epstein layer (Fig. 2.7 and Eq. 2.16), it multiplied the thickness parameter B in the topside by a so-called topside shape parameter k to fit observed vTEC.

$$vTEC = vTEC_{bot} + vTEC_{top} = 2\ N_{max}\ B_{bot} + 2\ N_{max}\ B_{top} \quad (2.15)$$

$$= 2\ N_{max}\ B_{bot}(1+k) \quad (2.16)$$

The DGR model formally became the NeQuick model after an additional modification of the topside thickness parameter B_{top}: this parameter received a height-increasing formulation (Fig. 2.12) to represent a simplified diffusive equilibrium (Leitinger et al., 2002).

More elaborate alternatives built on the same principles but needing longer calculations are not affected by the same topside limitations as NeQuick. These limitations are related to the topside ionospheric scale height defining the rate of electron density decrease with height and the $O^+ - H^+$ transition height where O^+ and H^+ densities become equal (Stankov et al., 2007). Such parameters are explicitly computed within COSTprof and NeUoG-plas, the two other models based on the DGR approach (Hochegger et al., 2000). These models consider diffusive equilibrium conditions more accurately. NeUoG-plas even includes a magnetic field aligned formulation for the plasmasphere (above $2000km$). A modification of NeQuick was proposed connecting it to the Gallagher plasmasphere model (Cueto et al., 2007). However it covers only low geomagnetic latitudes (between $\pm 40°$).

To remain computationally efficient and improve the topside representation, the NeQuick model received a new formulation for the topside shape parameter k. In NeQuick 1 and G, k is computed on the basis of two formulas, one for months between April and September and the other for the rest of the year (Eq. D.13). In NeQuick 2, it proceeds from a single formula (Eq. D.32). This formula was obtained from topside soundings data from the ISIS-2 satellite (Coisson et al., 2006). It provides electron density topside profiles closer to experimental ones as these profiles are usually understimated by NeQuick 1 at high and mid-latitudes and slightly overestimated at low latitudes.

This major evolution modified NeQuick intrinsic performances subsequently optimised through TEC data ingestion. By definition, ingestion minimises NeQuick mismodelling adapting its solar activity input. Hence this intrinsic mismodelling must be quantified to subsequently characterise ingestion effectiveness leading to the first research question of this thesis:

To which extent is NeQuick (and its latest evolutions) able to provide a realistic representation of the ionosphere without TEC adaptation?

2.2.2 Galileo algorithm performances

NeQuick provides *flexible solutions to accommodate TEC measurements*, another valuable feature in addition to the computational efficiency. Originally it has been designed to reproduce median values of the ionosphere electron density using a monthly solar activity index. Computing effective values of this index, NeQuick has then been used to model actual conditions thanks to the so-called data ingestion technique. Hence it is able to convert vTEC maps deduced from GPS measurements to electron density profiles (Nava et al.,

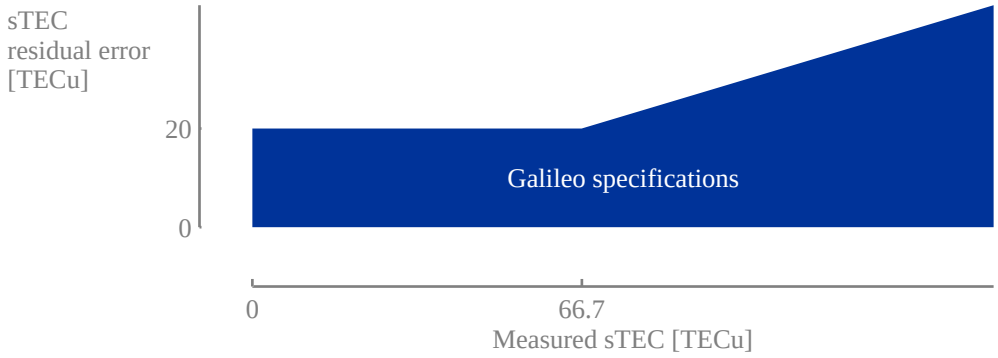

Figure 2.13: The Galileo algorithm specifications. To meet the specifications (filled area), the residual sTEC should remain smaller than $20 TECu$ or 30% of the measured sTEC, whichever is larger.

2005). To this extent, it is run at each grid point with the solar activity input value that minimises the difference between the vTEC value from the map and the integrated electron density profile from the model. Similarly it supplies a means to retrieve the electron density directly from sTEC measurements (Nava et al., 2006). In particular, it allows to reconstruct sTEC in directions and during periods not covered with such measurements. Added to NeQuick quick-run property, sTEC data ingestion was identified as an efficient technique to design the Galileo ionospheric correction.

Investigating sTEC data ingestion effectiveness contributes to the assessment of the Galileo algorithm performances. Formally these performances are subject to dedicated specifications (Arbesser-Rastburg, 2006): the residual sTEC error should not exceed 30% of the actual sTEC or $20TECu$, whichever is larger (Fig. 2.13). This residual error is equivalent to the residual ionospheric delay. Hence it characterises the ability of the algorithm to improve the pseudorange accuracy which influences the positioning accuracy. It depends on the combination of NeQuick intrinsic mismodelling and the way in which ingestion minimises this mismodelling with respect to sTEC data. Keeping in mind that NeQuick G does not include the latest topside modification, this combination defines the second research question of this thesis:

Taking into account NeQuick intrinsic weaknesses, how effectively can the model accommodate sTEC measurements, for Galileo in particular?

As a subquestion, the Galileo algorithm performances would be usefully compared to the GPS ICA results. These results are usually stated as a 50% RMS correction of the ionospheric range error.

2.2.3 Positioning performances

The positioning accuracy results from the propagation of pseudorange errors through the least-squares adjustment characterised by the *satellite sky distribution*. Mathematically it appears in the covariance matrix $\Sigma_{\hat{\mathbf{\Delta x}}}$. This matrix is obtained from the covariance propagation law applied to the positioning solution 2.6 (Hofmann-Wellenhof et al., 2008). It simplifies considering uncorrelated pseudoranges of equal precision (Eq. 2.17).

$$\Sigma_{\hat{\mathbf{\Delta x}}} = \left(A^T A\right)^{-1} \sigma_P^2 = Q_{\hat{\mathbf{\Delta x}}} \sigma_P^2 \tag{2.17}$$

In this case, it depends on the pseudorange precision σ_P, often referred to as User Equivalent Range Error (UERE), and the cofactor matrix $Q_{\hat{\mathbf{\Delta x}}}$. This matrix relates to the satellite sky distribution: it is computed from the design matrix A containing the unit vectors towards each satellite in view. Moreover it provides, through its diagonal elements, the information required to quantify the impact of the satellite sky distribution on the positioning solution by means of standard parameters. These parameters – subsumed under the

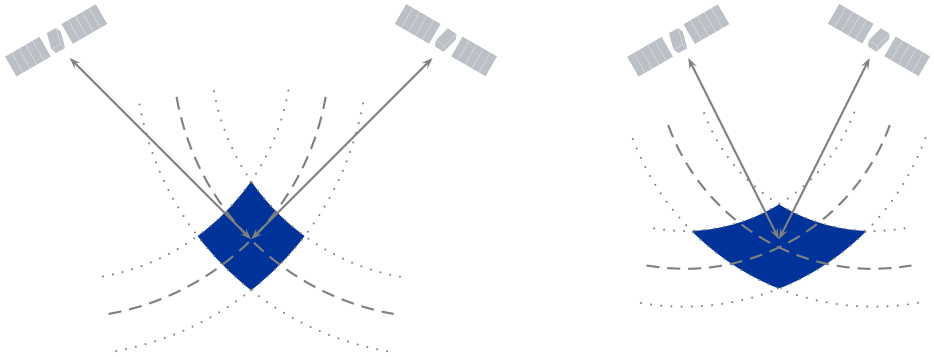

Figure 2.14: The influence of the receiver-satellite geometry on the positioning accuracy. For the same pseudorange errors (dotted arcs at each side of the dashed arcs), a poorer receiver-satellite geometry (right) leads to a wider uncertainty region around the true position (filled area) and a worse positioning accuracy.

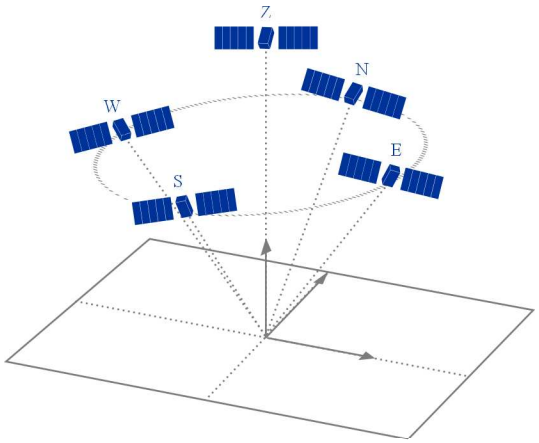

Figure 2.15: The simplest fictitious highly symmetrical satellite sky distribution. A satellite distribution involving 5 fundamental directions (northwards - N, eastwards - E, southwards - S, westwards - W - and at the zenith - Z) yields the simplest analytical expressions binding ionospheric delays to positioning errors.

term *dilution-of-precision* (DOP) – describe how the receiver-satellite geometry degrades the positioning accuracy basically determined by the measurement errors (Lonchay, 2009). Conceptually these errors define an uncertainty region around the true position more or less wide in function of the relative position of the satellites with respect to the receiver (Fig. 2.14). They have different influences in different coordinates: they are mapped onto the horizontal (resp. vertical) accuracy σ_H (resp. σ_V) through the $HDOP$ (resp. $VDOP$). Providing the appropriate coordinate transformation, these positioning accuracies are indeed computed from the diagonal elements of the covariance matrix obtained themselves from the corresponding elements of the cofactor matrix (Eq. 2.18 and 2.19). In particular, the vertical accuracy is usually worse than the horizontal: the projection of the satellite distribution on the horizontal plane appears rather homogeneous by comparison to the projection on the vertical axis limited at best to the upward half.

$$\begin{aligned}\sigma_H &= \sqrt{(\Sigma_{\hat{\mathbf{\Delta x}}})_{(1,1)} + (\Sigma_{\hat{\mathbf{\Delta x}}})_{(2,2)}} = \sqrt{(Q_{\hat{\mathbf{\Delta x}}})_{(1,1)} + (Q_{\hat{\mathbf{\Delta x}}})_{(2,2)}}\ \sigma_P \\ &= HDOP\ \sigma_P\end{aligned} \tag{2.18}$$

$$\sigma_V = \sqrt{(\Sigma_{\hat{\mathbf{\Delta x}}})_{(3,3)}} = \sqrt{(Q_{\hat{\mathbf{\Delta x}}})_{(3,3)}}\ \sigma_P = VDOP\ \sigma_P \tag{2.19}$$

Adopting a lower degree of simplification, the uncorrected ionospheric delay yields systematic effects on the positioning accuracy. Taking into account its directional variability (Section 2.1.2), it cannot actually be considered as a random variable affecting uncorrelated pseudoranges. Its influence becomes more intuitive thanks to a particular case of the positioning mathematical problem (Mohino, 2008). In this particular case, the ionospheric delay I^i towards satellite i replaces the corresponding observation ΔP^i to produce positioning errors induced only by the ionosphere (Eq. 2.20). These positioning errors adopt analytical expressions in a local reference frame (north N, east E, up U) and for a fictitious highly symmetrical satellite distribution. This distribution consists of one zenithal satellite and an even number of satellites at constant elevation η uniformly distributed in azimuth. The simplest example of such a distribution comprises five satellites, one at the zenith Z and the others towards each cardinal direction N, E, S and W (Fig. 2.15). It allows an analytical inversion of the matrix $A^T A$ to compute the cofactor matrix $Q_{\hat{\mathbf{\Delta x}}}$.

$$\mathbf{\Delta x} = \left(A^T A\right)^{-1} A^T\ \mathbf{I} \tag{2.20}$$

$$\mathbf{\Delta x} = \begin{pmatrix}\Delta N \\ \Delta E \\ \Delta U \\ \Delta b\end{pmatrix}, A = \begin{pmatrix}0 & 0 & -1 & 1 \\ \cos\eta & 0 & -\sin\eta & 1 \\ 0 & \cos\eta & -\sin\eta & 1 \\ -\cos\eta & 0 & -\sin\eta & 1 \\ 0 & -\cos\eta & -\sin\eta & 1\end{pmatrix}, \mathbf{I} = \begin{pmatrix}I^Z \\ I^N \\ I^E \\ I^S \\ I^W\end{pmatrix} \tag{2.21}$$

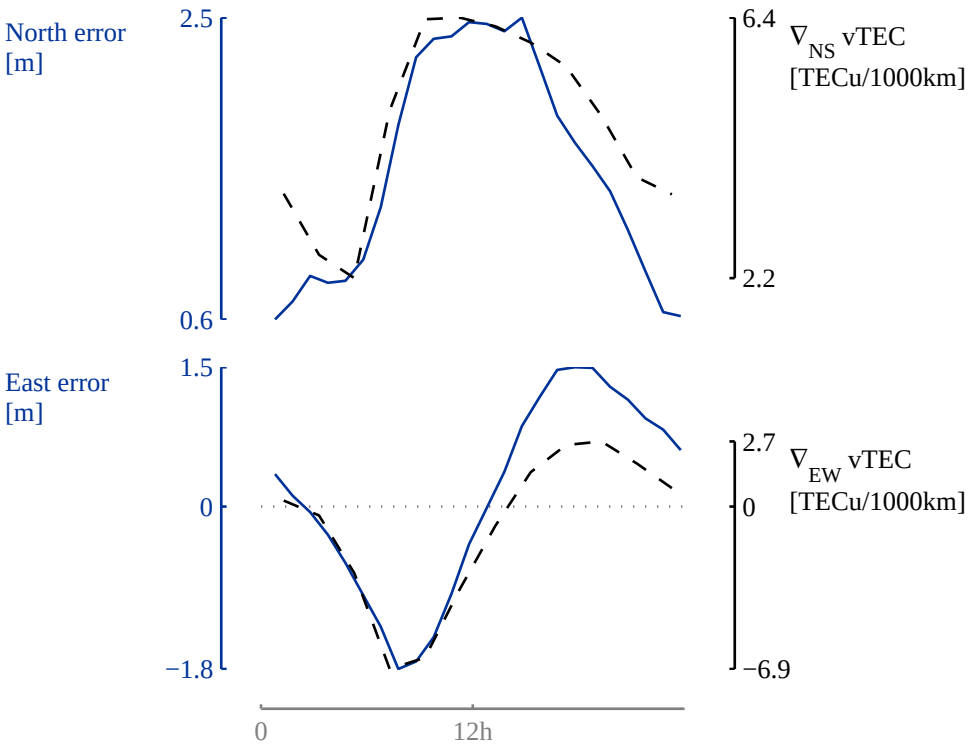

Figure 2.16: Relation between horizontal uncorrected positioning errors (solid lines) and TEC gradients ∇TEC (dashed lines). Without correction, the north (top plot) and east (bottom plot) positioning errors exhibit local-time profiles similar respectively to the north-south and east-west TEC gradients. These statistics correspond to yearly means at Brussels in 2002. The TEC gradients were deduced from TEC maps.

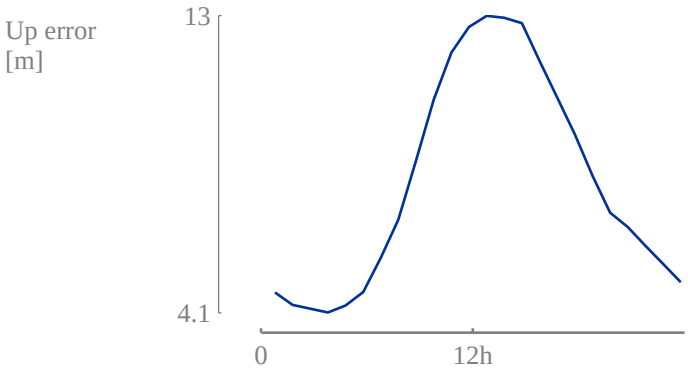

Figure 2.17: Local-time profile of the vertical uncorrected positioning error. Without correction, the up error exceeds horizontal ones. These statistics correspond to yearly means at Brussels in 2002.

$$\begin{cases} \Delta N &= \frac{1}{2\cos\eta}\left(I^S - I^N\right) \\ \Delta E &= \frac{1}{2\cos\eta}\left(I^W - I^E\right) \\ \Delta U &= \frac{1}{1-\sin\eta}\left(\overline{I} - I^Z\right) \\ \Delta b &= \frac{1}{1-\sin\eta}\left(\overline{I} - \sin\eta\ I^Z\right) \end{cases} \quad \text{with } \overline{I} = \frac{I^N + I^E + I^S + I^W}{4} \tag{2.22}$$

The accuracy of positions obtained without ionospheric correction depends on *TEC gradients* and vTEC. In the previous particular case, the horizontal errors ΔN and ΔE are finally function of the ionospheric delay differences along the respective axes (Eq. 2.22). These differences are equivalent to TEC gradients in the same direction which follow recognisable mean temporal evolutions at mid-latitudes (Fig. 2.16). For real satellite sky distributions, the equatorwards TEC gradients lead to an average north bias without proper correction, with a maximum around local noon. On the other hand, the larger TEC values eastwards in the morning (resp. westwards in the afternoon) provoke a negative (resp. positive) east bias. Finally the vertical error remains much larger than horizontal ones (Fig. 2.17). With the symmetrical satellite distribution, it equals the difference between a mean ionospheric delay $\overline{I}$ and the delay at the zenith equivalent to vTEC. It is hence positive on average as the ionospheric delay decreases with elevation. Yet it would intuitively have been negative considering pseudoranges lengthened after having crossed the ionosphere: all associated to positive elevations, these pseudoranges would simplistically have driven the receiver height below its actual level. However they also influence the fourth unknown which inclusion in the problem invalidates this reasoning.

The performances of an ionospheric correction in terms of position or delay are not strictly equivalent. Due to TEC spatio-temporal correlation, a given positioning improvement cannot simply be deduced from a DOP value and the corresponding ionospheric delay reduction. Among others, this reduction might not totally remove the systematic biases subsequently altering the positioning performances. Hence these performances deserve a specific treatment and the third research question of this thesis:

At which level does the Galileo Single Frequency Ionospheric Correction Algorithm improve the positioning accuracy?

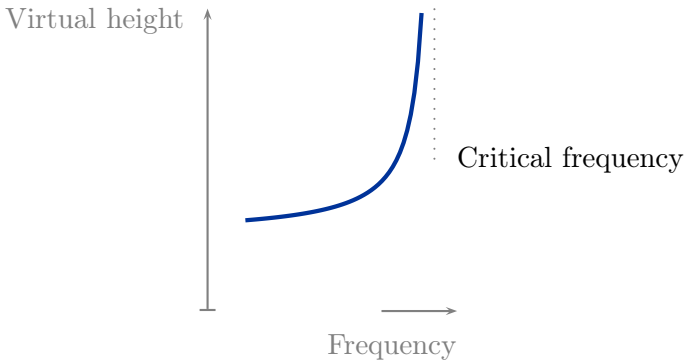

Figure 2.18: Ionogram (simplified scheme). An ionogram records the return time of vertically emitted signals reflected by the ionosphere. This time is converted to a virtual height and associated to the frequency of the corresponding signal. It draws so-called traces reaching at most the critical frequency. This frequency and larger ones do not allow vertically incident waves to be reflected by the ionosphere any more.

2.3 Research modes

In the manner of successive research cycles, a series of validation scenarios addressed the above-defined questions. They all began with the identification of reference *data from ionosondes and/or GPS* to compare NeQuick results with or to drive the model. They intended to assess the model running in a specific *operation mode*. They occasioned several *publications and communications* disseminating their results.

2.3.1 Ionosonde measurements

The ionosphere influences the propagation of radiowaves depending on their frequency. For high frequencies ($f > 100MHz$) employed for GNSS among others, it merely refracts radiowaves modifying their speed (Section 2.1.2) and possibly direction of propagation. For lower frequencies used for Amplitude Modulation (AM) radio broadcasting for instance, it reflects signals or even absorbs them. Neglecting the influence of the magnetic field, signals with a vertical direction of propagation bring the associated phase refractive index[13] n_φ (Eq. 2.23) to 0 when their frequency equals the plasma frequency f_p (Eq. 2.24).

$$n_\varphi^2(f) \simeq 1 - \left(\frac{f_p}{f}\right)^2 \tag{2.23}$$

$$\text{Reflection: } n_\varphi = 0 \Leftrightarrow f = f_p \tag{2.24}$$

Ionosondes exploit radiowave reflection to probe the ionosphere from the ground[14]. They emit pulsed signals vertically, sweeping frequencies from about 0.1 to more than 30 MHz. These signals are reflected as soon as the electron density encountered at a certain height yields a plasma frequency equal to the signal frequency. They are received back at the emitter after a time t. Measuring this time renders a diagram of a virtual height h' (Eq. 2.25) in function of the signal frequency, called *ionogram* (Fig. 2.18).

$$h' = \frac{c\,t}{2} \tag{2.25}$$

As the signal frequency is associated to a specific electron density, an ionogram allows to derive the *vertical electron density profile* after true height inversion.

[13] The phase refractive index characterises the propagation of a monochromatic signal i.e. oscillating at a pure, single frequency. To carry information, a real signal always involves a range of frequencies spread around the main carrier frequency. Hence its propagation is described by means of a group refractive index introduced previously (Eq. 2.9). This index is actually derived from the phase refractive index.

[14] Not unlike many references, this thesis introduces ionosondes as ground-based devices even if topside ionosondes exist as well.

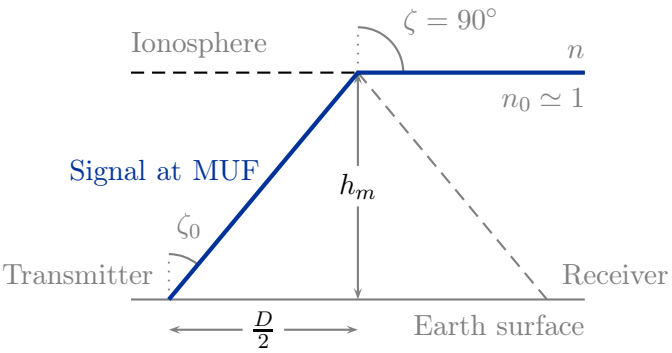

Figure 2.19: Signal transmitted at the Maximum Usable Frequency (MUF) experiencing total reflection on the ionosphere. To reach a receiver on Earth surface at distance D through ionospheric reflection, a transmitter also on the ground and broadcasting towards a zenith angle ζ_0 employs a signal frequency smaller than the MUF. The MUF induces total reflection (refraction angle $\zeta = 90°$) in the simplified case of a single ionospheric layer located at height h_m, of refraction index n and separated from the ground by a medium of refraction index $n_0 \simeq 1$.

This complex inversion is required as the virtual height is larger than the actual height. The virtual height is indeed obtained by multipling the half of time t by the speed of light c which is larger than the actual speed of propagation.

Ionograms extend until the *critical frequency* f_oF_2 linked to the peak electron density in the F_2 layer N_mF_2. They cover frequencies reflected by the ionosphere: the larger the signal frequency, the larger the plasma frequency and the electron density of the reflecting layer, the larger the height of reflection. The largest plasma frequency inducing reflection occurs at the F_2-layer peak. It is denoted critical frequency f_oF_2[15] and corresponds to the maximum electron density N_mF_2 (Eq. 2.26). It defines the frequency limit above which corresponding signals cross the ionosphere. Indeed these signals meet decreasing electron densities above the peak i.e. in the topside. Hence the topside is not accessible to an ionosonde.

$$N_mF_2 = 1.24\ 10^{10}\ (f_oF_2[MHz])^2 \tag{2.26}$$

Ionograms also supply the *transmission factor* $M(3000)F_2$ influenced by the F_2 peak height h_mF_2. They were originally used to find the optimum operation frequencies for High Frequency (HF) broadcasts. These broadcasts performed thanks to oblique reflection employ frequencies possibly larger than the critical frequency f_oF_2. According to Snell-Descartes law of refraction (Eq. 2.27), such frequencies experience refractive indices n preventing them from being refracted in the ionosphere if they remain below the so-called Maximum Usable Frequency (MUF). Assuming a unit refractive index n_0 below the ionosphere, the MUF allows a single solution for Snell-Descartes law: a refraction angle of 90° corresponding to total reflection (Fig. 2.19, Eq. 2.28).

$$n\ \sin\zeta = n_0\ \sin\zeta_0 \simeq \sin\zeta_0 \tag{2.27}$$

Total reflection: $\zeta = 90° \Leftrightarrow n = \sin\zeta_0$

$$= n(MUF) = \sqrt{1 - \left(\frac{f_p}{MUF}\right)^2} = \sqrt{1 - \frac{1}{M^2}} \tag{2.28}$$

$$f \leq MUF \Leftrightarrow n(f) \leq \sin\zeta_0 \Leftrightarrow \text{reflection} \tag{2.29}$$

The MUF equals the critical frequency at vertical and increases with the zenith angle ζ_0. Considering reflection on the F_2 layer, it is hence usefully normalised by f_oF_2 to yield the transmission factor $MF_2 = \frac{MUFF_2}{f_oF_2}$. The transmission factor depends on the distance D between the transmitter and the receiver and the height of the reflecting layer. On the one hand, it has been standardised for a distance of $3000km$ defining the $M(3000)F_2$ parameter read from ionograms. On the other hand, it is used to retrieve the F_2 peak height h_mF_2. In the case

[15] The second letter "o" stands for "ordinary" as the magnetic field actually provokes other types of reflected waves such as extraordinary waves (Davies, 1990).

of a simplified single reflecting layer of the refractive index n and located at the height h_m, this height is inversely proportional to $M(3000)F_2$ (Eq. 2.30)[16].

$$h_m = \frac{D}{2}\frac{1}{\tan\zeta_0} = \frac{D}{2}\sqrt{\frac{1}{\sin^2\zeta_0} - 1} = \frac{D}{2}\sqrt{\frac{1}{n^2} - 1} = \frac{D}{2}\frac{1}{\sqrt{M^2 - 1}} \tag{2.30}$$

Besides the main ionospheric characteristics f_oF_2 and $M(3000)F_2$ referred to as *ionosonde parameters* in the following, ionograms provide a series of predefined numbers thanks to a scaling procedure. Much more complex than the scheme previously illustrated, they exhibit features bounded by characteristic virtual heights or frequencies corresponding to basic measurements. Originally collected manually, these measurements are now more and more derived by autoscaling programs. However their reliability is still usefully checked by visual inspection as their manually scaled and autoscaled values possibly differ significantly (Bidaine, 2008; Bidaine & Warnant, 2010). These measurements serve various applications. In particular, a subset of them correspond to NeQuick core parameters, including f_oF_2 and $M(3000)F_2$, which drive the electron density profile formulation (Section 2.1.3). Considering their major importance, f_oF_2 and $M(3000)F_2$ measurements from worldwide ionosondes have been synthesised in the sixties in the shape of monthly median maps. In turn these maps also referred to as ITU-R coefficients were used to build models such as NeQuick or the International Reference Ionosphere (IRI).

To address the research questions, manually scaled ionosonde data were employed for different purposes. They were collected directly from ionosonde operators, e.g. for Dourbes data, or from the World Data Center (WDC) for Solar-Terrestrial Physics at Chilton, UK (`http://www.ukssdc.ac.uk/wdcc1/data_menu.html`). On the one hand (Section 2.3.3), they were used to drive NeQuick (Bidaine & Warnant, 2010, 2011). On the other hand, they were compared to the model results to investigate NeQuick representation of the F_2 peak parameters or the electron density profile (Bidaine et al., 2012). In particular, the measured electron density profile available up to the F_2 peak was integrated to provide a reference bottomside TEC value (Bidaine & Warnant, 2010). This value allows to distinguish the bottomside and topside contributions to the TEC and their corresponding mismodelling. Indeed it yields a value associated to the topside when subtracted from the vertical TEC obtained from GPS.

[16] h_mF_2 and $M(3000)F_2$ actually relate through a more complex formula taking into account the Earth curvature and the lower layers crossed before reflection.

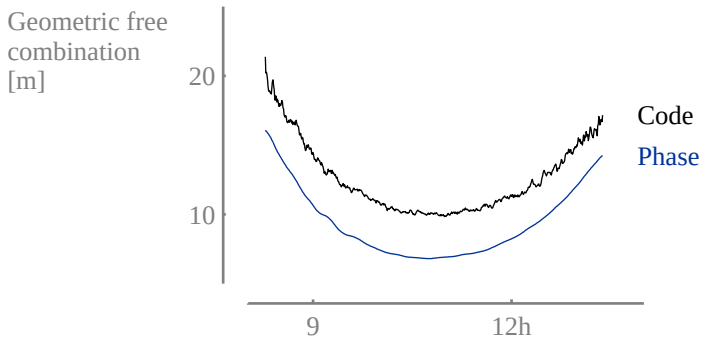

Figure 2.20: Code (rough curve) and phase (smooth curve) geometric free (GF) combinations. The phase GF combination is more precise (less noisy) but less accurate (due to the associated combination of ambiguities) than the corresponding code combination. It is illustrated for GPS satellite PRN 17, at Brussels on March 21^{st}, 2002.

2.3.2 GPS TEC

If the ionosphere basically induces undesirable effects on satellite positioning, the GPS also takes advantage of these effects to provide ionosphere measurements. These measurements primarily consist in sTEC values underlying the ionospheric delay (Eq. 2.10). This delay is involved in the code pseudorange P (Eq. 2.31) as well as in the phase pseudorange Φ_k expressed in meters (Eq. 2.32). This pseudorange ensues from the measurement of the beat phase between the carrier k ($k = 1, 2$; frequencies $f_1 = 1575.42\ MHz$ and $f_2 = 1227.6\ MHz$ for GPS) tracked by receiver p from satellite i and a replica generated by the receiver. It is prefered to derive ionosphere data as it is less noisy than code measurements. Similarly to the code pseudorange, it involves terms[17] depending on the signal frequency (the ionospheric delay I_k, the multipath effect $M_{k,\varphi}$, the receiver and satellite hardware delays p_k^i and $p_{p,k}$, the measurement noise $\varepsilon_{k,\varphi}$) or not (the geometric distance D, the satellite and receiver clock errors $\Delta t^i(t_e)$ and $\Delta t_p(t)$, the tropospheric delay T). However it comprises the so-called integer ambiguity N_k, an unknown number of wavelengths λ_k related to the (unknown) satellite-to-receiver distance at signal acquisition. This number remains constant as long as the corresponding carrier is continuously tracked.

$$P_k = D + c\left(\Delta t^i(t_e) - \Delta t_p(t)\right) + T + I_k + M_{k,g} - g_k^i + g_{p,k} + \varepsilon_{k,g} \tag{2.31}$$

$$\begin{aligned}\Phi_k = D + c\left(\Delta t^i(t_e) - \Delta t_p(t)\right) + T \\ +\lambda_k N_k - I_k + M_{k,\varphi} - p_k^i + p_{p,k} + \varepsilon_{k,\varphi}\end{aligned} \tag{2.32}$$

GPS TEC proceeds from *dual-frequency combinations*. In particular *geometric free* (GF) combinations are obtained from differences between pseudoranges measured on both carriers. Such differences eliminate frequency-independent terms. Considering the less noisy phase GF combination Φ_{GF} (Eq. 2.33, Fig. 2.20), the significant[18] remaining terms only include sTEC and a real combination N_{GF} of integer ambiguities.

$$\begin{aligned}\Phi_{GF} &= \Phi_1 - \Phi_2 \\ &\simeq -I_1 + I_2 + \lambda_1 N_1 - \lambda_2 N_2 = A\ sTEC + N_{GF}\end{aligned} \tag{2.33}$$

$$\begin{aligned}P_{GF} &= P_2 - P_1 \\ &= I_2 - I_1 + M_2 - M_1 - (g_2^i - g_1^i) + g_{p,2} - g_{p,1} + \varepsilon_2 - \varepsilon_1 \\ &= A\ sTEC + M_{GF} - g_{GF}^i + g_{p,GF} + \varepsilon_{GF}\end{aligned} \tag{2.34}$$

[17] In the following, the subscript p and superscript i are omitted in terms involving both as a single receiver and a single satellite are considered.

[18] Phase multipath, hardware delays and noise are usually neglected for dual-frequency TEC reconstruction.

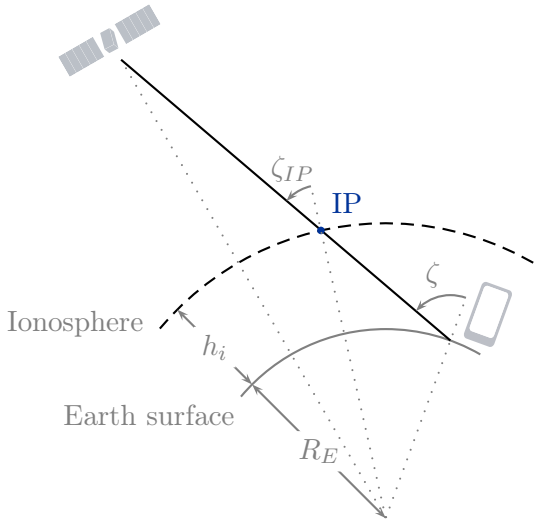

Figure 2.21: The ionospheric point (IP) and the thin shell approximation. The IP consists in the pierce point of the satellite-to-receiver path in a spherical shell representing the ionosphere. It is associated to the sTEC measurement corresponding to the path considered and depends on the ionospheric height h_i above Earth surface. It yields a satellite zenith angle ζ_{IP} computed from the surface zenith angle ζ and the Earth radius R_E.

To isolate sTEC, this combination is determined thanks to a given calibration technique. The most common technique is called *carrier-to-code levelling*: it computes N_{GF} from the difference between code and phase GF combinations (Eq. 2.35). This difference is averaged on a period of continuous tracking i.e. characterised by a single ambiguity. Therefore it is usually considered free of multipath and noise, both assumed zero-mean on the averaging period. On the contrary, it remains affected by code hardware biases, referred to as satellite and receiver *Differential Code Biases* (DCB) and assumed constant.

$$\begin{aligned} \langle \Phi_{GF} - P_{GF} \rangle &\simeq N_{GF} + g^i_{GF} - g_{p,GF} \\ \Rightarrow \tilde{\Phi}_{GF} = \Phi_{GF} - \langle \Phi_{GF} - P_{GF} \rangle &= A\ sTEC - g^i_{GF} + g_{p,GF} \end{aligned} \tag{2.35}$$

$$A = 40.3 \left(\frac{1}{f_2^2} - \frac{1}{f_1^2} \right) \simeq 0.105\ m\ TECu^{-1} \tag{2.36}$$

$$*_{GF} = *_2 - *_1 \text{ apart from } N_{GF} = \lambda_1 N_1 - \lambda_2 N_2 \tag{2.37}$$

Geometric-free combinations measured at one station constitute an adequate data set to compute sTEC above that station. In particular, the phase GF combination calibrated through carrier-to-code levelling directly provides sTEC thanks to a proper DCB estimation. This estimation results for example from the processing of a long time series of the code GF combination (Warnant, 1996; Warnant & Pottiaux, 2000): one combined satellite and receiver DCB $g_{p,GF} - g^i_{GF}$ – assumed constant in time – equals the average on a long period of the difference between P_{GF} and a polynomial sTEC approximation in latitude and local time. This estimation operationally tricky is not easily generalised to a large number of stations or to different regions in the world. It constitutes the main driver of TEC accuracy which amounts to $2-3 TECu$.

GPS sTEC is commonly converted to equivalent vTEC using a dedicated *mapping function*. The most widely used mapping function is defined in the framework of the thin-shell approximation. This approximation assimilates the ionosphere at a spherical layer of infinitesimal thickness at height h_i. This layer is pierced by the satellite line-of-sight at the *ionospheric point*[19] (IP; Fig. 2.21). This point is characterised by the satellite zenith angle ζ_{IP} the cosine of which yields the mapping function subsequently calculated from the zenith angle ζ of the satellite seen from the receiver and the Earth radius R_E (Eq. 2.38). Hence one IP is associated to one sTEC value, one equivalent vTEC and one mapping function for a given station.

$$vTEC = \cos \zeta_{IP}\ sTEC = \sqrt{1 - \left(\frac{R_E \sin \zeta}{R_E + h_i} \right)^2}\ sTEC \tag{2.38}$$

[19]This short naming is prefered to the complete designation "ionospheric pierce point" found in many references as the present thesis employs no other definition of ionospheric points.

Geometric-free combinations measured at several stations allow to build vTEC maps. In particular, *Global Ionospheric Maps* (GIM) are produced by the International GNSS Service (IGS) (Dow et al., 2009) since 1998 (Hernández-Pajares et al., 2009). Nowadays they are computed by four Ionosphere Associate Analysis Centers (IAAC) leading to corresponding GIM types: the Center for Orbit Determination in Europe (CODE), the European Space Agency (ESA), the Jet Propulsion Laboratroy (JPL) and the Universitat Politècnica de Catalunya (UPC). They are also merged in a fifth combined product denoted IGS. Most of them proceed from the resolution of a system of equations corresponding to carrier-to-code levelled observations $\tilde{\Phi}_{GF}$ obtained from a large number of worldwide distributed stations (Orus, 2005). Instead of sTEC unknowns, these equations involve the associated mapping functions based on a 450-km thin-shell height and a vTEC approximation (characteristic of the GIM type) depending on many parameters. These parameters constitute the unknowns together with the satellite and receiver DCB.

Coming back to single-station sTEC computation, GIM enable another technique to calibrate the phase GF combination without DCB estimation. Considering a satellite-receiver pair and a continuous tracking period, this calibration technique derives the related ambiguity from the average difference between the phase GF combination and synthetic sTEC values (Orus et al., 2007b). Each of these values is converted from the GIM vTEC at the corresponding IP by means of the mapping function. Hence this technique is not directly affected by DCB errors, code multipath or noise but depends on the average GIM sTEC accuracy on a continuous tracking period. Compared to the previous technique based on carrier-to-code levelling, it provides spatially consistent sTEC data more easily for large numbers of stations throughout the world. However these data are larger by several $TECu$ on average (Bidaine & Warnant, 2009b; $6.8 TECu$ for UPC GIM calibration at Brussels in 2002).

Similarly to ionosonde measurements, GPS TEC data were used in the framework of this thesis both to drive NeQuick and validate its results. On the one hand, TEC data have been ingested into the model following different schemes. These schemes involved mainly sTEC calibrated at ESA by means of UPC (Bidaine & Warnant, 2011) or IGS maps (Bidaine et al., 2012) but also directly GIM (Section 4.2.2) available from IGS (`http://igscb.jpl.nasa.gov/components/prods.html`). On the other hand, NeQuick results have been compared to GPS TEC derived from UPC (Bidaine & Warnant, 2010, 2011) or IGS (Bidaine et al., 2012; Chapter 4) GIM calibration. In particular, these results have been analysed through vTEC statistics (Bidaine & Warnant, 2010, 2011) focusing first on a limited number of degrees of freedom of the model errors. These statistics were based on vTEC profiles computed from high elevation sTEC (Warnant & Pottiaux, 2000): every 15 minutes, sTEC measurements associated to IP not further than $200 km$ from the station were selected, converted to vertical and averaged into a vTEC reference value.

2.3.3 NeQuick uses

Taking into account the characteristics of the above-described data, several operation modes of the NeQuick model have been adopted to address the research questions. They were built for three versions of the model: NeQuick 1 and 2 (Section 2.2.1) as well as NeQuick G (Section 2.2.2). They were implemented in Fortran (NeQuick 1 and 2 original language) and C (NeQuick G official version) and embedded into a dedicated Matlab tool suite for interfacing and analysis. They provided material mainly for three articles in international peer-reviewed journals summarised in next chapter.

The first operation mode referred to as *ionosonde parameters constrain* allows to study the intrinsic formulation of NeQuick electron density profile (Section 3.1). This formulation is derived from ionosonde parameters obtained, for a standard use of the model, from the ITU-R maps (Section 2.1.3). These maps exhibit their own level of accuracy and, above all, only provide monthly median values of f_oF_2 and $M(3000)F_2$. Strictly speaking, they do not constitute an intrinsic characteristic of NeQuick and should therefore not influence the evaluation of the model ability to provide a realistic daily profile without TEC adaptation. Hence this evaluation results from the replacement of the ITU-R maps by actual ionosonde measurements of f_oF_2 and $M(3000)F_2$ (Bidaine & Warnant, 2010). It quantifies the mismodelling strictly related to the profile formulation through vTEC comparison with GPS measurements. sTEC is indeed not directly available as ionosonde data (and consecutive NeQuick profiles integrated into vTEC) are only obtained at vertical.

The following operation modes enable the investigation of TEC adaptation, especially in the framework of the Galileo algorithm (Section 3.2).

- On the one hand, GPS *sTEC data ingestion* representative for the procedure followed at each GSS was applied (Section 2.1.3). Given the shape of the sTEC RMS difference function to minimise (Fig. 2.9), this procedure uses an inverse parabolic interpolation without derivatives (Brent, 1973) to determine daily effective ionisation levels Az at each station. These ionisation levels provided as input to NeQuick correspond to vTEC (and sTEC) modelled values. These values account for the best TEC representation reachable with daily Az at each station. Therefore, they constitute an important point of comparison with respect to other operation modes.

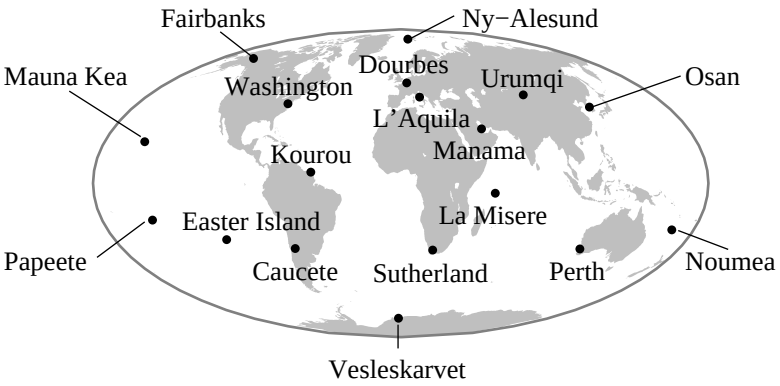

Figure 2.22: Location of the GPS stations selected to simulate the Galileo algorithm broadcast coefficients. These stations are representative for the GSS of the IOV phase.

- On the other hand, *broadcast coefficients* were simulated from the same modip interpolation performed by GCC (Bidaine & Warnant, 2011). This interpolation combined effective ionisation levels derived at 18 GPS stations representative for the GSS of the Galileo *In-Orbit Validation* (IOV) phase[20] (Fig. 2.22). Regarding simulated broadcast coefficients, these results primarily consist in vTEC (and sTEC) statistics compared to the previous operation modes.

The last operation mode integrates NeQuick in position computations characteristic of a typical mass-market single-frequency receiver (Section 3.3). Such a receiver performs *single-point single-epoch* (SPSE) *positioning*: it uses code pseudorange measurements, broadcast orbits, clocks and hardware biases as well as a simple tropospheric model. Hence SPSE positioning was operated thanks to the gLAB software tool suite (Hernandez-Pajares et al., 2010). This suite developped in C (and available from `http://www.gage.es/gLAB`) was modified to include ionospheric corrections based on the NeQuick model (Bidaine et al., 2012). It was run with GPS observations measured on the first carrier frequency (L_1) and broadcast ephemerides, both obtained from the IGS in the shape of RINEX files (`http://igscb.jpl.nasa.gov/components/data.html`). It provided positioning errors for permanent stations the position of which is known at sub-centimetre level. Applying various ionospheric corrections, these errors were analysed to quantify the accuracy improvement with respect to an uncorrected case.

2.3.4 Publications and communications

Besides the three main peer-reviewed articles constituting the core of this thesis, the research presently reported lead to a number of publications available from ORBi (ULg on-line repository).

Bidaine, B., Prieto-Cerdeira, R., & Orus, R. (2006). NeQuick: In-Depth Analysis and New Developments. In *Proceedings of the 3rd ESA Workshop on Satellite Navigation User Equipment Technologies NAVITEC 2006*. Available at `http://orbi.ulg.ac.be/handle/2268/1556`.

Bidaine, B., & Warnant, R. (2007a). Assessment of the NeQuick Model at Mid-latitudes using GPS TEC and Ionosonde Data. In *IRI/COST 296 WORKSHOP*, Prague (Czech Republic), July 10th to 14th, 2007. Oral communication. Available at `http://orbi.ulg.ac.be/handle/2268/1562`.

[20] This phase was initiated on October 21st, 2011 with the launch of the two first Galileo operational satellites. It will count four satellites and 18 GSS. It will offer first experimental data to compare with this thesis results.

Bidaine, B., & Warnant, R. (2007b). Assessment of the NeQuick Model at Mid-latitudes using GPS TEC and Ionosonde Data. In *Proceedings of the First Colloquium Scientific and Fundamental Aspects of the Galileo Programme*. Available at http://orbi.ulg.ac.be/handle/2268/1561.

Bidaine, B., & Warnant, R. (2007c). Ionosphere Modelling for GALILEO Single Frequency Users. In *Seminar "Spatial Data Research in Belgium"*, Brussels (Belgium), October 17th, 2007. Poster. Available at http://orbi.ulg.ac.be/handle/2268/1563.

Bidaine, B. (2008). *Combining Ionosonde and GPS TEC Data to Assess NeQuick Formulation*. Short Term Scientific Mission report, COST Action 296. Available at http://orbi.ulg.ac.be/handle/2268/1548.

Bidaine, B., & Warnant, R. (2008a). Modelling the Ionosphere over Europe: Investigation of NeQuick Formulation. In *5th European Space Weather Week*, Brussels (Belgium), November 17th to 21st, 2008. Poster. Available at http://orbi.ulg.ac.be/handle/2268/1564.

Bidaine, B., & Warnant, R. (2008b). Modelling the Ionosphere over Europe: Investigation of NeQuick Formulation. In *5th European Space Weather Week*, Brussels (Belgium), November 17th to 21st, 2008. Oral communication. Available at http://orbi.ulg.ac.be/handle/2268/1565.

Bidaine, B., & Warnant, R. (2008c). Towards an Improved Single-Frequency Ionospheric Correction: Focus on Mid-Latitudes. In *Proceedings of the 4th ESA Workshop on Satellite Navigation User Equipment Technologies NAVITEC 2008*. Available at http://orbi.ulg.ac.be/handle/2268/1551.

Bidaine, B., & Warnant, R. (2009a). Ionosphere Modelling Based on the NeQuick Model and GNSS Data Ingestion. In *Proceedings of the Second International Colloquium - Scientific and Fundamental Aspects of the Galileo Programme*. Available at http://orbi.ulg.ac.be/handle/2268/19132.

Bidaine, B., & Warnant, R. (2009b). Measuring Total Electron Content with GNSS: Investigation of Two Different Techniques. In *Proceedings of the 11th International Conference on Ionospheric Radio Systems and Techniques (IRST 2009)*, pp. 201–206. London (UK): Institution of Engineering and Technology - IET. doi:10.1049/cp.2009.0063. ISBN 0781849191234. Available at http://orbi.ulg.ac.be/handle/2268/1553.

Warnant, R., Foelsche, U., Aquino, M., Bidaine, B., Gherm, V., Hoque, M. M., Kutiev, I., Lejeune, S., Luntama, J. P., Spits, J., Strangeways, H. J., Wautelet, G., Zernov, N., & Jakowski, N. (2009). Mitigation of ionospheric effects on GNSS. *Annals of Geophysics*, 52 (3-4), 373–390. Available at http://orbi.ulg.ac.be/handle/2268/1924.

Bidaine, B. (2009). Modélisation de l'ionosphère pour les utilisateurs Galileo simple fréquence. In *Journées de Géomatique Liège - Montpellier - Sherbrooke 2009*, Liège (Belgium), May 11th to 13th, 2009. Oral communication. Available at http://orbi.ulg.ac.be/handle/2268/12637.

Bidaine, B., & Warnant, R. (2010). Assessment of the NeQuick model at mid-latitudes using GNSS TEC and ionosonde data. *Advances in Space Research*, 45 (9), 1122–1128. doi:10.1016/j.asr.2009.10.010. Available at http://orbi.ulg.ac.be/handle/2268/26082.

Haralambous, H., & Bidaine, B. (2010). Comparison of GPS-derived vTEC over Cyprus with NeQuick Model. In P. Doherty, M. Hernández-Pajares, J.-M. Juan, J. Sanz, & A. Aragon-Angel (Eds.), *Proceedings of the International Beacon Satellite Symposium 2010 (BSS 2010)*. Barcelona (Spain): CIMNE. Available at http://orbi.ulg.ac.be/handle/2268/22225.

Bidaine, B., Nava, B., Stankov, S., & Warnant, R. (2010). M-Ingestion: Simultaneous Ingestion of Ionosonde and GNSS Data into the NeQuick Model. In P. Doherty, M. Hernández-Pajares, J.-M. Juan, J. Sanz, & A. Aragon-Angel (Eds.), *Proceedings of the International Beacon Satellite Symposium 2010 (BSS 2010)*. Barcelona (Spain): CIMNE. Available at http://orbi.ulg.ac.be/handle/2268/40738.

Bidaine, B. (2010). Modélisation de l'ionosphère pour les utilisateurs Galileo simple fréquence. In *1ère Journée des Doctorants du Centre de Géosciences*, Liège (Belgium), January 21st, 2010. Oral communication. Available at http://orbi.ulg.ac.be/handle/2268/32000.

Bidaine, B., & Warnant, R. (2011a). Galileo Single Frequency Ionospheric Correction: Performances in Terms of Position. In *Proceedings of the 13th International Ionospheric Effects Symposium IES2011*. Available at http://orbi.ulg.ac.be/handle/2268/88442.

Bidaine, B., & Warnant, R. (2011b). Ionosphere modelling for Galileo single frequency users: illustration of the combination of the NeQuick model and GNSS data ingestion. *Advances in Space Research*, 47 (2), 312–322. doi:10.1016/j.asr.2010.09.001. Available at http://orbi.ulg.ac.be/handle/2268/72765.

Bidaine, B., Lonchay, M., & Warnant, R. (2012). Galileo Single Frequency Ionospheric Correction: Performances in Terms of Position. *GPS Solutions*, published online. doi:10.1007/s10291-012-0261-0. Available at http://orbi.ulg.ac.be/handle/2268/117284.

Performances

The Galileo correction performances experienced by a single frequency user will depend on how the ingestion and positioning operations will transpose the intrinsic mismodelling of the NeQuick model into final coordinates. In particular, NeQuick topside simplification considered as the counterpart for the model computational efficiency (Section 2.2.1) should be compensated for by sTEC data ingestion. However, as the ionospheric delays affecting pseudo-ranges combine destructively during the computation of horizontal positions (Section 2.2.3), sTEC data ingestion might yield residual errors impacting positioning more than expected from TEC statistics.

The characterisation of the Galileo correction performances distinguishes the influence of successive NeQuick operation modes in comparable situations. To this extent, it first relies on *yearly error statistics* considering trends more than specific cases. Before Galileo deployment, these statistics were built from GPS measurements prefiguring Galileo data. They were collected at locations presenting *co-located ionosonde and GPS receiver* to enable NeQuick first operation mode (ionosonde parameters constrain; Section 2.3.3). They cover a *high solar activity* period (2002) to capture larger ionospheric effects and to employ more reliable data.

This chapter summarises the achievements of this thesis previously published in three main peer-reviewed articles (Appendices A to C). Not unlike the research questions (Section 2.2), it addresses *NeQuick* intrinsic representation of the ionosphere, the impact of *TEC adaptation* (for Galileo in particular) and the correction level provided in terms of *positioning*.

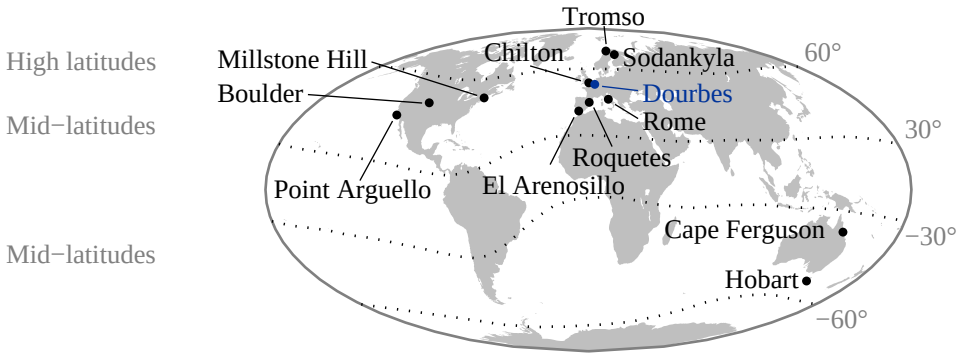

Figure 3.1: Location of the first set of GPS stations selected as test sites. These stations belong to mid/high latitudes. They are further characterised in Tab. B.1.

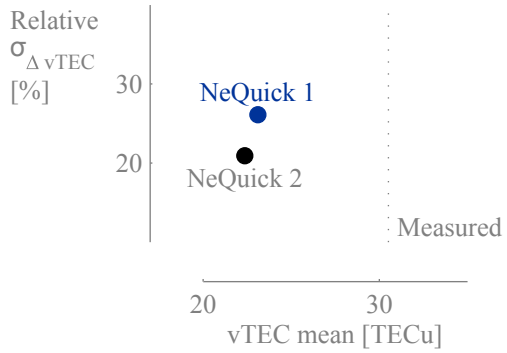

Figure 3.2: Yearly vTEC performances of the NeQuick model operated with ionosonde parameters constrain in 2002. The mean modelled vTEC underestimates the mean measured value by about $8TECu$. The standard deviation of differences with measurements $\sigma_{\Delta vTEC}$ reaches between 20 and 27% of the mean measured vTEC depending on the model version.

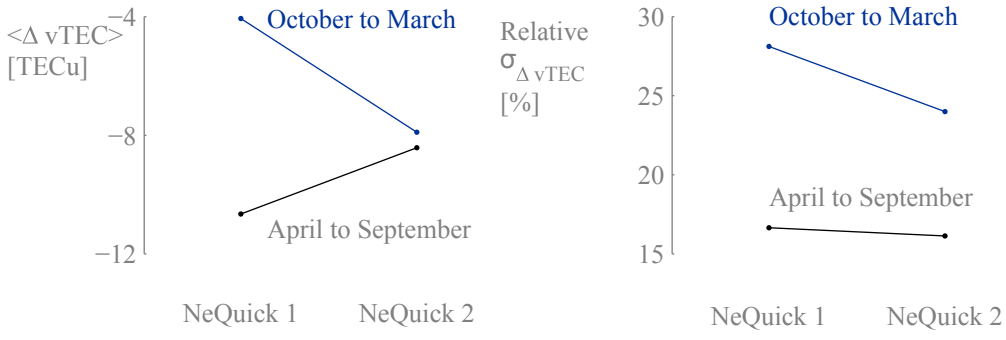

Figure 3.3: Evolution of half-yearly vTEC performances between NeQuick versions operated with ionosonde parameters constrain. The mean difference with measurements $\langle \Delta vTEC \rangle$ becomes more homogeneous throughout the year with NeQuick 2. With NeQuick 2, the standard deviation $\sigma_{\Delta vTEC}$ decreases more in the period from October to March than in the other one.

3.1 NeQuick model

The characterisation of NeQuick intrinsic performances through ionosonde parameters constrain has been undertaken at various *mid- and high-latitude stations* (Fig. 3.1). These stations were selected according to the collaborative research context of this thesis: Dourbes (Bidaine & Warnant, 2007) was followed by two other European stations (Bidaine & Warnant, 2008a) and 9 additional locations (Bidaine & Warnant, 2009a) for which manually scaled ionosonde data are available for 2002 from the COST database at Chilton WDC. These ionosonde data were used to constrain NeQuick and compute vTEC values at the twelve selected stations in 2002 every 15 minutes. These modelled values were compared to reference vTEC obtained from GPS phase measurements calibrated by means of UPC GIM.

NeQuick 1 exhibits a vTEC underestimation and a standard deviation of vTEC differences with measurements amounting both to around $7.5 TECu$ or *25%* of the mean measured vTEC (Fig. 3.2). On the one hand, the underestimation increases by 10% with NeQuick 2. However it must be interpreted with caution considering the observed differences between GPS TEC calibration techniques (Section 2.3.2). It might indeed be partly attributed to the measurements and not only to the model. On the other hand, the standard deviation decreases by 20% with *NeQuick 2* accounting for *better performances* of this latest version. Globally the best results occur in mid-latitude Europe and the worst in high-latitude Europe among the regions investigated. In addition the results improve with NeQuick 2 in all regions (Fig. B.5).

The *topside shape parameter* k largely influences NeQuick performances. Indeed NeQuick 1 performances differ significantly between the 6-month periods corresponding to each k formula (Eq. D.13) incorporated in this version of the model (Fig. 3.3). On the contrary, NeQuick 2 produces much similar statistics between both periods thanks to its new single k formula (Eq. D.32). In particular the mean difference between measured and NeQuick 1 vTEC for the period between October and March exceeds by $6.6 TECu$ its counterpart for the rest of the year. With NeQuick 2, both means tighten at $0.5 TECu$ from each other consistently with the hypothesis of a contribution from the measurements to the observed bias. The standard deviation for NeQuick 1 and the half of the year including winter months reaches nearly twice the value derived for the other half. It decreases by 15% with NeQuick 2 against 3% for the other value emphasising the larger mismodelling for October to March. This distinct, yet favourable evolution clearly appears in monthly statistics for individual stations (Fig. A.7 and B.6).

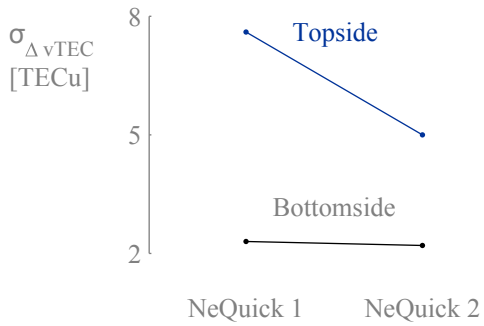

Figure 3.4: Evolution between NeQuick versions operated with ionosonde parameters constrain of the yearly standard deviation of vTEC differences dissociated between topside and bottomside. The standard deviation $\sigma_{\Delta vTEC}$ decreases more for the topside contribution than for the bottomside one.

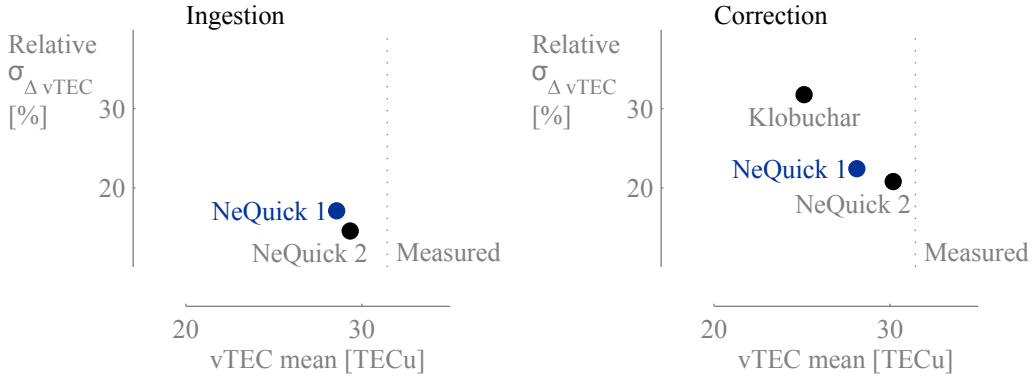

Figure 3.5: Yearly vTEC performances of the NeQuick model operated with sTEC data ingestion (left plot) and simulated or real ionospheric corrections (right plot) in 2002. The mean modelled vTEC underestimates the mean measured value by between 1 and $4TECu$ depending on NeQuick version and operation mode. The standard deviation of differences with measurements $\sigma_{\Delta vTEC}$ reaches between 14 and 23% of the mean measured vTEC with larger values for simulated ionospheric corrections.

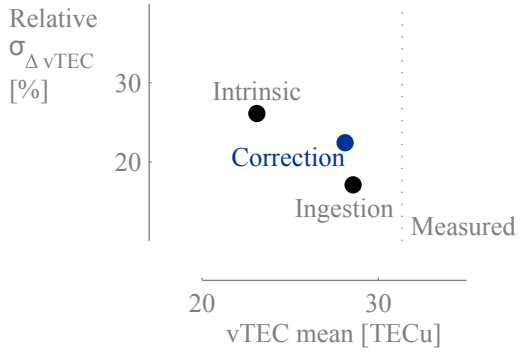

Figure 3.6: Yearly vTEC performances of NeQuick 1 compared between the first three operation modes. The mean modelled vTEC underestimates less the mean measured value with the simulated ionospheric correction, similarly to sTEC data ingestion. The standard deviation $\sigma_{\Delta vTEC}$ decreases less with the correction than with ingestion.

The topside contributes the most to the global mismodelling. It is virtually dissociated from the bottomside subtracting from GPS vTEC the integrated bottomside electron density profile measured by an ionosonde. It accounts on average for more than 75% of vTEC at Dourbes in 2002 (Fig. A.6). At the same location, it is associated to a negative mean of TEC differences between reference and NeQuick values, likewise the bottomside and the whole TEC. Considering NeQuick 1, it involves a standard deviation of $7.6 TECu$ i.e. more than 3 times larger than for the bottomside (Fig. 3.4). This standard deviation falls by a third with NeQuick 2 whereas it remains similar for the bottomside.

3.2 Ingestion and Galileo correction

For the two following operation modes, an effective ionisation level Az obtained directly or indirectly from TEC adaptation drives NeQuick solar activity input to model TEC (Section 2.3.3). Therefore modelled vTEC has first been studied to evaluate in which respect this ionisation level allows to reduce the effect of NeQuick intrinsic weaknesses described in previous section. Modelled sTEC has then been assessed to quantify the ability of the Galileo algorithm to correct the ionospheric delay.

3.2.1 vTEC

Daily sTEC data *ingestion* into NeQuick 1 yields a vTEC underestimation slightly smaller than $3 TECu$ and a standard deviation reaching about *17%* of the mean measured vTEC for the twelve selected stations in 2002 (Fig. 3.5, left plot). With NeQuick 2, both statistics decrease by 27% and 15% respectively. Among the regions investigated, mid-latitude Europe presents the best statistics and high-latitude Europe the worst. All regions show better statistics with NeQuick 2 (Fig. B.7).

NeQuick 1 fed with effective ionisation levels interpolated from simulated broadcast coefficients – consistently with the future *Galileo correction* – produces a vTEC underestimation slightly larger than $3 TECu$ and a *22%* standard deviation (Fig. 3.5, right plot). Hence it performs twice and 1.5 times better than the Klobuchar model. NeQuick 2 enables 62% and 7% reductions respectively. Finally the NeQuick models induce the same regional statements as previous operation modes whereas the Klobuchar model provides better statistics in North America than in other regions as expected from its integration in the American GNSS (Fig. B.9).

TEC adaptation partially compensates for NeQuick intrinsic mismodelling. For NeQuick 1, sTEC ingestion absorbs 61% of the underestimation obtained with the first operation mode (Fig. 3.6). It also cuts the standard deviation

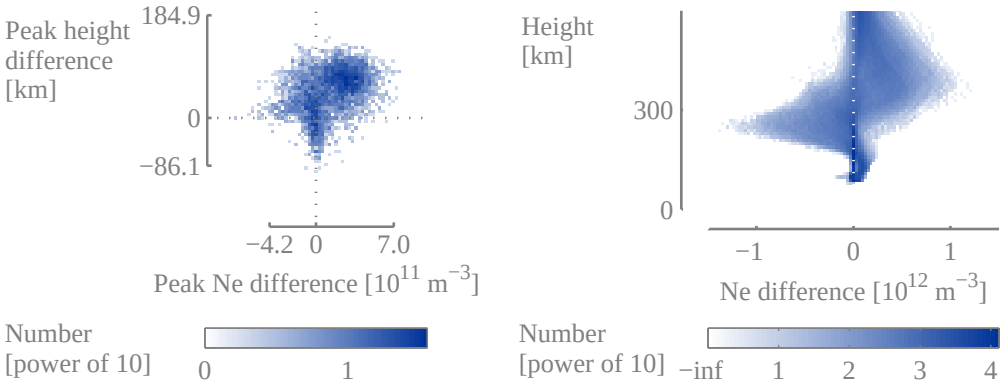

Figure 3.7: Yearly distributions of the differences of peak electron density and height (left plot) and electron density profile (right plot) between hourly manually scaled data from Dourbes digisonde and NeQuick 1 operated with sTEC data ingestion. sTEC data ingestion generally occasions an uplifted over-ionized peak of the electron density profile (left plot). This profile is consequently stretched with underestimated electron densities at fixed lower heights and overestimated concentrations at larger altitudes (right plot). The limited portion of the topside actually not probed but modeled by the digisonde is only shown for illustration.

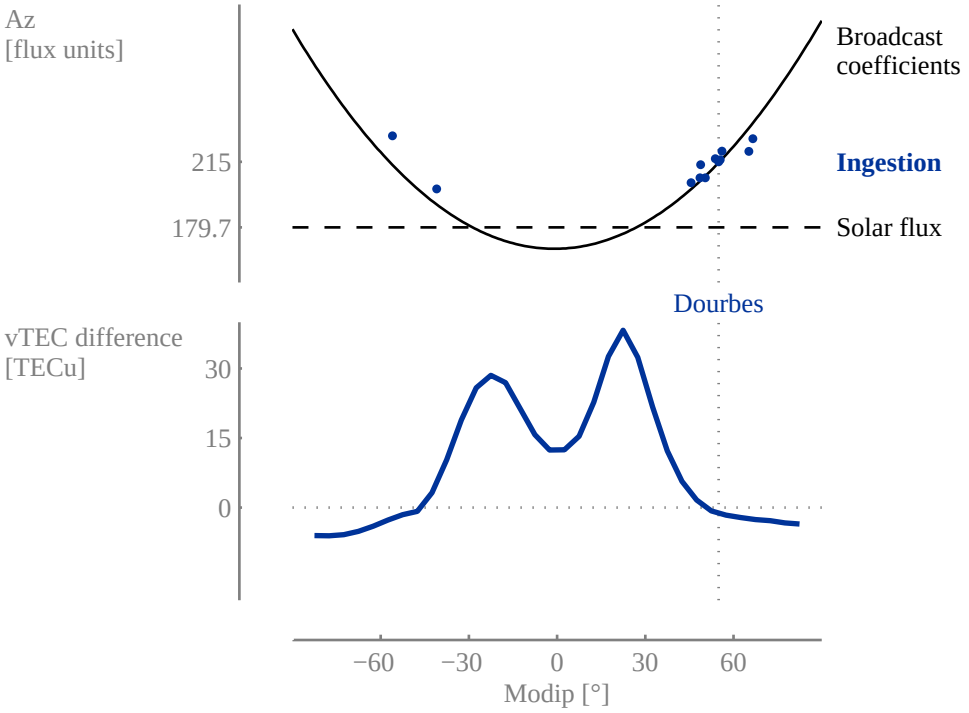

Figure 3.8: Modip dependence of the yearly mean of various ionisation levels (top plot) and the yearly mean vTEC difference between UPC GIM and NeQuick 1 driven by Dourbes Az (bottom plot). The effective ionisation levels at test stations (dots) as well as the Az interpolated from simulated broadcast coefficients (continuous line) decrease with the absolute value of modip. On the contrary, Dourbes Az induces overestimated vTEC differences (weighted means for 5° modip bins from maps of vTEC differences) towards the equator (thick line).

by one third. However this standard deviation raises again when using simulated broadcast coefficients. These coefficients are interpolated from effective ionisation levels of the previous day. Consequently they induce an additional mismodelling due more to the *day-to-day variability* of TEC than to the interpolation. These observations remain valid for NeQuick 2 (Fig. B.11).

TEC adaptation provokes a *distortion of the electron density profile* corresponding to a bottomside-topside balance. To absorb the TEC underestimation observed at the selected stations in 2002, sTEC ingestion renders Az values much larger than solar activity proxies such as the solar flux (Fig. 3.8, top plot). These values are mainly employed to interpolate the ITU-R coefficients to the given solar activity level and compute the ionosonde parameters f_oF_2 and $M3000(F_2)$ (Section 2.3.1). In turn these parameters swell the electron density N_{max}^{F2} and height h_{max}^{F2} of the F_2-layer peak (Fig. 3.7, left plot). This uplifted over-ionised peak subsequently stretches the electron density profile in electron density and height. Obtained from sTEC ingestion at Dourbes and compared to Dourbes digisonde measurements, this profile adopts first too weak then too strong electron densities for increasing fixed heights (Fig. 3.7, right plot). Applying the same TEC dissociation as in previous section, this stretched profile results in contributions to TEC respectively overestimated for the bottomside and remaining underestimated for the topside. Hence the topside underestimation stated for ionosonde parameters constrain is somehow partially compensated for by a bottomside inflation.

TEC adaptation is conditioned by a TEC *sensitivity to Az varying with modip*. The smaller the absolute value of modip, the smaller the Az needed to fit the measured sTEC in the RMS sense in the framework of ingestion (Fig. 3.8, top plot). Therefore the effective ionisation levels derived at the selected stations in 2002 are well approximated on average by the parabolic interpolation based on the simulated broadcast coefficients (Section 2.1.3). For the present experiment, these ionisation levels generally exceed their equivalent obtained from broadcast coefficients. They justify vTEC mean values larger than with the simulated Galileo correction, consistently with previous observations (Fig. 3.6). Similarly the effective ionisation level computed at Dourbes induces a vTEC underestimation with respect to UPC GIM at Dourbes modip (Fig. 3.8, bottom plot). On the contrary, this Az leads to a large overestimation at smaller modip in absolute value. This overestimation supports the need for smaller ionisation levels at lower latitudes.

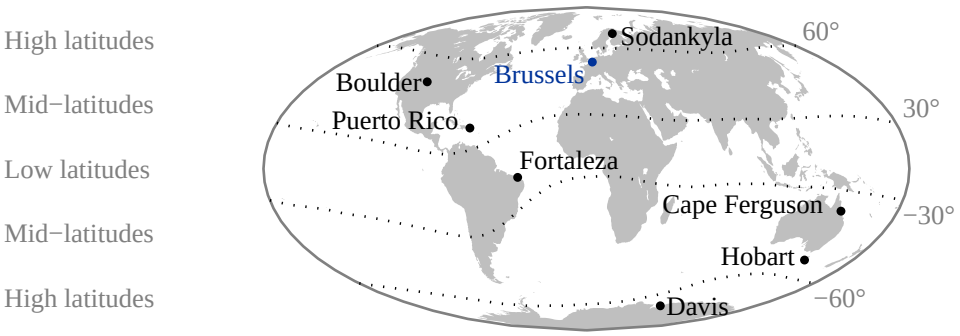

Figure 3.9: Location of the second set of GPS stations selected as test sites. These stations cover all modip bands. They are further characterised in Tab. C.1.

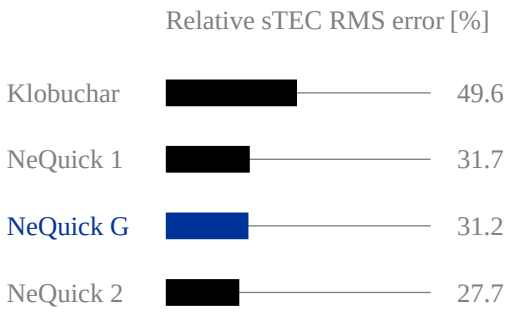

Figure 3.10: Yearly sTEC performances of the ionospheric corrections in 2002. The RMS difference between measured and NeQuick sTEC ranges between 27% and 32% of the mean measured sTEC depending on the model version.

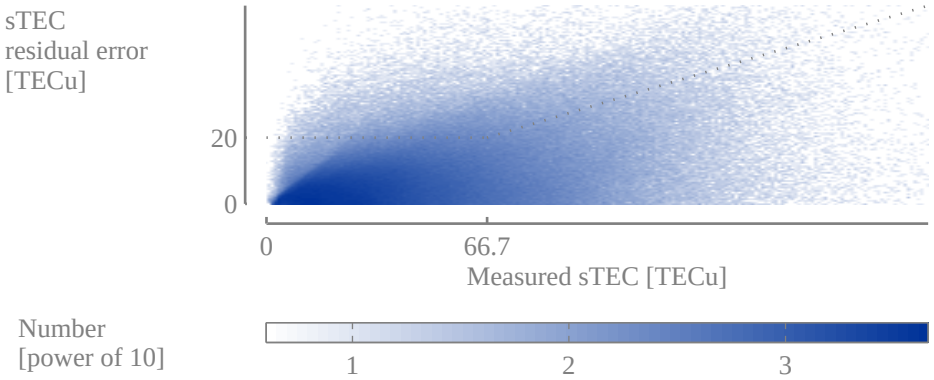

Figure 3.11: sTEC residual errors from NeQuick G compared to the Galileo algorithm specifications in 2002. 93% of the residual errors meet the specifications (below the dotted line).

3.2.2 sTEC

The sTEC analysis (as well as the rest of this thesis) employs a research framework differing in three aspects following historical choices.

- First a subset of stations was isolated in the modip bands already considered. It was completed by *additional stations* to cover all bands and better represent a global picture (Fig. 3.9).
- Second the *sTEC data* were *calibrated by means of* the *IGS* combined product instead of UPC GIM as a generalisation.
- Third the focus was attributed to the *official NeQuick version for Galileo*, referred to as NeQuick G, only available after the publication of the two first articles presented in appendix. This version uses the same topside formulation as NeQuick 1 so that previous statements related to that formulation remain conceptually valid for NeQuick G.

NeQuick G models sTEC with a *31% RMS residual error* when it is operated in combination with simulated broadcast coefficients (Fig. 3.10). This residual error relates to a 44-$TECu$ mean measured sTEC for the selected sites and year. The sTEC residual error and mean measured sTEC exceed their vTEC counterparts previously illustrated because of the sTEC directional variability (Section 2.1.2) and the modified station set. Larger TEC measurements and mismodellings are indeed expected at low elevation and low latitudes where one of the new test sites is located. The sTEC residual error is quantified by means of a RMS value for the sake of comparison with the performance indicator commonly used for the Klobuchar model. Admittedly the RMS constitutes a meaningful, single measure of model errors. It actually corresponds to the combination of the mean m and the standard deviation s (RMS $\simeq \sqrt{m^2 + s^2}$) which remain usefully considered to characterise separately the central tendency and the dispersion of mismodellings. Hence, for NeQuick G, the RMS almost equals the standard deviation as the mean error is much smaller ($-1.7TECu$ i.e. 4% of the mean measured sTEC). It increases slightly for NeQuick 1 (by 2%) and decreases by 11% for NeQuick 2. It is 1.6 times larger with the Klobuchar model and involves a much larger underestimation ($-10.8TECu$ for the mean vs. $19TECu$ for the standard deviation). It adopts the smallest values at high mid-latitudes (Brussels, Boulder and Hobart) and the largest at low latitudes (Fortaleza).

NeQuick G *complies with the Galileo algorithm specifications* for the stations and year of study. These specifications state that the residual error should be smaller than 30% of the actual sTEC or $20TECu$, whichever is larger (Section 2.2.2). In the present analysis, 93% of the residual errors meet this criterium (Fig. 3.11). This proportion is only slightly smaller for NeQuick 1 and larger for NeQuick 2 (less than 1% in both cases). By comparison with

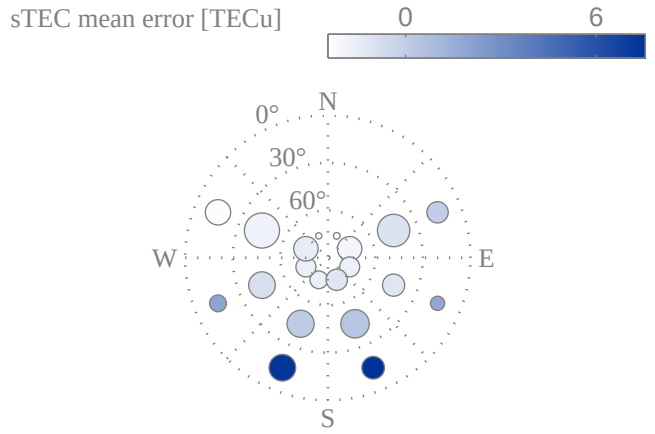

Figure 3.12: Directional dependence of the yearly mean sTEC difference between measurements and NeQuick G driven by the Az interpolated at Brussels from simulated broadcast coefficients. NeQuick G induces a sTEC mean overestimation southwards. sTEC errors correspond to mean differences with measured values for 30° elevation and 45° azimuth bins and the circle surface to the number of values in each bin.

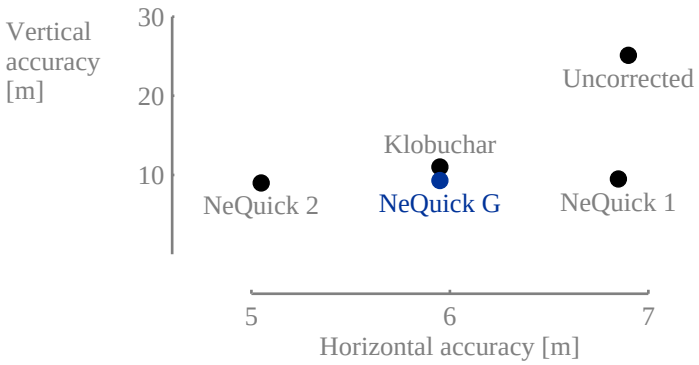

Figure 3.13: Yearly positioning performances of the ionospheric corrections in 2002. The corrections improve more the vertical accuracy – between 9 and $11m$ – than the horizontal one – between 5 and $7m$. These numbers correspond to the 95^{th} percentile of absolute horizontal and vertical positioning errors.

the other versions, the compliant data for NeQuick 2 include more large sTEC measurements (larger than $\frac{20TECu}{30\%} \simeq 66.7TECu$, associated to large residual errors) but less smaller sTEC measurements. Similarly to sTEC RMS error, the compliance level is generally larger at high mid-latitudes and smaller at low latitudes.

TEC adaptation is conditioned by the *directional dependence* of the sTEC mismodelling translating into a north-south balance. Daily sTEC ingestion results in effective ionisation levels depending on modip (Section 3.2.1). In particular, the Az computed for NeQuick G at mid-latitudes exceeds lower latitude ionisation levels. Hence this value implies a vTEC overestimation at lower latitudes (Fig. 3.8, bottom plot) but also a sTEC overestimation equartorwards from a mid-latitude station (Fig. 3.12). Consequently it corresponds to a minimum RMS difference involving a set of modelled sTEC values on average overestimated towards the equator and underestimated towards the pole. Furthermore it is even larger due to the satellite sky distribution: at a mid-latitude station, this distribution does not exhibit any satellite in a portion of the sky towards the pole, where smaller sTEC values would have been observed.

3.3 Positioning

Considering the last operation mode, NeQuick G provides *positioning accuracies amounting to* $6m$ *horizontally and* $9.3m$ *vertically* (Fig. 3.13). These accuracies correspond to the 95^{th} percentile of absolute horizontal and vertical positioning errors for the stations and period of interest. These metrics are regularly used in service specifications, e.g. 15 and $35m$ for the Galileo single frequency Open Service (Hofmann-Wellenhof et al., 2008). With a simulated ionospheric correction based on NeQuick G, the 95^{th} percentile of horizontal (resp. vertical) errors decreases by 14% (resp. 63%) with respect to the uncorrected case. By comparison, it is reduced by 1% (resp. 62%) with NeQuick 1, 27% (resp. 64%) with NeQuick 2 and 14% (resp. 56%) with the Klobuchar model. The corrections generally yield the best positioning accuracies at high mid-latitudes, the largest vertical errors at low latitudes but the largest horizontal errors at low mid-latitudes (Puerto Rico and Cape Ferguson), unlike TEC[1].

The *north error* contributes the most to the limited improvement of the horizontal accuracy supplied by the simulated Galileo ionospheric correction. In any case, this correction would never completely eliminate the reported positioning errors which are not only caused by the (residual) ionospheric delay but also by other effects considered as random (Section 2.1.1). Taken this

[1]The spatio-temporal variability of positioning performances is further discussed in Section C.2.3.

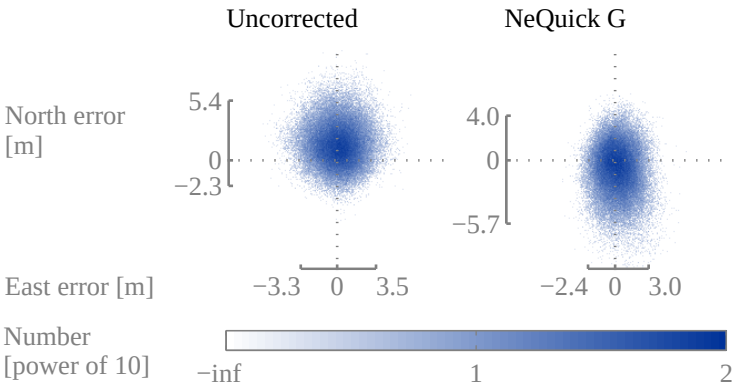

Figure 3.14: Yearly distributions of the horizontal positioning errors at Brussels, uncorrected (left plot) and corrected with NeQuick G (right plot). The distributions exhibit mean biases towards the north and south directions respectively. The axes represent 2-σ intervals around corresponding means.

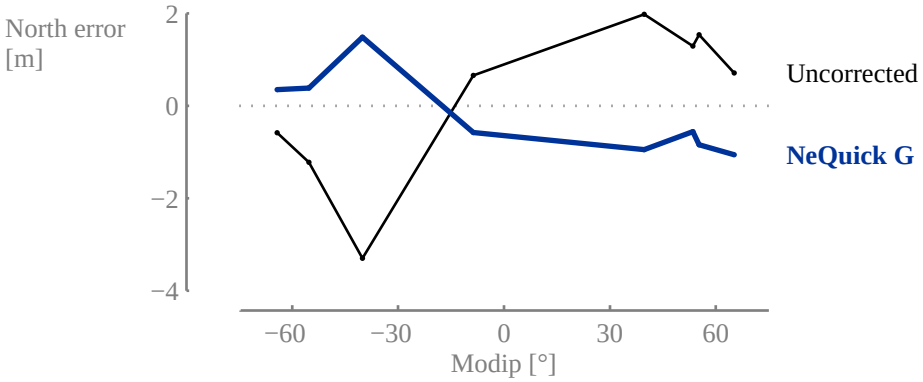

Figure 3.15: Modip dependence of the yearly mean north error obtained with and without the ionospheric correction based on NeQuick G. NeQuick G (thick line) overcorrects the north bias (continuous line) generally positive (resp. negative) in the north (resp. south) hemisphere with the exception of Fortaleza.

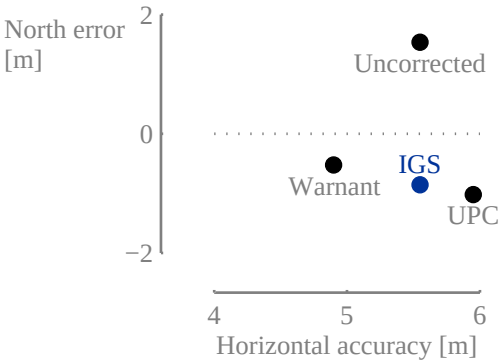

Figure 3.16: Relation between the yearly mean north error and horizontal accuracy obtained with NeQuick G at Brussels from the ingestion of different sTEC data sets. The horizontal accuracy improves and the absolute mean north error decreases when ingesting sTEC data from carrier-to-code leveling instead of GIM calibration.

observation into account, the corrections exhibit improvements of the vertical accuracy from the uncorrected case consistent with the vTEC residual errors previously depicted (Section 3.2.1). Indeed the vertical accuracy primarily depends on vTEC (Section 2.2.3). On the other hand, the horizontal accuracy is driven by TEC gradients which justifies why sTEC and positioning residual errors are not directly correlated (Fig. C.5). At mid-latitudes, these gradients induce a horizontal bias towards the poles without ionospheric correction (Fig. 3.14, left plot). Inversely the equatorwards bias obtained with the simulated Galileo correction (Fig. 3.14, right plot) suggests an overestimation of north-south TEC gradients. Together with the larger dispersion observed along the north axis than along the east one, it supports the attention dedicated to the north error in the following.

NeQuick G renders a mean north error ensuing from a *biased representation of TEC gradients*. These gradients point equatorwards except between the crests of the equatorial anomaly i.e. at low latitudes (Section 2.1.2). In the uncorrected case, they induce positive (resp. negative) north biases at northern (resp. southern) stations as well as at Fortaleza ($\mu = -8.7°$) belonging to southern low latitudes (Fig. 3.15). Moreover they reach their extrema at low mid-latitudes, not unlike the mean north error and the horizontal accuracy (Fig. C.8). On the other hand, the mean north error takes opposite signs after the introduction of the simulated ionospheric correction based on NeQuick G. Accordingly NeQuick G overestimates north-south TEC gradients consistently with the modip variability of TEC sensitivity to Az (Fig. 3.8, bottom plot) and the directional dependence of the sTEC mismodelling (Fig. 3.12). The other simulated corrections are subject to similar reasoning (Section C.3.2).

The north error and the horizontal accuracy are *sensitive to the sTEC calibration technique*. By comparison to GIM calibration, a technique such as carrier-to-code levelling possibly produces smaller sTEC on average (Section 2.3.2). In this case, it leads to smaller effective ionisation levels, a smaller profile distortion (Section 3.2.1), less stretched horizontal TEC gradients and better positioning results (Fig. 3.16). Nevertheless these results remain characterized by the influence of the mean north error on the horizontal accuracy. Hence this influence represents a major driver in the design of variants for the Galileo algorithm.

Variants

In the quest for the best real-time ionospheric effect mitigation technique for single frequency users, the Galileo correction algorithm offers building blocks for alternative procedures. Such procedures possibly designed and maintained by third parties would supply NeQuick-dedicated coefficients through other communication channels than the Galileo Signal In Space. Providing a compliant coefficient definition with Galileo navigation message, they would allow the users to benefit quasi-blindly from an ionospheric correction potentially more flexible in space and time.

The definition of variants explores three variation levels matching the constitutive steps of the Galileo algorithm (Section 2.1.3; which characteristics are recalled in brackets).

- The *model adaptation* produces a set of effective parameters. It depends on the ingested data (single-station sTEC measurements) and the optimisation criterium (RMS minimization).
- The *broadcast information synthesis* determines a number of coefficients (3) from the effective parameters (modip interpolation) with a given spatio-temporal resolution (global, daily).
- The *broadcast information processing* is performed by the receiver to retrieve effective parameters from the coefficients (receiver-modip interpolation).

This chapter first considers single-level variants to propose *answers to NeQuick G discrepancies* reported in previous chapter. Then it investigates *regional correction procedures* combining all variation levels.

4.1 Potential answers to identified discrepancies

The previous diagnosis of Galileo correction discrepancies suggests which variation level to challenge in order to cope with undesirable effects. The electron density profile distortion consecutive to sTEC data ingestion could be limited thanks to a more advanced model adaptation scheme: exploiting ionosonde measurements to define additional effective parameters yields *multiple ingestion*. Regarding ingested data characteristics, the inconsistencies between sTEC measurement techniques might be handled with a different optimisation criterium rendering *variance-driven ingestion* among others. Finally envisaging the effective ionisation level sensitivity, the excessive TEC gradients could be reduced acting on broadcast information synthesis, with an increased *ionisation level spatio-temporal resolution*, and processing, with a modified *scope* for the receiver.

4.1.1 Multiple ingestion

The multiple ingestion – or m-ingestion – concept tackles NeQuick *slab thickness* mismodelling (Buresova et al., 2009). The slab thickness equals the ratio between vTEC and the vertical profile peak electron density. As standard sTEC ingestion produces by definition an optimised TEC representation but possibly less realistic peak parameters (Section 3.2.1), the slab thickness suffers from the same collateral effects. Hence it should benefit from adapting NeQuick simultaneously to TEC and peak parameter measurements.

M-ingestion introduces three effective parameters (Bidaine et al., 2010).

- The first parameter drives the peak electron density function itself of the F_2-layer critical frequency f_oF_2 (Section 2.3.1): similarly to the standard Az, $Az_{f_oF_2}$ corresponds to the effective solar flux minimising the RMS difference between modelled and measured f_oF_2 respectively obtained from the CCIR coefficients and an ionosonde.
- The second parameter controls the peak height depending on the transmission factor $M(3000)F_2$ among others: for the sake of parallelism, $Az_{M(3000)F_2}$ optimises the RMS difference between $M(3000)F_2$ ITU-R maps and ionosonde measurements.
- The third parameter modulates NeQuick F_2 bottomside thickness: the multiplicative coefficient α proceeds from the minimisation of the RMS difference between modelled and measured sTEC, given the two other effective parameters computed beforehand.

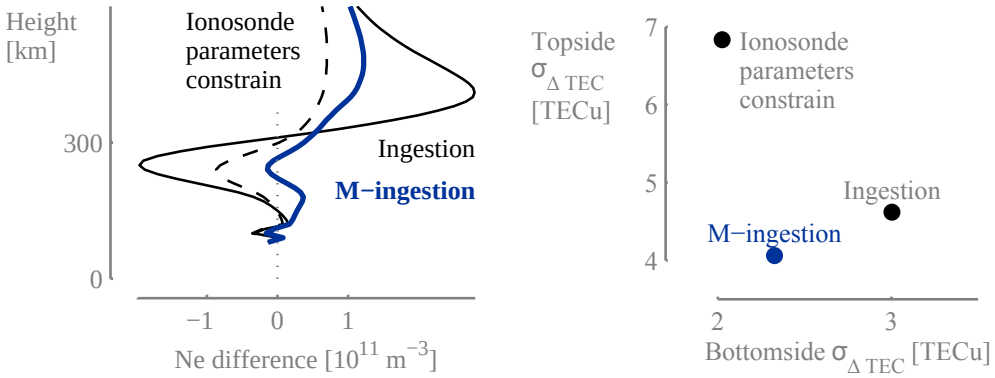

Figure 4.1: Yearly mean profile of the electron density difference between hourly manually scaled data from Dourbes digisonde in 2002 and various NeQuick operation modes including m-ingestion (left plot) and comparison between the yearly standard deviation of vTEC differences dissociated between topside and bottomside (right plot). Contrary to standard daily sTEC ingestion (continuous line), daily m-ingestion (thick line) does not stretch the vertical profile of electron density Ne (left plot) which remains similar to NeQuick intrinsic results obtained from ionosonde parameters constrain (dashed line). Hence it renders more realistic bottomside and topside TEC (right plot). The TEC statistics $\sigma_{\Delta TEC}$ consist in standard deviations of hourly differences with reference values. For the bottomside, the reference values correspond to integrated bottomside electron density profiles measured by the digisonde. For the topside, they result from the difference between GPS-derived vTEC and ionosonde-derived bottomside TEC. The reference TEC also used for (m-)ingestion is obtained from IGS GIM calibration.

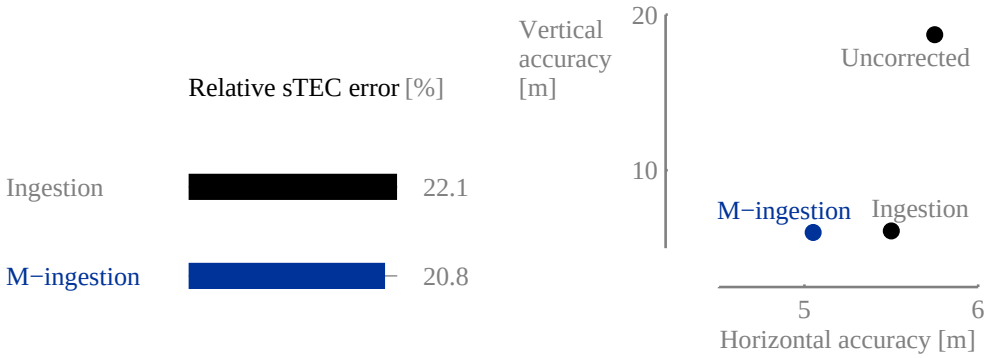

Figure 4.2: Yearly performances in terms of sTEC (left plot) and positioning (right plot) of the NeQuick model operated with m-ingestion compared to standard ingestion at Dourbes in 2002. Both the relative sTEC RMS error (left plot) and the positioning errors (right plot) decrease thanks to m-ingestion.

Daily m-ingestion curbs the electron density profile distortion observed for standard ingestion. At Dourbes in 2002, it removes the mean peak over-ionisation and depresses its uplift. Instead of the alternatively underestimated and overestimated electron densities for increasing fixed heights, it preserves on average the intrinsic shape of NeQuick profile distributing apparently the TEC mismodelling on all altitudes (Fig. 4.1, left plot). Hence the TEC mismodelling is shared differently between bottomside and topside (Fig. 4.1, right plot). On the one hand, the bottomside TEC is largely affected by standard ingestion: its differences from the integrated bottomside ionosonde profile, negative on average when constraining NeQuick with ionosonde peak parameters (Section 3.1), become positive and the standard deviation of these differences increases significantly. With m-ingestion, both the mean and standard deviation of its differences decrease. On the other hand, the topside TEC, already improved with standard ingestion, further augments on average towards the reference value thanks to m-ingestion and the associated standard deviation diminishes.

M-ingestion enhances NeQuick performances both in terms of sTEC and positioning. It gives indeed access to sTEC as it provides peak parameters necessary for electron density computation not only at vertical, an advantage by comparison to the so-called ionosonde parameters constrain technique. By the way, it yields a smaller RMS error than standard ingestion at Dourbes in 2002 (Fig. 4.2, left plot). Furthermore it can be operated to correct pseudoranges not only enabling positioning but improving its accuracy (Fig. 4.2, right plot).

4.1.2 Variance-driven ingestion

Variance-driven ingestion – or v-ingestion – formally assumes the existence of an *unknown common bias* affecting sTEC measurements. This bias plays the role of a residual receiver DCB which would have subsisted after ambiguity resolution, the fundamental difference between various sTEC calibration techniques (Section 2.3.2). It does not alter positioning as a delay common to all pseudoranges lodges itself in the synchronisation error (Mohino, 2008). However it modifies NeQuick ingestion results and potentially accounts for the variable positioning performances associated to various sTEC data types (Section 3.3): it is not simply compensated by an equal diminution of all modelled sTEC values ensuing from a smaller effective ionisation level cæteris paribus.

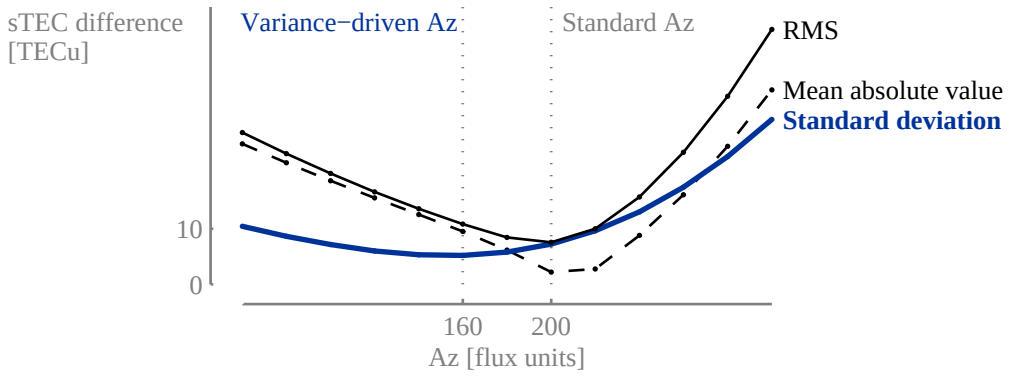

Figure 4.3: Statistics of the difference between modelled and measured sTEC in function of the daily ionisation level Az at Brussels on September 1^{st}, 2002. The effective ionisation level adopts a smaller value with v-ingestion, minimising the standard deviation of sTEC differences (thick line), than with standard ingestion, optimising the RMS (continuous line). The RMS appears clearly influenced by the mean asbolute error (dashed line). These statistics were computed for 20-unit Az steps ingesting data calibrated by IGS GIM.

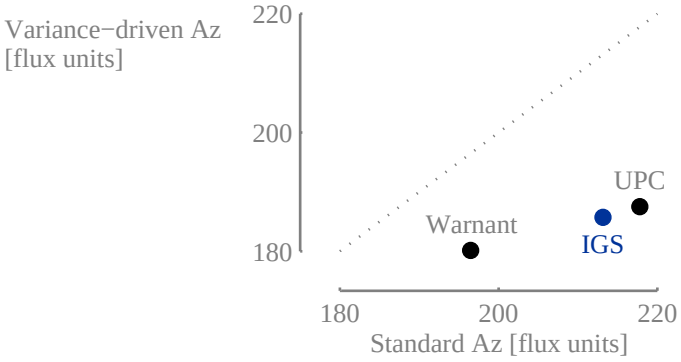

Figure 4.4: Yearly mean effective ionisation level Az obtained at Brussels from v-ingestion compared to standard ingestion using different sTEC data sets. The effective ionisation level becomes smaller with v-ingestion than with standard ingestion, especially using GIM-calibrated sTEC but also with carrier-to-code levelled data (Warnant). It falls within a narrower interval around the IGS-related reference case.

V-ingestion minimises the variance of the differences between modelled and measured sTEC instead of their RMS. It proceeds from an elementary least-squares adjustment characterised by quasi-trivial observation equations binding each couple i of modelled and measured sTEC values within a specific data set (Eq. 4.1). The solution of this adjustment consists in the ionisation level $\hat{A}z$ and bias $\hat{B}$ which minimise the sum squared residuals ν_i (Eq. 4.2): $\hat{B}$ equals the mean of the differences between modelled and measured sTEC and $\hat{A}z$ consequently optimises their variance (Eq. 4.3).

$$sTEC_{mod,i}(Az) - B = sTEC_{meas,i} + \nu_i \tag{4.1}$$

$$\begin{aligned} \left(\hat{A}z, \hat{B}\right) &= \arg\min \boldsymbol{\nu}^T \boldsymbol{\nu} \\ &= \arg\min \sum_i \left(sTEC_{mod,i}(Az) - sTEC_{meas,i} - B\right)^2 \end{aligned} \tag{4.2}$$

$$\Rightarrow \begin{cases} \hat{B} = \left\langle sTEC_{mod}(\hat{A}z) - sTEC_{meas} \right\rangle \\ \hat{A}z = \arg\min \mathrm{Var}\left(sTEC_{mod}(Az) - sTEC_{meas}\right) \end{cases} \tag{4.3}$$

Daily v-ingestion produces on average smaller effective ionisation levels than standard ingestion. In general different Az values minimise the absolute mean, the standard deviation and the RMS of sTEC errors (Fig. 4.3). As opposed to the modelled sTEC, the mean error monotonously decreases with Az. At some point, it reaches smaller values by comparison to the standard deviation and controls the RMS minimisation[1]. Hence the minimum absolute mean and RMS errors are obtained from generally larger Az values for data sets with larger mean sTEC than others. On the other hand, the minimum standard deviation, equivalent to the minimum variance driving v-ingestion, provides ionisation levels less dependent on the data set (Fig. 4.4). The yearly mean Az at Brussels in 2002 take more similar values than for standard ingestion. They are still sorted according to sTEC measurement orders of magnitude, the smallest for the data generated by using carrier-to-code levelling (Warnant & Pottiaux, 2000), the largest associated to UPC GIM calibration (Orus et al., 2007b). These effective ionisation levels occasion residual TEC underestimations – larger than for standard ingestion by definition – and standard deviations ranked likewise.

[1] As a reminder, the RMS combines the mean and the standard deviation (Section 3.2.2).

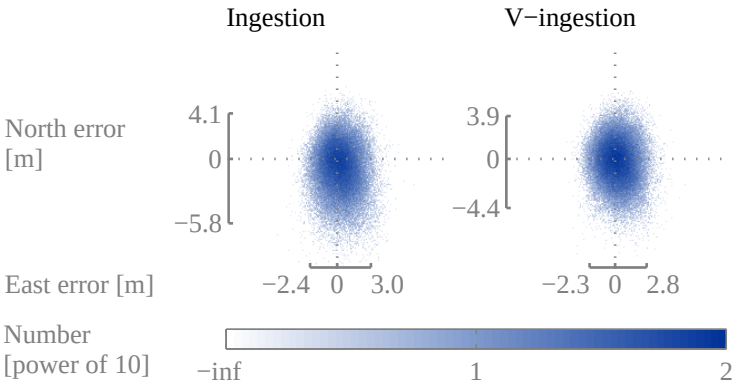

Figure 4.5: Yearly distributions of the horizontal positioning errors at Brussels, corrected with NeQuick and standard ingestion (left plot) or v-ingestion (right plot). V-ingestion of IGS-calibrated sTEC significantly reduces the south offset due to NeQuick overcorrection from standard ingestion. It also restricts the north and east 2-σ intervals depicted by the axes.

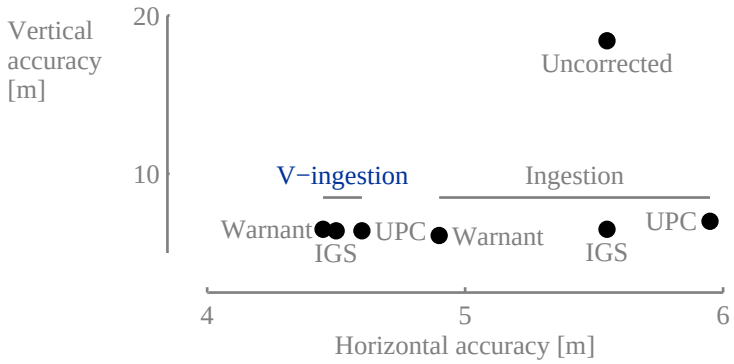

Figure 4.6: Yearly positioning performances of the NeQuick model operated with v-ingestion compared to standard ingestion at Brussels in 2002. V-ingestion yields smaller horizontal errors also more consistent among ingested data sets, not unlike the effective ionisation level Az.

The effective ionisation levels computed with v-ingestion raise the positioning accuracy when injected into NeQuick to model the ionospheric delay instead of standard ones. These Az suppress the mean sTEC overestimation southwards observed at Brussels in 2002 (Section 3.2.2) and induce a smaller south bias in the horizontal error distribution (Fig. 4.5): they apparently reduce the north-south TEC gradient mismodelling. They allow significant improvements for all TEC calibration techniques considered with respect to ingestion, ending up with more similar horizontal accuracies (Fig. 4.6). These horizontal accuracies remain mainly affected by the TEC gradient mismodelling intrinsically due to the model but presumably amplified by TEC measurements discrepancies. These discrepancies formally attributed to a residual receiver DCB are not necessarily really determined by v-ingestion (as the adjusted bias also receives the average intrinsic mismodelling). Nevertheless v-ingestion effectively mitigates excessive north-south TEC gradients.

4.1.3 Spatio-temporal effective ionisation level resolution

Intuitively, the closer the source of sTEC measurements from the location of interest and the more real-time the effective ionisation level supplied to NeQuick, the more realistic the model results. Hence these results in terms of positioning accuracy would possibly benefit from a larger spatio-temporal resolution of the broadcast information dedicated to the ionospheric correction than the global daily framework employed by the Galieo algorithm. Their sensitivity to Az variations depends on space and time and impacts the representation of TEC horizontal gradients among others (Section 3.3). They are driven by the correlation between different ionospheric scenarios: how far and how long does an ionisation level remain effective for positioning?

Daily Az *values computed from nearby measurements* instead of broadcast coefficients *do not necessarily induce more accurate horizontal positions*. Yet they could be expected to outperform other values until a given correlation distance. According to Klobuchar & Kunches (2000b), the correlation distance separates two locations at which ionospheric measurements exhibit a correlation coefficient larger than a certain threshold. It coincides to a certain percentage improvement when using at one place the measurement from the other instead of monthly average conditions. In this respect, a minimal 28% improvement ensues from correlation distances of 3000 km in longitude and 1700 km in latitude at mid-latitudes. Such distances would theoretically never be exceeded with about 100 worldwide stations providing ionospheric information in their surroundings[2]. For NeQuick, the correlation distance concept is

[2]The Earth surface ($4\pi R_E^2 \simeq 5.1\ 10^8 km^2$) approximately corresponds to 100 rectangles 3000-km long and 1700-km large ($5.1\ 10^6 km^2$).

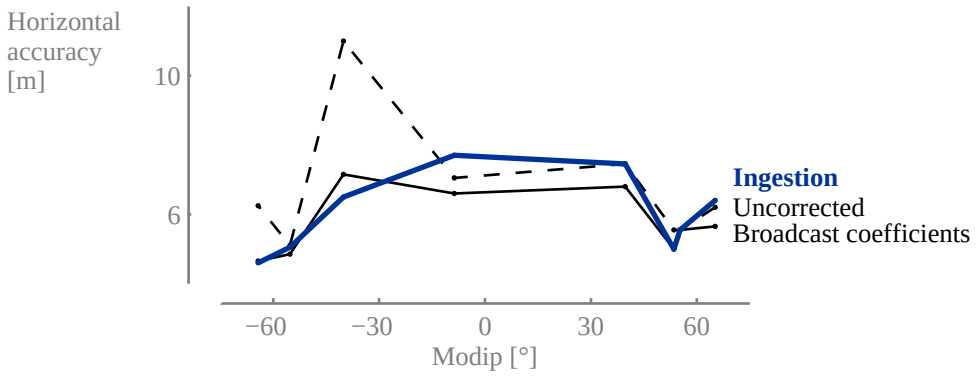

Figure 4.7: Modip dependence of the yearly horizontal performances of the NeQuick model operated with ingestion compared to broadcast coefficients. Despite their larger spatial ionosphere correlation, daily effective ionisation levels obtained from local sTEC ingestion (thick line) instead of simulated global broadcast coefficients (continuous line) do not necessarily provide a better horizontal accuracy by comparison to the uncorrected case (dashed line).

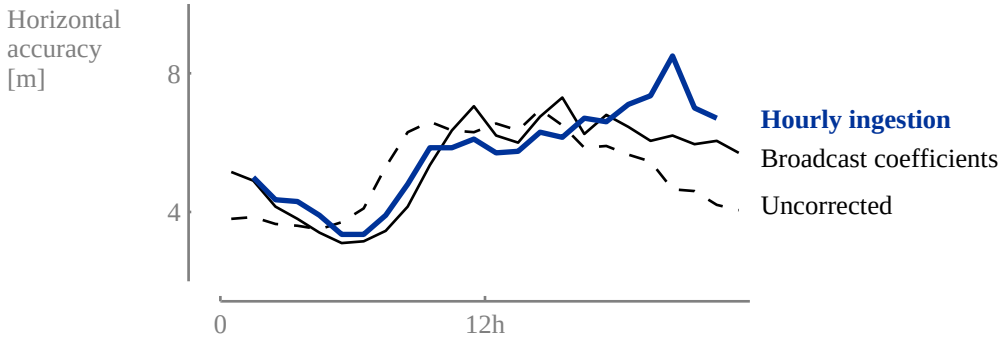

Figure 4.8: Local-time dependence of the yearly horizontal performances of the NeQuick model operated with hourly ingestion compared to broadcast coefficients at Brussels. Despite their larger temporal ionosphere correlation, hourly effective ionisation levels obtained at Brussels from local sTEC ingestion (thick line) instead of simulated global broadcast coefficients (continuous line) do not necessarily provide a better horizontal accuracy by comparison to the uncorrected case (dashed line).

usefully interpreted bearing in mind the definition of Az: an effective ionisation level should remain better than other values, in particular the monthly smoothed sunspot number suited for NeQuick monthly median original operation, within such a distance from its associated spot. Inversely it leads to the best sTEC representation at this location, in particular by comparison to the value deduced from simulated broadcast coefficients. Surprisingly it does not always imply smaller horizontal positioning errors (Fig. 4.7): in 2002, it improves the positioning accuracy at Cape Ferguson and Davis ($\mu = -40.1°$ and $-64.3°$) but even amplifies the errors for four of the remaining test sites. Indeed it enables NeQuick to better model TEC but not necessarily horizontal TEC gradients: at Fortaleza for example ($\mu = -8.7°$), the yearly mean Az is larger than the value obtained from broadcast coefficients, decreasing TEC underestimation but not TEC gradient mismodelling (Section C.4.1).

Similarly *sub-daily effective parameters*, based on more recent TEC data than the day before and more frequently updated than once a day, *do not automatically suffice to improve horizontal positioning*. Again they could be supposed to better capture the ionosphere temporal variability, at least at short term. For instance, a useful time frame for multiplicative TEC predictions based on nowcasted measurements instead of monthly median values is limited to 2 to 3 hours (Klobuchar & Kunches, 2000a). Regarding NeQuick, a shorter ingestion time frame e.g. 1 hour decrease the global sTEC RMS error but appears less reliable as the satellite sky distribution is scarcer for an hour than an entire day. Furthermore it lacks to provide a better horizontal accuracy, at least at Brussels in 2002 (Fig. 4.8): it renders excessive night-time TEC gradients in particular from a smaller Az sensitivity in that period and consecutive larger Az values.

4.1.4 Effective ionisation level scope

Given the effective ionisation level spatial sensitivity, processing broadcast information not only using the receiver modip makes sense. From the point of view of a static Galileo user, one Az value will be computed at current location and remain valid to model the ionospheric delays towards any satellite for the whole day (until the broadcast coefficients are updated). However this value is maybe not the most appropriate both for southwards and northwards incoming signals for instance. Obtained directly from sTEC ingestion, it would indeed have lead to overestimated (resp. underestimated) delays southwards (resp. northwards) and a mean north overcorrection (Section 3.2.2). Further exploiting the parabolic interpolation against modip introduced to fit ingestion results (Section 2.1.3), it could be usefully reduced (resp. raised) for southwards (resp. northwards) satellite links adapting its scope.

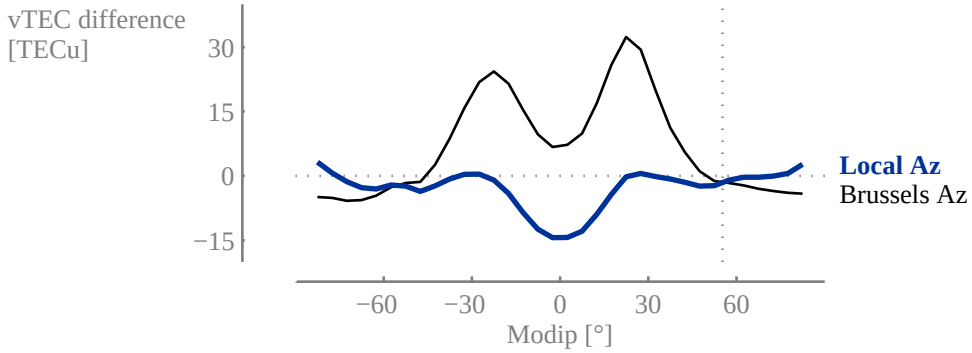

Figure 4.9: Modip dependence of the yearly mean vTEC difference between IGS GIM and NeQuick driven by the local Az compared to Brussels Az. The vTEC difference roughly equals 0 around Brussels (vertical dotted line) using the daily effective ionization level computed locally from simulated broadcast coefficients (thick line) unlike its value derived at Brussels (thin line).

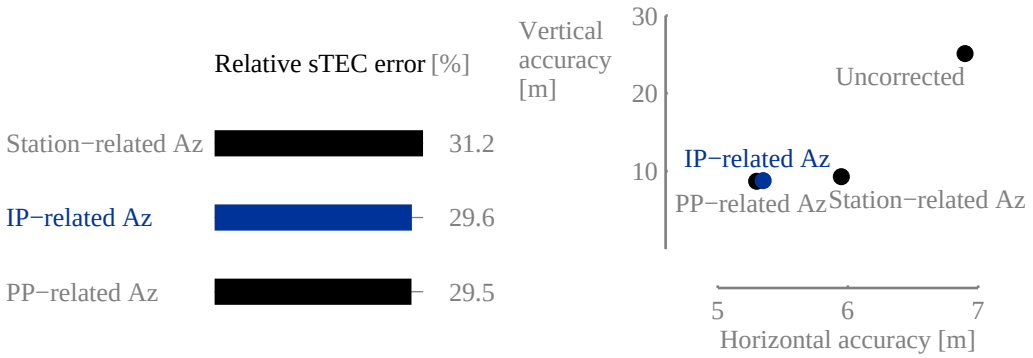

Figure 4.10: Yearly performances in terms of sTEC (left plot) and positioning (right plot) of ionospheric corrections based on the NeQuick model and various effective ionisation level scopes in 2002. The effective ionisation level related either to the ionospheric point (IP) or to the physical point (PP) improves the sTEC RMS (left plot) and positioning (right plot) performances of the Galileo correction for the selected test sites.

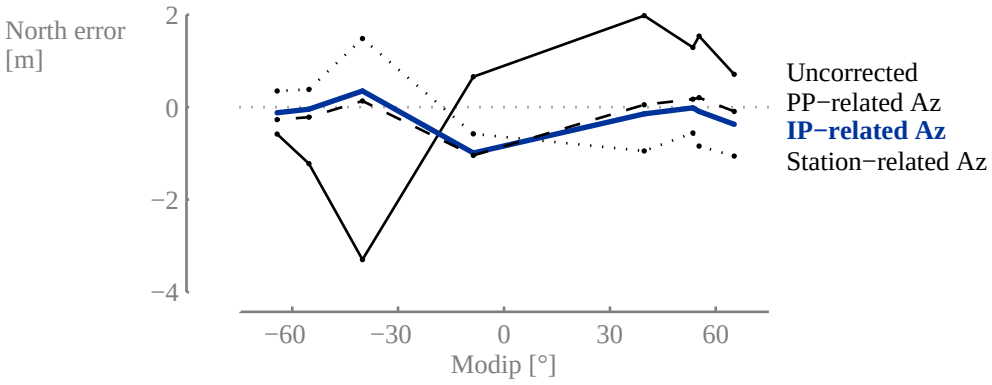

Figure 4.11: Modip dependence of the yearly mean north error obtained with ionospheric corrections based on NeQuick and various effective ionisation level scopes. The IP- (thick line) and PP-related Az (dashed line) neutralise the mean north overcorrection yielded by the station-related Az (dotted line) by comparison to the uncorrected case (continuous line) with the exception of Fortaleza ($\mu = -8.7°$).

A *local Az related to the region actually crossed by navigation signals* copes with excessive equatorwards TEC gradients. At Brussels in 2002, these mean excessive gradients ensue from the use of a single daily ionisation level calculated either from the simulated broadcast coefficients or sTEC ingestion (Fig. 4.9). Indeed ingestion balances the influence of regions of variable mismodelling probed by sTEC measurements, leaving a systematic slant depending at least on modip. This slant is materialised by a mean overestimated (resp. underestimated) vTEC equatorwards (resp. polewards). Hence it is overcome interpolating Az from the broadcast coefficients at the modip below each integration point: at smaller (resp. larger) modip in absolute value, the consecutive smaller (resp. larger) mean Az decreases (resp. increases) vTEC accordingly.

An effective ionisation level related either to the ionospheric point (IP, Section 2.3.2) or to the physical point (PP) improves the Galileo correction performances. It is respectively derived for each satellite direction[3] or separately for each integration point. For the selected test sites in 2002, it inflates the sTEC underestimation at least by 50% with respect to the standard station-related Az but erodes the standard deviation of sTEC differences between measured and modelled values by at least 5%. Consequently it induces a smaller sTEC RMS error shrinking just below 30% (Fig. 4.10, left plot) and a slightly larger compliance with the Galileo algorithm specifications reaching 94%. In terms of positioning, it enhances the horizontal accuracy by 10% and the vertical by 5%, gaining at least $0.5m$ in both cases (Fig. 4.10, right plot).

The absolute mean north error generally decreases thanks to an adaptative Az scope, partially explaining the better positioning accuracies. The mean north error takes positive (resp. negative) values without correction in the north (resp. south) hemisphere and appears overcorrected with the station-related Az (Fig. 4.11). Besides a smaller dispersion of the horizontal distributions, it fades with the IP/PP-related ionisation level. On the contrary, it enlarges at Fortaleza ($\mu = -8.7°$) which already needed special discussions about the standard Galileo correction discrepancies (Section 3.3). Indeed it proceeds from more complex gradients pointing south on average despite the southern location. Hence these north-south TEC gradients are amplified by the smaller low-latitude Az provided by local parabolic interpolation (Fig. 4.9). Apparently they would have benefited from a larger ionisation level between the crests.

Finally considering computation time, the IP-related effective ionisation level offers an efficient solution for its smaller associated number of operations and its comparable modelling performances by comparison to the PP-related Az. The PP-related Az occasions sTEC (resp. position) run times 1.5 (resp. 2.5) times larger[4] than the station- or IP-related Az i.e. about 1 (resp. 8)

[3] For the sake of consistency with GIM, the employed modip corresponds to IP belonging to a 450-km high thin shell.

[4] These values were obtained from Fortran programs and gLAB run for Brussels station

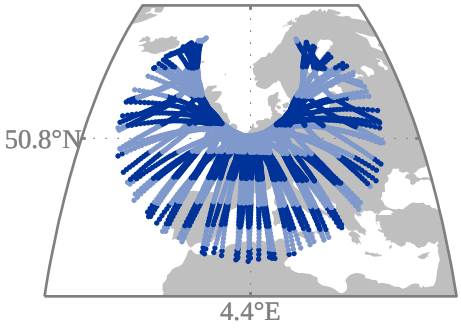

Figure 4.12: Ionospheric points used for parametrised ingestion at Brussels (50.8°N, 4.4°E) on January 1^{st}, 2002. To perform modip parametrised ingestion, the sTEC measurements are sorted according to the modip of their corresponding IP. In this example, all possible GPS satellite directions above a 5° elevation mask every 2 minutes are grouped in 2.5° bins (alternatively light and dark).

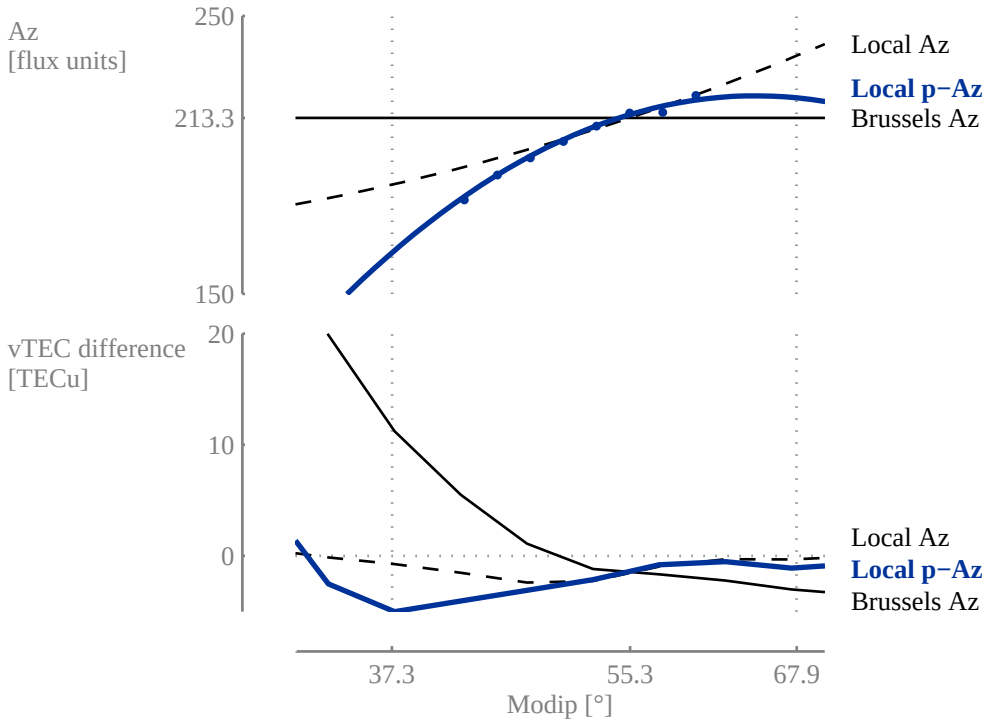

Figure 4.13: Modip dependence of the yearly mean of various ionisation levels (top plot) and the yearly mean vTEC difference between IGS GIM and NeQuick driven by local $p-Az$ compared to local and Brussels Az (bottom plot). P-ingestion (thick lines) at Brussels generates effective ionisation levels decreasing southwards on a yearly mean basis (top plot), like the local Az based on global broadcast coefficients (dashed lines). Consequently it produces a more stable yearly mean vTEC difference with IGS GIM (bottom plot) by comparison to Brussels Az (continuous lines). The vertical dotted lines enclose the IP in sight from Brussels.

$10^{-2}s$. These run times are more affected by the adaptation of internal parameters (such as the CCIR coefficients) to successive ionisation levels than by the multiplication of Az evaluations from broadcast coefficients. When performed at each integration point, these evaluations constrain several internal parameters to be updated several hundred to thousand times more often depending on the integration routine (Knezevich & Radicella, 2004).

4.2 Regional correction procedures

Following the interest of the compatibility with the global Galileo algorithm and the adaptative Az scope, regional correction procedures would advantageously provide broadcast information describing a modip-dependent effective ionisation level. Hence they would rely on model adaptation techniques producing effective parameters suited for modip interpolation. For operational purposes, they could more efficiently involve sTEC measurements in the framework of *parametrised ingestion* or GIM for *TEC map ingestion*. These two variants would also enable *extensions* potentially useful for specific situations.

4.2.1 Parametrised ingestion

Parametrised ingestion – or p-ingestion – breaks down a sTEC data set according to the value of one or several chosen parameters and computes *effective ionisation levels for predefined value ranges of these parameters*. Standard sTEC ingestion minimises NeQuick mismodelling towards a given data set. When this data set is split depending on time for example, ingestion replaces the original single ionisation level by as much Az as new subsets e.g. 24 when passing from daily to hourly ingestion: the process is parametrised with time. Remembering the systematic sTEC mismodelling previously identified, it should benefit from a modip parametrisation. Classifying sTEC measurements in bins of IP modip (Fig. 4.12), p-ingestion supplies corresponding Az values referred to as p-Az (Fig. 4.13, top plot). These p-Az are subsequently interpolated against modip[5] synthesising regional substitutes for the global broadcast coefficients.

and January 3^{rd}, 2002 on a computer equipped with a 2.00 GHz Intel Core2 Duo processor and 2 Go RAM.

[5]The results in this thesis proceed from a weigthed interpolation using the final RMS reached by the optimisation in each bin.

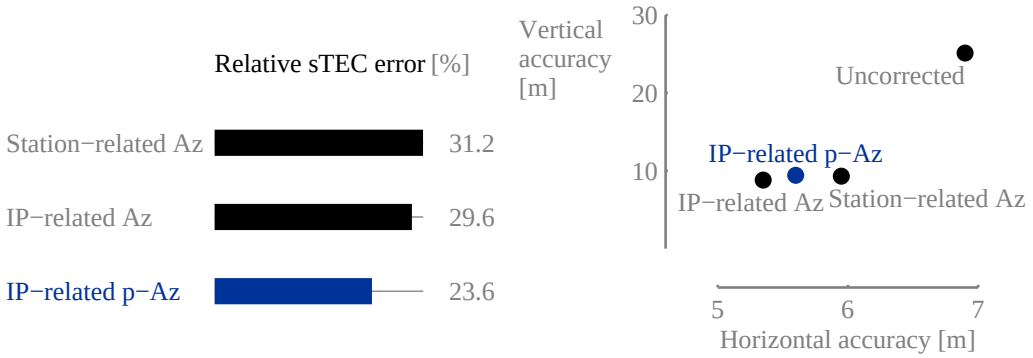

Figure 4.14: Yearly performances in terms of sTEC (left plot) and positioning (right plot) of ionospheric corrections based on the NeQuick model and p-ingestion compared to former procedures in 2002. The effective ionisation level p-Az based on information synthesised from p-ingestion and related to the IP limits better the sTEC RMS (left plot) then the positioning errors (right plot) left by the Galileo correction for the selected test sites in 2002.

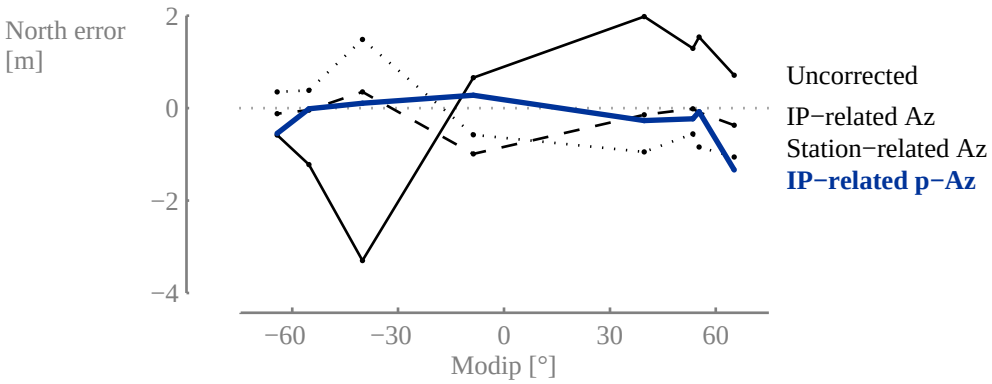

Figure 4.15: Modip dependence of the yearly mean north error obtained with ionospheric corrections based on NeQuick and p-ingestion compared to former procedures. Apart from high latitudes, the IP-related p-Az (thick line) copes better with the uncorrected yearly mean north bias (continuous line) than the station-related Az (dotted line), not unlike the IP-related Az (dashed line).

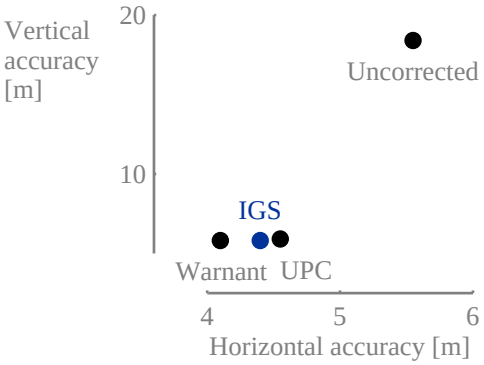

Figure 4.16: Yearly positioning performances of NeQuick operated with p-ingestion and different sTEC data sets at Brussels in 2002. P-ingestion of sTEC data calibrated following (Warnant & Pottiaux, 2000) offers the best correction.

The local p-Az calculated from a second-order modip interpolation approaches the TEC gradient modelling improvement provided by the local Az based on global broadcast coefficients. For Brussels in 2002, the yearly mean p-Az decreases southwards as expected from the sTEC mean overestimation in this direction. Becoming smaller than Brussels Az, it depresses the yearly mean vTEC difference (Fig. 4.13, bottom plot) too much however by comparison to the local Az. Following on average a concave function of modip, it remains indeed below the convex parabola corresponding to global broadcast coefficients.

Regarding sTEC and positioning, the ionisation level derived at IP from p-ingestion results drives NeQuick more effectively than the standard station-related Az. Interpolated from three coefficients representing p-Az dependence on modip, it decreases both the absolute mean and the standard deviation of sTEC differences at the selected sites in 2002: its associated RMS error amounts to 76% and 80% of those obtained with previously described station- and IP-related Az (Fig. 4.14, left plot). Hence it reinforces the Galileo specifications compliance level up to 97%. However it renders only about half of the horizontal positioning improvement reached when processing global broadcast information with an adaptative Az scope (Fig. 4.14, right plot).

The IP-related p-Az adequately handles the north overcorrection induced by the station-related Az. In 2002, it performs the best at southern mid-latitudes (Cape Ferguson and Hobart i.e. $\mu = -40.1°$ and $-55.3°$) and slightly worse at northern mid-latitudes (Brussels, Boulder and Puerto Rico i.e. $\mu = 55.3°$, $53.5°$ and $39.7°$) (Fig. 4.15). At high latitudes (Sodankyla and Davis i.e. $\mu = 65.2°$ and $-64.3°$), it seems impacted by the poorer satellite sky distribution and the less effective model adaptation to low elevation sTEC measurements. At these stations, it degrades indeed both the mean north error and the horizontal accuracy confirming the influence of the first in the second. This influence is questionable at low latitudes (Fortaleza): indeed the north bias resulting from the average mismodelling of more complex TEC gradients is smaller but does not imply a better horizontal accuracy.

Similarly to v-ingestion, p-ingestion yields more homogeneous positioning performances among various ingested sTEC data types. In particular it reduces the 95^{th} percentile of horizontal errors by 0.8 to $1.5m$ with respect to standard ingestion (Fig. 4.16). Taking the Az variability into account, its adatative Az scope compensates possible remaining common biases in sTEC measurements. It goes even further as p-ingestion of sTEC data calibrated following (Warnant et Pottiaux, 2000) offers the best correction at Brussels in 2002.

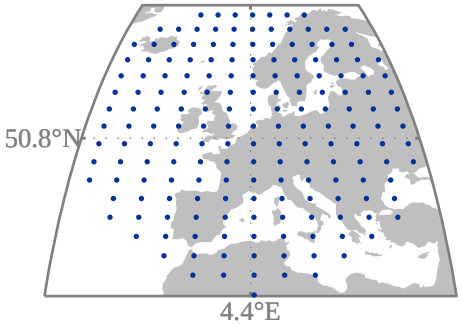

Figure 4.17: Grid points used for TEC map ingestion at Brussels (50.8°N, 4.4°E). The second proposed regional correction procedure exploits effective ionisation levels obtained from TEC map ingestion at grid points in sight of a specific location.

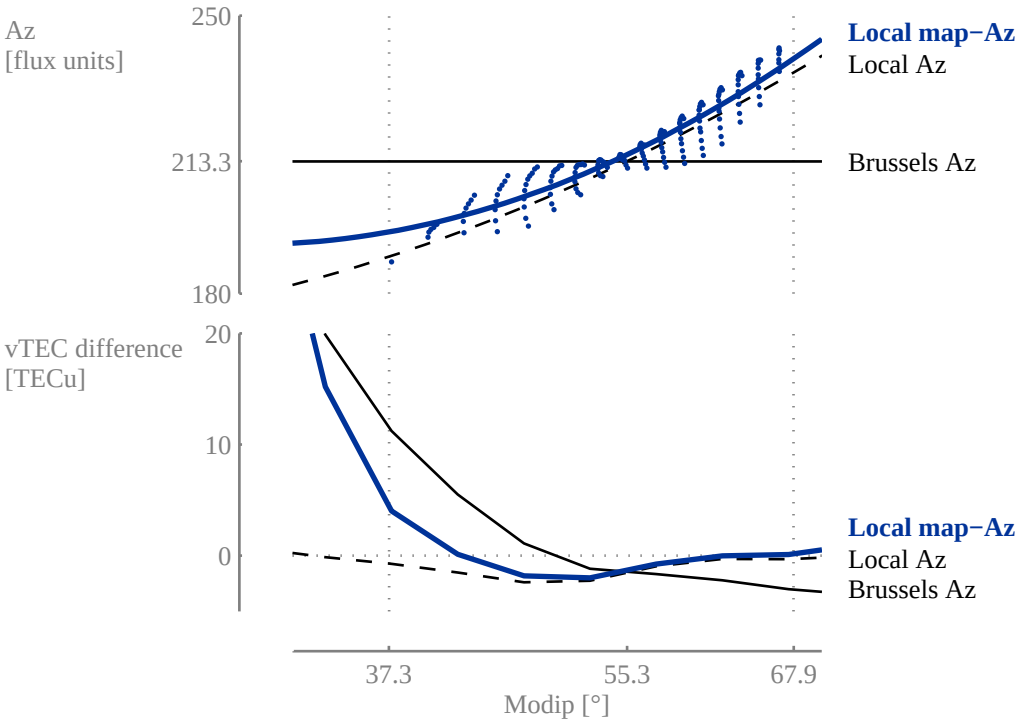

Figure 4.18: Modip dependence of the yearly mean of various ionisation levels (top plot) and the yearly mean vTEC difference between IGS GIM and NeQuick driven by local $map - Az$ compared to local and Brussels Az (bottom plot). The effective ionisation level supplied by TEC map ingestion around Brussels (thick lines) adequately declines southwards on a yearly mean basis (top plot), similarly to the local Az based on global coefficients (dashed lines). Consequently it produces a more stable yearly mean vTEC difference with IGS GIM (bottom plot) by comparison to Brussels Az (continuous lines). The vertical dotted lines enclose the IP in sight from Brussels.

4.2.2 TEC map ingestion

Leaving the single-station approach, NeQuick enables the computation of *world-wide grids of effective parameters* fitting GIM (Nava et al., 2005). Standard GIM (Section 2.3.2) consist in global vTEC maps of 2.5° latitude, 5° longitude and 2-h time resolution. For each grid point, they provide 12 values per day[6] available for ingestion into the NeQuick model: minimising the RMS difference between these values and corresponding modelled vTEC, ingestion produces daily Az maps. These maps constitute the basic information for a regional correction procedure. Such a procedure first isolates the grid points in sight of a specific location, assimilating them at 450-km high IP (Fig. 4.17). Second it extracts polynomial coefficients from the modip interpolation[7] of corresponding Az values denoted map-Az (Fig. 4.18, top plot).

Thanks to three regional coefficients, TEC map ingestion successfully assists NeQuick in modelling TEC gradients. The yearly mean vTEC difference with IGS GIM becomes successively slighlty negative and positive with decreasing modip from Brussels considering local effective parameters deduced from map-Az interpolation around Brussels in 2002 (Fig. 4.18, bottom plot). It is larger than its counterpart based on global coefficients interpolated locally, like the ionisation levels themselves, at a different level however for various modip consistently with the variable Az sensitivity.

[6]The even-hour IONEX format affords a 13^{th} value since November 3^{rd}, 2002.

[7]The results in this thesis proceed from a weigthed interpolation using the cosine of latitude equilibrating the growing number of grid points on a parallel with increasing latitude.

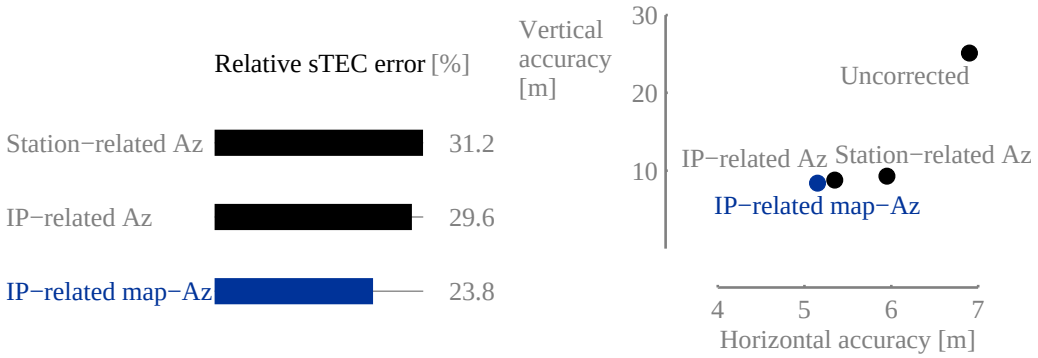

Figure 4.19: Yearly performances in terms of sTEC (left plot) and positioning (right plot) of ionospheric corrections based on the NeQuick model and TEC map ingestion compared to former procedures in 2002. The effective ionisation level map-Az based on information synthesised from TEC map ingestion and related to the IP outperforms its equivalent obtained from global coefficients both in terms of sTEC RMS error (left plot) and positioning accuracy (right plot) for the selected test sites.

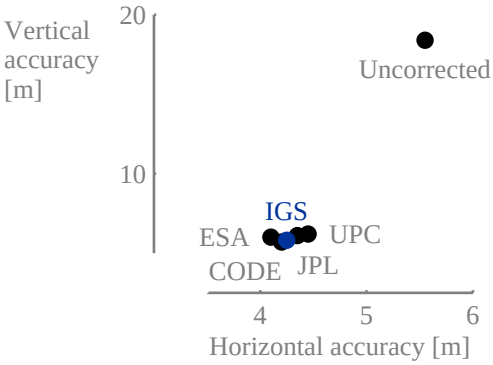

Figure 4.20: Yearly positioning performances of NeQuick operated with TEC map ingestion and different GIM at Brussels in 2002. The ingestion of various GIM provide consistent positioning accuracies.

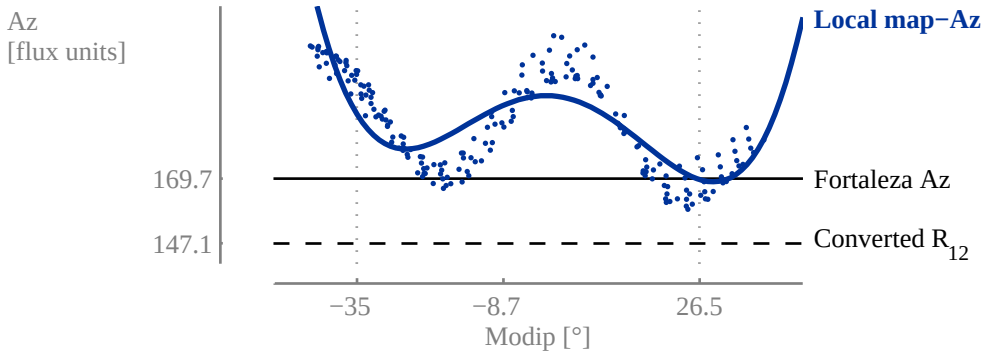

Figure 4.21: Modip dependence of the yearly mean of various ionisation levels including local map-Az obtained from extended TEC map ingestion around Fortaleza. Five coefficients better describe the modip dependence of ionisation levels obtained from TEC map ingestion (thick line). They imply local map-Az larger than the Az derived at Fortaleza from global coefficients (continuous line) or the converted monthly smoothed sunspot number (dashed line).

NeQuick driven by an IP-related map-Az enhances both the sTEC and positioning performances. For the stations and year of interest, it exhibits sTEC statistics rather similar to p-ingestion ones i.e. a 24% smaller RMS error with respect to the simulated standard Galileo correction (Fig. 4.19, left plot) and a 97% compliance level with the corresponding specifications. It ouperforms the positioning accuracies reached with global broadcast coefficients whichever Az scope (Fig. 4.19, right plot). Both horizontal and vertical positioning errors decrease by at least $0.8m$ compared to the station-related Az implementation, meaning 13% and 10% improvements respectively. The horizontal improvement partially originates in a smaller average north bias which nearly follows the same trend among stations as using the IP-related Az. Once again the global enhancement hides worst results at low latitudes as both the horizontal 95^{th} percentile and the mean north error degrade at Fortaleza.

Positioning accuracies obtained from the ingestion of GIM computed by individual centres are consistent with the results of the combined product. At Brussels in 2002, they differ by less than $0.5m$ horizontally as well as vertically (Fig. 4.20). Noticeably horizontal accuracies rank in the same order as corresponding yearly mean Az parabolas within the modip interpolation range. This order fits vTEC orders of magnitude with the largest for UPC and the intermediate for IGS GIM (Bidaine & Warnant, 2009b).

4.2.3 Extensions

Theoretically the concept of variance-driving is applicable in the framework of parametrised ingestion, extending it into a *hybrid ingestion* scheme. Modip p-ingestion absorbs the bias between various sTEC data sets but does not formally account for it. By minimising the variance of sTEC mismodelling within each modip bin, it generates smaller p-Az values still decreasing with decreasing modip around Brussels in 2002. It slightly depresses horizontal positioning errors derived from the ingestion of IGS and UPC GIM-calibrated sTEC (by 0.15 and $0.25m$ respectively, comparing 95^{th} percentiles), contrary to code-to-carrier levelling as well as vertical errors.

Practically now low latitudes require further imagination to accommodate the complexity of the ionosphere in this part of the world. This complexity yields a larger Az variability not correctly represented by a second-order polynomial of modip. At Cape Ferguson (southern low mid-latitudes), a *fourth-order interpolation* of p-Az values already ameliorates corrected positions by $0.25m$ horizontally and $0.5m$ vertically. Similarly for TEC map ingestion, it fits better the ionisation levels larger between the crests of the equatorial anomaly (Fig. 4.21), where vTEC is actually smaller. However it is affected by instabilities at the borders of the interpolation region characterising growing orders of polynomial adjustments. It recovers operational bounds thanks to a wider modip range which is only accessible for map-Az.

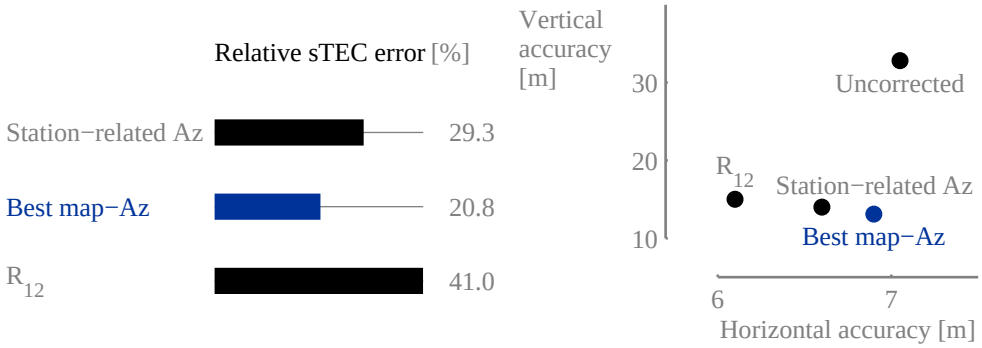

Figure 4.22: Yearly performances in terms of sTEC (left plot) and positioning (right plot) of ionospheric corrections based on the NeQuick model and extended TEC map ingestion compared to former procedures at Fortaleza in 2002. An effective ionisation level computed at each integration point from a fourth-order interpolation based on TEC map ingestion improves sTEC RMS statistics (left plot) as well as the vertical positioning accuracy but not the horizontal correction (right plot).

The best performances from IGS GIM ingestion at Fortaleza in 2002 proceed from PP-related effective ionisation levels computed by means of five coefficients based on an extended interpolation region. They consist in a 21% relative sTEC RMS error i.e. 29% better than using the station-related Az (Fig. 4.22, left plot) originating in a removed underestimation and a 19% smaller standard deviation. They raise the Galileo specifications compliance from 86% to 92%. They involve the best vertical positioning accuracy but unfortunately not smaller horizontal errors than the simulated standard Galileo correction (Fig. 4.22, right plot). In this situation, these errors appear critically influenced by the average ionisation level more than its spatial variability as the monthly smoothed sunspot number R_{12}, much smaller than other values when converted to flux units, provides an even better horizontal correction. They are very likely depending on the vertical electron density profile distortion and the combination of Ne discrepancies at smaller heights, near the receiver and larger altitudes, further from the user. In this case, these discrepancies do not usefully compensate despite the adaptative Az scope following which the ionisation level does not evolve monotonously on slant paths.

Conclusion

The Galileo Single Frequency Ionospheric Correction Algorithm will serve mass-market navigation receivers with a means to account for a major error source affecting their positioning accuracy. This algorithm is based on NeQuick, an empirical model deriving the electron density profile from characteristic points of this profile. It should be assessed in different situations and at various levels to quantify its performances. Hence it raised three research questions.

To which extent is NeQuick (and its latest evolutions) able to provide a realistic representation of the ionosphere without TEC adaptation?

Taking into account NeQuick intrinsic weaknesses, how effectively can the model accommodate sTEC measurements, for Galileo in particular?

At which level does the Galileo Single Frequency Ionospheric Correction Algorithm improve the positioning accuracy?

These questions have been tackled thanks to ground-based measurements collected worldwide, at several tens of locations, in 2002. These measurements enabled either to drive the NeQuick model or to characterise its results. They were obtained from ionosondes – providing various parameters related to the vertical electron density profile from radiowave reflection – and GPS receivers – supplying TEC from ionosphere refraction.

This chapter concludes an independent investigation of the Galileo ionospheric correction. It summarises NeQuick and Galileo correction performances, emphasising the main lessons learnt. Finally it discusses perspectives brought by this PhD research.

Table 5.1: NeQuick and Galileo correction performances. NeQuick and Galileo correction performances have been investigated for different versions of the NeQuick model and compared to the Klobuchar model. They have been quantified through different statistics for each parameter of interest: the relative standard deviation for vTEC, the relative RMS difference for sTEC and 95^{th} percentiles for positioning errors.

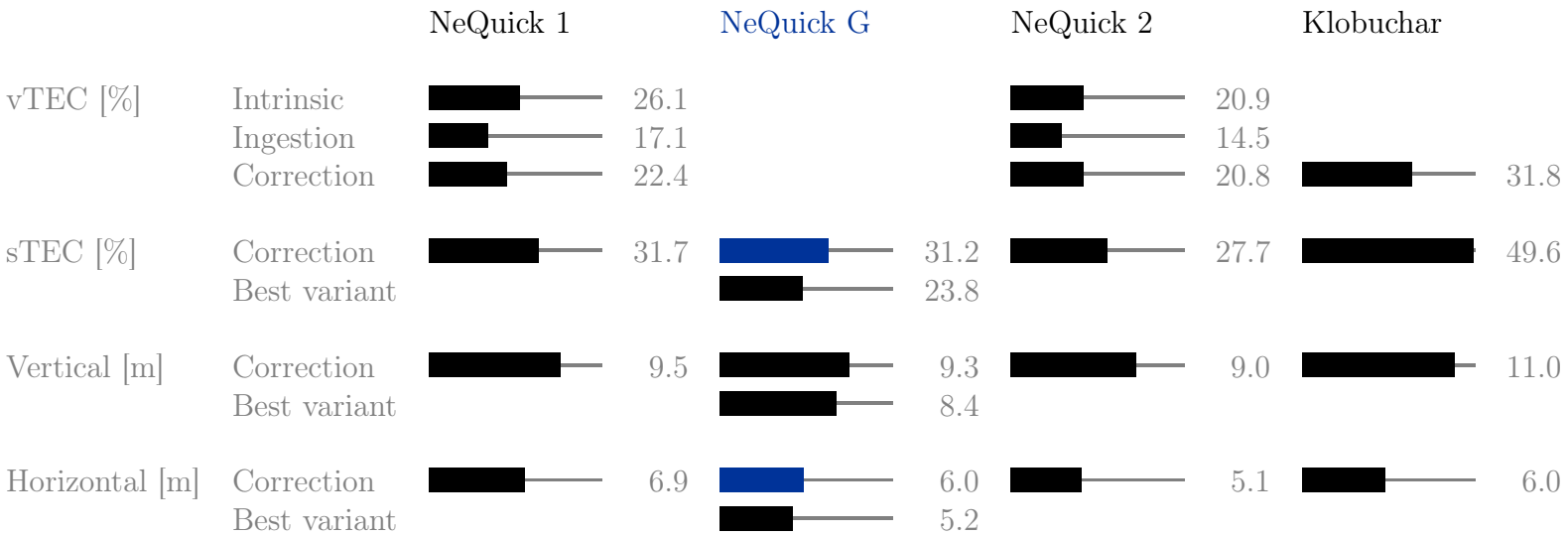

5.1 Galileo correction performances

Several indicators usefully synthesise NeQuick and Galileo correction performances (Tab. 5.1): the smaller the indicator, the better the associated performance. These indicators depend on the investigated parameter.

- Vertical TEC (vTEC) is characterised by the relative standard deviation of differences between measured and modelled values. The standard deviation better accounts for the performances of NeQuick first operation mode. It is indeed not influenced by potential discrepancies associated to measurement techniques which have shown significant mean differences.
- Slant TEC (sTEC) is examined by means of the relative Root Mean Square (RMS) difference between measured and modelled values. The RMS is involved in ionospheric correction specifications.
- Positioning errors are summarised by their 95^{th} percentile. The 95^{th} percentile is often employed for positioning service specifications.

Several ionospheric models have been considered. NeQuick G is put forward because it constitutes the official version for Galileo. NeQuick 1 was privileged at the beginning of the research because NeQuick G was not yet officially available. Noticeably NeQuick 1 shares the same formulation as NeQuick G for the topside, the upper – and larger – part of the electron density profile. NeQuick 2 was assessed to quantify the impact of its new topside formulation. The Klobuchar model, implemented in the GPS, is provided for the sake of comparison.

vTEC residual errors of the NeQuick model range between 14 and 26%. They correspond to a mean measured vTEC of $31 TECu$. They amount to 26% for NeQuick 1 used in its first operation mode. This operation mode, referred to as ionosonde parameters constrain, represents the intrinsic behavior of the model. Indeed it investigates how NeQuick derives electron density profiles from actual ionosonde measurements (Section 3.1). NeQuick 1 second operation mode yields vTEC residual errors decreasing to 17%. This mode involves sTEC data ingestion: it employs daily effective ionisation levels computed at each station in order to minimise NeQuick mismodelling with respect to daily sets of sTEC measurements from that station (Section 3.2.1). For NeQuick 1 third operation mode, vTEC residual errors raise back to 22%. These errors represent Galileo correction vTEC performances: indeed they relate to effective ionisation levels interpolated from simulated broadcast coefficients based on previous-day ingestion.

sTEC residual errors deduced from simulated Galileo corrections based on different NeQuick versions vary between 28 and 32%. They are associated to a mean measured sTEC of $44 TECu$. They amount to *31% for NeQuick G*

in particular. They adopt larger values than for vTEC. They indeed cover various elevations inducing longer paths through the ionosphere among others and have been computed for a different station set (Section 3.2.2).

Positioning residual errors resulting from the application of simulated Galileo corrections reach 9 to 9.5m vertically and 5.1 to 6.9m horizontally. They are respectively much smaller and comparable to the uncorrected vertical and horizontal positioning errors (25.1 and 6.9m). *For NeQuick G*, they equal *9.3 and* 6m. They correspond to NeQuick last operation mode, the most meaningful for Galileo end-users. Noticeably they do not only translate ionospheric mismodellings as they remain influenced by other error sources (Section 3.3).

The best results from variants have been obtained from a regional procedure based on TEC map ingestion. This procedure supplied sTEC residual errors 24% smaller than for the official algorithm, as well as vertical and horizontal positioning errors 10% and 13% smaller respectively. It relies on simulated broadcast coefficients interpolated from grids of effective ionisation levels (Section 4.2.2).

The findings of this thesis are *consistent with previous or simultaneous investigations.*

- In parallel of this thesis, several studies have been conducted to quantify the Galileo algorithm performances. According to Prieto-Cerdeira et al. (2006), the specifications are met more than 95% of the time during the high solar activity year investigated (2000). During that year, the residual RMS error does not exceed 30%. Orus et al. (2007a) stated an error of 30% for the same year embedding NeQuick 2 in the algorithm. They also showed a large decrease of the average mismodelling (60% to 80% in relative error) down to below 1$TECu$. Orus & Prieto-Cerdeira (2008) examined a low solar activity year (2007) in the framework of the Galileo In-Orbit Validation Element (GIOVE) mission[1]. They obtained 40% RMS errors and improvements from NeQuick 2 between 1% and more than 10%. For two later low solar activity years (2008-2009) within the same mission, Hidalgo et al. (2009) observed more than 97% residual errors falling within specifications and corresponding to an 8$-TECu$ RMS.

- The Galileo algorithm outperforms the GPS ICA in terms of sTEC. According to Feess & Stephens (1987), the residual RMS error of the GPS ICA reaches 40% in the years 1980 to 1983 (high and medium solar activity). In 2000, the residual vertical RMS error amounts to 54% compared to measurements collected over oceans from the TOPEX altimetric satellite (Orus et al., 2002). For the same year, Radicella et al. (2008) compared the GPS ICA and the Galileo algorithm built on NeQuick 2. They reported daily 95th percentiles of the sTEC mismodelling ranging

[1]This mission involved two experimental satellites launched in 2005 and 2008.

from 20 to 70$TECu$ for NeQuick 2 and values larger by about 20$TECu$ for the GPS ICA.

- A few earlier works ended up with different ionospheric impact on different dimensions as well as different correction levels on pseudorange or positions. According to Allain & Mitchell (2009), the majority of the positioning error caused by the ionosphere impacts the vertical component and the largest errors occur at midday. Belabbas et al. (2005) compared the ionospheric error left by the NeQuick and Klobuchar model at pseudorange and position levels during a high solar activity year (2000). They reported better performances with NeQuick at pseudorange level but not necessarily at position level. Orus & Prieto-Cerdeira (2008) confronted both models at low latitudes for a low solar activity year (2007). They did not either observe significant positioning performance differences.

The above-described *performances largely depend on the modelling of the topside*. This part of the electron density profile is represented in the same way for NeQuick 1 and G, accounting for the similar sTEC performances. Hence NeQuick 1 and G are equivalent regarding main conclusions including early ones drawn only for NeQuick 1. On the contrary, NeQuick 2 benefits from a more realistic topside formulation explaining most of its better performances.

sTEC performances meet the Galileo algorithm specifications requesting simplistically 30% residual errors. These performances proceed from the effectiveness of sTEC data ingestion illustrated for vTEC comparatively to NeQuick intrinsic behaviour. However they deteriorate because of TEC day-to-day variability which is also visible from vTEC statistics. They indeed result from broadcast information pragmatically computed by means of TEC measurements from the day before.

sTEC and positioning performances are not directly related to one another. TEC and vertical positioning exhibit consistent correction levels but not horizontal positioning. Horizontal positioning is indeed altered by TEC gradients and not by independent TEC values or delays. In other words the uncorrected ionospheric delays cannot be considered as random. In addition, their mean value only modifies the common bias i.e. the fourth unknown of the positioning problem. Hence they would rather be taken into account by means of their standard deviation in a typical error budget dedicated to positioning.

The Galileo correction performances associated to several discrepancies *could be improved thanks to different variants*. In particular variants employing an adaptative effective ionisation level scope adequately deal with north-south TEC gradients overcorrected by the original algorithm. Such variants compute at least one effective ionisation level per satellite direction instead of one per receiver location. They are also much less affected by potential measurement biases.

5.2 Perspectives

The present thesis provides tools for *further investigation of the Galileo algorithm*.

- The first tools – the engineered scenarios and associated operation modes of the NeQuick model – could be revisited at other locations and solar activity levels as well as during successive phases of Galileo deployment. Consisting in simulations, they indeed lead to conclusions which could be validated on real case studies, employing Galileo navigation signals and resulting positioning solutions. Such case studies could be produced not later than late 2012 with the first four satellites simultaneously operational.

- The second tools – single-level variants – could be considered for implementation. These variants indeed imply minor modifications in the current definition of the Galileo algorithm but potentially significant improvements. At system level, upgrading the model version to NeQuick 2 basically consists in replacing two formulas of the topside description by a single one. Applying variance-driven ingestion – or v-ingestion – would only affect the optimisation criterium, minimising the variance of mismodellings instead of their RMS. Both these variants do not influence the synthesis and processing of broadcast information. At user level, opting for an adaptative scope of the effective ionisation level would slightly modify the broadcast information processing of the software embedded in Galileo receivers. This variant should improve the positioning accuracy at least at mid-latitudes, where most of Galileo single frequency users will operate.

Future research in the field of the one presented in this thesis will benefit from the *evolution of ionosphere monitoring techniques*.

- Ionosondes have proven their interest, either for model design or validation. However they constitute complex – hence expensive – instruments requiring careful post-processing for ionospheric parameters identification. Therefore they are deployed sparsely across the world and are not easily exploited for global ionosphere modelling. In particular they enabled the proof of concept of multiple ingestion or m-ingestion, a technique adapting NeQuick simultaneously to TEC and ionosonde measurements. Unfortunately this technique suffers from the limited availability and robustness of ionosonde data which would be mandatory in an operational system.

- GNSS TEC monitoring has shown its influence on NeQuick usage, regarding both model adaptation and performance evaluation. Indeed it exhibits discrepancies between different dual-frequency techniques (Ciraolo et al., 2007; Conte et al., 2011). On the one hand, these discrepancies possibly amplify NeQuick intrinsic weaknesses in the framework of data ingestion. On the other hand, they complicate the interpretation of the model results. Hopefully they will be better characterised thanks to more accurate techniques potentially ensuing from triple-frequency measurement combinations (Spits & Warnant, 2011). Such techniques will indirectly profit ionosphere modelling.

The present thesis contributes to *innovation in ionosphere modelling*.

- It demonstrates the potential of concurrent exploitation of ionosonde and GNSS data, not unlike concomitant research. In particular, both kinds of data permit to constrain the peak and thickness of the electron density profile at the same time in the framework of m-ingestion. Similarly they enable the local electron density profile reconstruction in real-time (Stankov et al., 2011) taking into account separately the distribution of major ions (O^+ and H^+). Undeniably they foster research hopefully converging to global operational models.

- It presents prototypical procedures appealing further developments. For instance, m-ingestion provides effective parameters candidates for spatial interpolation, like standard ingestion within the Galileo algorithm. It would define three sets of coefficients to retrieve multiple effective parameters at distant locations.

- It suggests the investigation of composite procedures. For example, m-ingestion could be applied in combination with TEC map adaptation. First it would derive the two effective ionisation levels related to the peak of the electron density profile from measurements collected at a number of ionosondes within a given area. Then it would extract the third effective parameter from the adaptation to TEC maps covering this area. Hence it would create corresponding maps of the thickness modulator α. These maps could be reduced into monthly median sets of coefficients subsequently incorporated in the core data underlying NeQuick.

The present thesis proposes *regional correction procedures* which could be *futher investigated and developed towards operationality*. These procedures – parametrised ingestion or p-ingestion, and TEC map ingestion – support the interest of an effective ionisation level scope. Indeed both of them potentially supply broadcast coefficients best interpolated by single-frequency users at least for each satellite direction. In addition, TEC map ingestion offers promising perspectives.

- It could yield a better spatio-temporal availability of broadcast information than p-ingestion. It benefits from advanced spatial interpolation techniques exploited for global TEC maps. These maps indeed combine GNSS data from hundreds of stations around the world. They are routinely generated at a 2-hour rate and disseminated via the internet with a 10-day latency for the final products. However predicted products have recently been designed and proposed for download (García-Rigo et al., 2011). Such products consist in 1 or 2-day forecasts of global vTEC maps. Hence they could be ingested into NeQuick to provide broadcast information for the day regarded by the forecast.

- It enables flexible data management, with a variable degree of centralisation. First, it can involve a centralised model adaptation, contrary to any other ingestion scheme. In such a case and for global TEC maps, it would generate effective ionisation level grids valid for the whole world. It would ressemble the computation of Klobuchar-style ionospheric coefficients best fitting CODE TEC maps performed at CODE since 2000 (Schaer, 2001). Second, it can employ a decentralised broadcast information synthesis. Within a given region, it would then derive broadcast coefficients from the interpolation of the corresponding subset of effective ionisation levels extracted from the global grid.

- It can accommodate various sources of ionospheric data, including regional TEC maps and results from tomography.

The proposed regional procedures could be implemented in the framework of *assisted GNSS* (A-GNSS). A-GNSS consists in providing a GNSS user with information he would normally receive from the satellites, through an alternative communication channel (van Diggelen, 2009). A-GNSS mainly allows to decrease drastically the time needed to compute a first position after receiver power-up. It also supplies a means to dispatch adapted coefficients dedicated to the ionospheric correction. It could indeed transmit through mobile networks a navigation message containing these adapted coefficients swapped for the original ones. Relieving the need for fully independent infrastructures, A-GNSS could stimulate the deployment of alternative procedures for the Galileo single frequency ionospheric correction algorithm, yielding an Assisted Ionospheric Correction Algorithm (A-ICA). Indeed it already serves numerous smartphones which will probably be the first to actually use Galileo thanks to its interoperability with GPS. These smartphones will be the first to make *Galileo a part of our daily lives*.

A

(Bidaine and Warnant, 2010)

Assessment of the NeQuick model at mid-latitudes using GNSS TEC and ionosonde data

Abstract The **modelling of the Total Electron Content (TEC)** plays an important role in global navigation satellite systems (GNSS) accuracy, especially for **single-frequency receivers**, the most common ones constituting the mass market. For the latter and in the framework of Galileo, the **NeQuick model** has been chosen for correcting the ionospheric error contribution and will be integrated into a global algorithm providing the users with daily updated information.

In order to reach the ionosphere error correction level objective, the model itself as well as its use for Galileo are **investigated**. In our comparison process, we take advantage of various ionosphere data from several European stations (Dourbes in Belgium, El Arenosillo and Roquetes in Spain) where **ionosonde and GPS TEC data** are available for different solar activity levels. These data allow us to study NeQuick representation of the ionosphere at **mid-latitudes**. Constraining the model with ionosonde measurements, we investigate the difference between GPS-derived vertical TEC and corresponding values from NeQuick for a **high solar activity level** (year 2002). With this approach, we reach **residual errors of less than 20% in standard deviation**. We especially highlight the **improvements from the latest (second) version** of NeQuick and show the **critical importance of the topside** formulation.

Keywords ionosphere, Total Electron Content (TEC), NeQuick, topside, mitigation, Global Navigation Satellite Systems (GNSS)

A.1 Introduction

The **ionosphere**, the part of the atmosphere extending between 50 and several thousand kilometers from earth surface, produces different effects on Global Navigation Satellite Systems (GNSS) (Kintner & Ledvina, 2005). The major influence from its intrinsic electron concentration N_e $[electrons\ m^{-3}]$ concerns the time of flight of navigation signals depending on their frequency f $[Hz]$ and on the total content in free electrons of the ionosphere. For code measurements, the consecutive **pseudorange error** I_g $[m]$ is obtained as follows at first approximation.

$$I_g = \frac{40.3}{f^2} \int_{sat.}^{rec.} N_e \, ds = \frac{40.3}{f^2} sTEC \tag{A.1}$$

This slant *"total electron content"* $(sTEC)$ is defined as the integral of the electron density on the path between the satellite and the receiver. Its units are $[electrons\ m^{-2}]$ or more generally TEC units $[TECu = 10^{16}\ el.m^{-2}]$, one $TECu$ inducing an error of 0.16 m for the L_1 carrier (1575.42 MHz) and it can be converted to vertical TEC $(vTEC)$ by means of a mapping function. As every ionospheric parameter, the value of TEC depends on different factors such as location, time of the day, season, solar or geomagnetic activity.

TEC modelling reveals itself of first importance especially for *single frequency receivers*, the most common ones constituting the mass market, but also for multiple-frequency devices. The latest will indeed comprise a *fallback mode* in single frequency within the framework of critical applications such as civil aviation where the level of precision must be guaranteed in all circumstances. For Galileo single frequency users, the ionospheric error correction algorithm uses the **NeQuick** model to compute TEC (Prieto-Cerdeira et al., 2006; Orus et al., 2007a). Understanding its *weaknesses and evolutions* and *validating* its results constitutes then a task of prime order to reach the best correction level. Therefore *different situations* have to be considered: different latitude regions (space conditions), different hours, seasons and years (time conditions) and specific phenomena occurrence (magnetic storms, Travelling Ionospheric Disturbances - TIDs). In addition the results can be compared to *different data sets* among which GPS $sTEC$ or $vTEC$ measurements, Global Ionospheric Maps (GIMs) of $vTEC$, ionosonde profiles, topside soundings.

For instance, Coisson et al. (2004) compared GIMs obtained using different empirical models with monthly median maps computed on the basis of GIMs produced by the Center for Orbit Determination in Europe (CODE). They reported NeQuick to be the model with the more stable behaviour in time and space. They also performed a $sTEC$ analysis involving nine European and North American stations on a geogmagneticaly quiet day during a period of high solar activity and they obtained an RMS value of 13.2 $TECu$ or 33.8%.

Another interesting study broadening the scope of the potential tests involving NeQuick examines its performances in the framework of the Galileo Single Frequency Ionospheric Correction Algorithm (Orus et al., 2007a). Considering a high solar activity year (2000), it states an error of 30% for the latest version of the model and improvements at almost all latitudes by comparison to the previous version. It also shows a large decrease of the global bias (60% to 80% in relative error) down to below 1 $TECu$ for the whole year 2000. For the present study, we chose to investigate NeQuick performance at mid-latitudes using ionosonde and GPS TEC data.

A.2 Tools and method

A.2.1 NeQuick model

NeQuick belongs to the "DGR family" of ionospheric models known as "**profilers**" (Di Giovanni & Radicella, 1990; Radicella & Zhang, 1995). They indeed fit analytical functions on a set of anchor points, namely the E, F_1 and F_2 layer peaks, to represent these principal ionospheric layers and compute the electron density profile. NeQuick is the simplest one and was adopted by the ITU-R recommendation for TEC modelling (Hochegger et al., 2000). The NeQuick model is divided into two regions (Radicella & Leitinger, 2001): the *bottomside*, up to the F_2-layer peak, consists of a sum of five semi-Epstein layers[1] (Rawer, 1982) and the *topside* is described by means of an only sixth semi-Epstein layer with a height-dependent thickness parameter.

To compute the parameters for the Epstein layers[2], the thickness parameters B^L_{bot} and B^L_{top} and the anchor points coordinates i.e. peaks electron density NmL and height hmL, NeQuick employs the *ionosonde parameters*, f_oE, f_oF_1, f_oF_2 and $M(3000)F_2$. These critical frequencies and transmission factor are themselves obtained from empirical equations among which the CCIR maps (ITU, 2009b) for the F_2 characteristics[3] so that a monthly median situation is represented. However the power of NeQuick consists in its ability to accommodate other sources of data for these parameters e.g. measured values.

NeQuick FORTRAN 77 code was submitted to and accepted by the ITU-R in 2000 and revised in 2002. It is downloadable from the Internet (ITU, 2009a), is referred to either as *version 1* or ITU-R and constitutes the current baseline for Galileo. This package includes also numerical integration subroutines allowing to compute $vTEC$ and $sTEC$.

[1] The prefix "semi" means that different thickness parameters are used below and above the layer peak.

[2] L stands for the layer index which possible values are E, F_1 and F_2.

[3] Note that NeQuick f_oE and f_oF_1 should be referred to as *effective* critical frequencies as their definition does not correspond exactly to the cited reference ITU-R recommendation.

Since then the model has undergone a series of evolutions leading to a **second version** (Nava et al., 2008; Bidaine et al., 2006) available from the model designers.

- *Bottomside simplifications* and associated changes in the calculation of the E and F_1 peak amplitudes and f_oF_1 (Leitinger et al., 2005) allow to avoid some unrealistic features.
- Topside soundings data from the ISIS-2 satellite were processed to modify the formulation of the *shape parameter* k involved in the *topside* thickness parameter calculation (cf. appendix A.5). It was previously computed on the basis of two formulas, one for months between April and September and the other for the rest of the year, which are replaced by a single one in NeQuick 2. Coisson et al. (2006) showed that the new formulation provides electron density profiles closer to experimental ones, where NeQuick 1 tends to underestimate the electron density at high and mid latitudes and slightly overestimate at low latitudes.
- Finally a *new modified dip latitude (MODIP) file* was introduced for MODIP interpolation in the framework of CCIR maps use.

Consequently potential improvements need to be assessed through different methods among which the one described in next section.

A.2.2 Analysis method

Among the different analysis methods using NeQuick in different ways, we chose as a first step to **uncouple NeQuick formulation from its underlying data** (Bidaine & Warnant, 2007). To this extent, we replaced the CCIR maps of f_oF_2 and $M(3000)F_2$ by their measured values by means of an ionosonde, which we call ionosonde parameters from now on. In other words, we constrained the model to a daily behaviour, anchoring it in a real ionosphere, instead of considering the monthly median output.

Given this use of NeQuick, we compared its results using **two kinds of measurements**: $vTEC$ or simply TEC from now on, the valuable parameter for navigation purpose, computed by GPS and vertical electron density profiles from an ionosonde. We took there advantage of collocated independent data, a part exploited to constrain the model and the other as reference.

We developed software enabling us to browse measured and modelled TEC and electron density profiles as well as input data. We also included a module allowing to **analyse statistically TEC differences** computing mainly bias $\overline{\Delta TEC}$ and standard deviation $\sigma_{\Delta TEC}$ for each year, month, day and UT in a month or year as follows.

Figure A.1: Collocated digisondes and IGS/EUREF stations

Table A.1: Characteristics of the data sets

Station	Code	Latitude [°N]	Longitude [°E]	Time interval
Digisondes providing f_oF_2 and $M(3000)F_2$ every hour				
Dourbes	DB049	50.1	4.6	01/02 to 29/04
				16/05 to 20/11
				25/11 to 31/12
Roquetes	EB040	40.8	0.5	01/01 to 31/12
El Arenosillo	EA036	37.1	-6.7	01/01 to 08/02
				12/02 to 24/07
				26/10 to 31/12
GPS stations providing TEC every quarter				
Dourbes	dour	50.1	4.6	01/01 to 31/12
Roquetes	ebre	40.8	0.5	01/01 to 31/12
San Fernando	sfer	36.5	-6.2	01/01 to 31/12

$$\overline{\Delta TEC} = \langle TEC_{meas} - TEC_{mod} \rangle \tag{A.2}$$

$$\sigma_{\Delta TEC} = \sqrt{\left\langle \left(TEC_{meas} - TEC_{mod} - \overline{\Delta TEC} \right)^2 \right\rangle} \tag{A.3}$$

$$*_{Relative} = \frac{*}{\langle TEC_{meas} \rangle} \tag{A.4}$$

$$\text{Evolution} = \frac{*_{NeQuick\ 2} - *_{NeQuick\ 1}}{*_{NeQuick\ 1}} \tag{A.5}$$

<> denotes a mean on a given period of the specified expression and $*$ either the bias $\overline{\Delta TEC}$ or the standard deviation $\sigma_{\Delta TEC}$.

In the following sections, we adopt **four different approaches**:

- we compare the global TEC behaviour of each version of the model with GPS TEC examining *yearly statistics*,
- we highlight the influence of the *modification of the topside shape parameter k* considering separately the periods corresponding to both formula in NeQuick 1,
- we show the critical importance of the topside *splitting TEC* between its bottomside and topside contributions
- and we confirm our observations examining *monthly statistics*.

A.2.3 Data sets

We gathered manually validated ionosonde parameters and electron density profiles obtained by **digisondes** and **GPS** $sTEC$ **data calibrated by means of Global Ionospheric Maps (GIM)**[4]. TEC is computed based on the geometry-free combination of phase measurements. Phase ambiguities are estimated using precise sTEC values obtained from TEC maps (Orus et al., 2007b). Consequently potential problems related to code hardware delays, multipath and noise (Ciraolo et al., 2007) are reduced as no pseudorange measurement is directly involved in TEC computation. To obtain $vTEC$, we selected $sTEC$ values corresponding to an elevation greater than 61.8°, we converted them to vertical using a mapping function associated to a 400-km thin shell height and we computed their mean over 15-minute periods (equivalent to having selected subionospheric points within a radius of 200 km around the station; similar to (Warnant & Pottiaux, 2000)).

[4]The data set used was computed at the European Space Agency (ESA) using GIMs produced by the Universitat Politècnica de Catalunya (UPC).

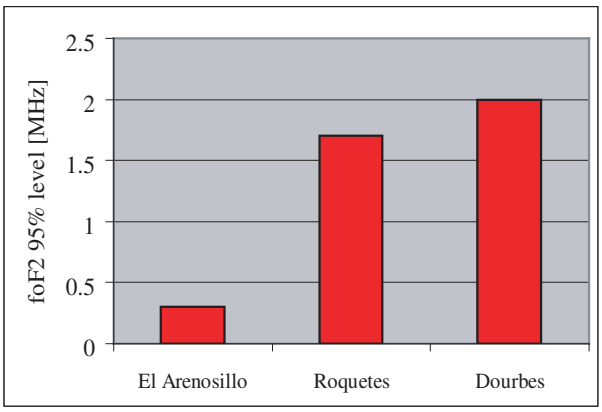

Figure A.2: Influence of ionosonde scaling validation on f_oF_2

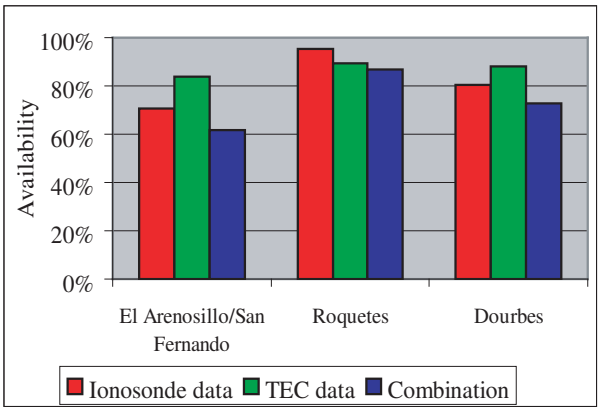

Figure A.3: Data availability

We fixed the framework of this study over a **high solar activity** period (year 2002) and **mid-latitudes** selecting three European locations with collocated digisonde and IGS/EUREF station (cf. fig. A.1 and table A.1).

Finally we highlight the **interest of manual validation** of ionosonde parameters showing the 95% percentile of f_oF_2 differences between auto-scaled and manually validated values (cf. fig. A.2). We also give the **availability** levels of each kind of data and for their combined use (cf. fig. A.3). We count maximum 35040 GPS TEC values (one every quarter) and 8760 DGS parameters couples and profiles (soundings every hour). We explain partially the lower availabilities

- for El Arenosillo digisonde, by a lack of data between July 25th and October 25th,
- for Dourbes digisonde, because of January is missing
- and for TEC data, because of the odd-hour IONEX format for the GIM leads to a systematic gap between 23 and 1 UT.

A.3 Analysis

A.3.1 Yearly statistics

Examining yearly statistics allows us first to observe the **influence of latitude**: TEC mean decreases northwards (cf. fig. A.4). We also state an average **underestimation** of both versions of the model even larger (around 20%) for NeQuick 2. Hovewer biases have to be interpreted with caution. Indeed previous studies comparing different GPS TEC reconstruction techniques show that biases of several $TECu$ can appear between them (Prieto-Cerdeira et al., 2006; Orus et al., 2007a; Bidaine & Warnant, 2009b). These biases are related to the levelling techniques used by the different authors to compute phase ambiguities. Therefore the interpretation of the detected biases of the model is difficult. Nevertheless the **lower (around 20%) standard deviation** obtained for NeQuick 2 indicates us an improvement from the second version of the model.

A.3.2 Influence of k unification

As described in section A.2.1, the major modification between both NeQuick versions is related to the topside. The two formulas (one for April to September and the other for October to March) for the shape parameter k in NeQuick 1 were replaced by a single one in NeQuick 2 (cf. appendix A.5). It reveals

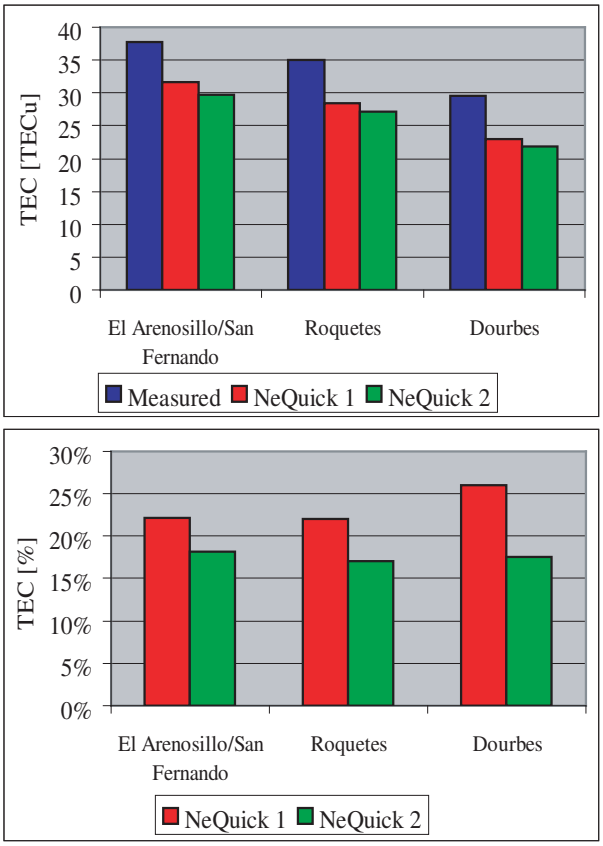

Figure A.4: Yearly TEC mean (top) and relative standard deviation (bottom)

thus itself interesting to **compute statistics separately for each period corresponding to the two former formulas**.

We then observe different performances for each period especially regarding statistics evolution from one version to the other (cf. fig. A.5). For April to September, we state a lower (20%) bias and slightly larger standard deviation in NeQuick 2. For October to March however, the bias, lower than for the first period in NeQuick 1, becomes much larger (200%)[5] and the standard deviation, larger between April and September for the first version of the model, decreases by about 15% in the second version. This **second period becomes hence more homogenous** with the first one and mostly influences the global statistics.

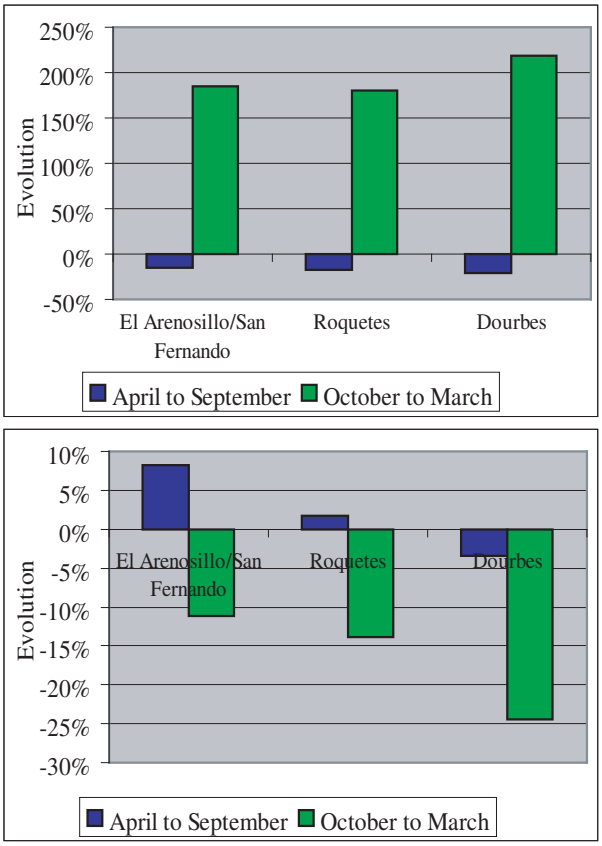

Figure A.5: Evolution of TEC bias (top) and standard deviation (bottom) between NeQuick versions

[5]This high percentage is due to the low value of NeQuick 1 bias (around 2.5 $TECu$).

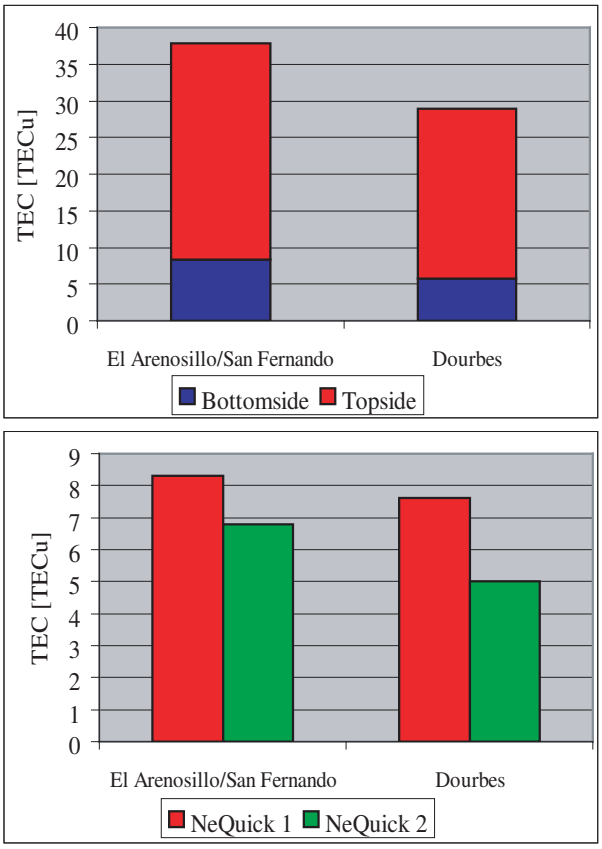

Figure A.6: Proportion of TEC within bottomside and topside (top) and yearly topside TEC standard deviation (bottom)

A.3.3 TEC splitting

To feel even more confident about the impact of the modification in the topside formulation, we could advantageously **distinguish between bottomside and topside contributions to the TEC**. To this extent, we integrated the bottomside electron density profile from the digisondes to compute the bottomside TEC[6]. Then we subtracted this value to the GPS TEC to obtain an estimate of the topside TEC for which conclusions have to be drawn with caution as it includes the whole GPS TEC uncertainty.

This procedure enables us to highlight the **large proportion of TEC lying within the topside** (more than 75% on average, cf. fig. A.6). We thus put into perspective the importance of the bottomside formulation – eventually slightly worse with NeQuick 2 – justifying the interest of the simplifications introduced in the second version of the model (cf. section A.2.1). We also observe the **favourable evolution of the topside statistics** corresponding to the global values and driving them.

A.3.4 Monthly statistics

A last interesting insight to handle NeQuick formulation and the consequences of its modification consists in examining monthly statistics. To this extent, we chose Roquetes for its higher data availability. Fig. A.7 highlights the **double behaviour** described in section A.3.2 **for NeQuick 1** and the **homogenisation** from the topside shape parameter k unification **in NeQuick 2**. We also note an improvement in bias and standard deviation for August and September (idem for Dourbes), two months missing in El Arenosillo data set (cf. section A.2.3). If they had been present, they would apparently have influenced positively the various statistics presented in previous subsections.

A.4 Conclusion and perspectives

As a corner stone in the Galileo single frequency ionospheric correction algorithm, the **NeQuick model is improved** thanks to several studies. The present assessment lies within this scope insofar as it investigates the model and its latest developments for three mid-latitude stations collecting collocated ionosonde and GPS TEC data.

Conditioning NeQuick with ionosonde data, we first analysed statistically the difference between GPS-derived vertical TEC for Dourbes, Roquetes and El Arenosillo/San Fernando stations and corresponding modelled values for the

[6]We have not had access to profiles for Roquetes digisonde yet so that we did not apply TEC splitting to that station.

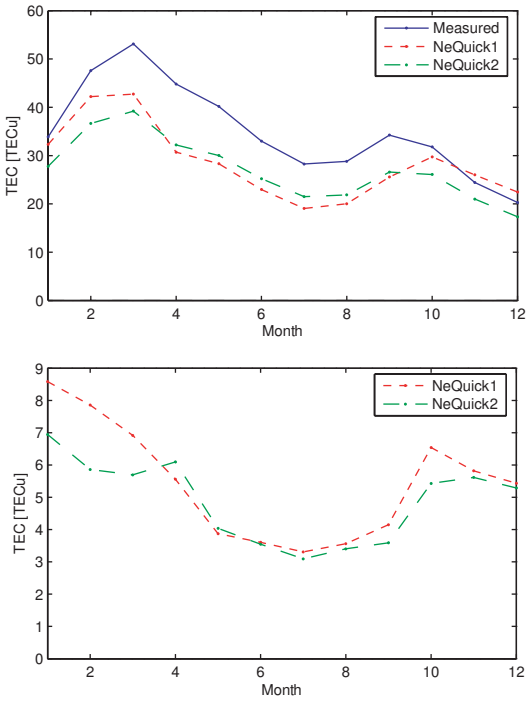

Figure A.7: Monthly TEC mean (top) and standard deviation (bottom) for Roquetes

last solar maximum in 2002. We found **standard deviations decreasing by 20% to reach less than 20% in relative values with NeQuick 2**; biases increasing by 20% up to 25% (care must be taken about GPS TEC data regarding the bias).

To explain this progress, we highlighted the influence of the **unification of the topside shape parameter** k as the two former formulas corresponded with periods exhibiting opposite behaviours. We also showed the **importance of the topside** accounting for 75% of the TEC on average and we confirmed all our observations examining **monthly statistics**.

The present study constitutes a basis of comparison for further investigation of more global uses of the model. We will indeed be able to observe how **data ingestion** techniques can accommodate the remaining mismodelling as well as the adaptation of the CCIR maps to daily situations. Finally we will assess the **Galileo single frequency ionospheric correction algorithm** with potential suitable evolutions of NeQuick.

A.5 NeQuick topside electron density

The topside is defined as the region of the ionosphere above the F_2-layer peak. To compute its electron density, the NeQuick model uses a semi-Epstein layer with a maximum corresponding to the F_2-layer peak (electron density N_mF_2 and height h_mF_2) and a height-dependent thickness parameter H.

$$N_{top}(h) = 4\ N_mF_2\ \frac{e^{\frac{h-h_mF_2}{H}}}{\left(1+e^{\frac{h-h_mF_2}{H}}\right)^2} \tag{A.6}$$

The height-dependent thickness parameter H is calculated by means of a semi-thickness parameter $B_{top}^{F_2}$ associated to the topside part of the F_2-layer.

$$H = B_{top}^{F_2}\left(1+\frac{12.5(h-h_mF_2)}{100B_{top}^{F_2}+0.125(h-h_mF_2)}\right) \tag{A.7}$$

$B_{top}^{F_2}$ relies itself on its bottomside equivalent $B_{bot}^{F_2}$ through the topside shape parameter k. Both their formulation have been modified in the new version of NeQuick.

In NeQuick 1, two additional auxiliary parameters ν and x are used and k is defined differently for two six-months periods.

$$B_{top}^{F_2} = \frac{k\ B_{bot}^{F_2}}{\nu}$$

$$k = \begin{cases} -7.77 + 0.097 \left(\frac{h_m F_2}{B_{bot}^{F_2}} \right)^2 + 0.153\ N_m F_2 & \text{from October to March} \\ 6.705 - 0.014\ R_{12} - 0.008\ h_m F_2 & \text{from April to September} \end{cases} \tag{A.8}$$

$$2 \leq k \leq 8$$

$$\nu = (0.041163\ x - 0.183981)\ x + 1.424472$$

$$x = \frac{k\ B_{bot}^{F_2} - 150}{100}$$

In NeQuick 2, the additional parameters disappear and a single formula is introduced for k.

$$B_{top}^{F_2} = k\ B_{bot}^{F_2}$$

$$k = 3.22 - 0.0538\ f_o F_2 - 0.00664\ h_m F_2 + 0.113 \frac{h_m F_2}{B_{bot}^{F_2}} + 0.00257\ R_{12} \tag{A.9}$$

$$k \geq 1$$

(Bidaine and Warnant, 2011)

Ionosphere modelling for Galileo single frequency users: illustration of the combination of the NeQuick model and GNSS data ingestion

B

Abstract The ionospheric effect remains one of the main factors limiting the accuracy of Global Navigation Satellite Systems (GNSS) including Galileo. For single frequency users, this contribution to the error budget will be mitigated by an algorithm based on the NeQuick global ionospheric model. This quick-run empirical model provides flexible solutions for combining ionospheric information obtained from various sources, from GNSS to ionosondes and topside sounders. Hence it constitutes an interesting simulation tool not only serving Galileo needs for mitigation of the ionospheric effect but also widening the use of new data.

In this study, we perform slant TEC data ingestion – the optimisation procedure underlying the Galileo single frequency ionospheric correction algorithm – into NeQuick for a dozen locations around the world where both an ionosonde and a GPS receiver are installed. These co-located instruments allow us to compare measured and modelled vertical TEC showing for example global statistics or dependence towards latitude. We analyse measurements for the year 2002 (high solar activity level) giving an insight into the situation we could observe when Galileo reaches its Full Operation Capability, during the next solar maximum.

At last we compare Galileo and GPS ionospheric corrections. For Galileo, we end up with an underestimation of 11% and 4% depending on the version of NeQuick embedded in the algorithm, as well as a 22% standard deviation. This means respectively twice, five and 1.5 times better than GPS.

Keywords GNSS, Galileo, Ionospheric correction, Single frequency, NeQuick, Data ingestion

B.1 Introduction

The accuracy of GNSS-based positioning/navigation is influenced by errors induced by the satellite, receiver, and propagation medium (Hofmann-Wellenhof et al., 2008). The first two categories include for instance the biases due to the satellite and receiver clocks. The last category comprises influences on the propagation of navigation signals within the Earth atmosphere. Two cases are usually distinguished corresponding to two parts of the atmosphere: the neutral part is referred to as the troposphere and the region containing free electrons the ionosphere.

The ionosphere is known to induce scintillations and time delays among other effects (Arbesser-Rastburg & Jakowski, 2007). The latter constitutes the major error source for ranging applications. For code measurements, it leads to a pseudorange error $[m]$

$$I_g = \frac{40.3}{f^2} \int_{sat.}^{rec.} N_e \; ds = \frac{40.3}{f^2} sTEC \tag{B.1}$$

where f denotes the signal frequency $[Hz]$, Ne the electron concentration $[electrons\ m^{-3}]$ and $sTEC$ the slant total electron content $[el.m^{-2}]$. As every ionospheric parameter, the value of TEC depends on different factors such as location, time of day, season, solar or geomagnetic activity. It is more generally measured in TEC units $[TECu = 10^{16}\ el.m^{-2}]$.

Various strategies exist to mitigate the ionospheric effects on GNSS (Warnant et al., 2009). They depend on the application, more or less precise, and on the availability of one or more signal frequencies. For multi-frequency devices, the ionospheric delay can be mitigated by means of specific combinations of measurements, taking advantage of the dispersive property of the ionosphere. On the contrary, single frequency navigation – our field of investigation – requires an ionospheric model, for TEC in particular. For the Global Positioning System (GPS), the Single Frequency Ionospheric Correction Algorithm (SF ICA) is based on the Bent model (Klobuchar, 1987). It uses eight broadcast coefficients from the navigation message to compute vertical TEC ($vTEC$). Assuming a thin shell ionosphere, $sTEC$ is then computed by means of an appropriate mapping function and converted to time delay. This technique is supposed to provide a 50% root-mean-square (RMS) correction of the ionospheric time delay.

In the case of Galileo, the NeQuick model will be used together with three broadcast coefficients that will permit to compute the electron density along the satellite-to-receiver ray-path. Subsequently the electron density values will be integrated to obtain the corresponding $sTEC$ (Arbesser-Rastburg, 2006). According to its specification, this method should exhibit a maximum residual error of 20 $TECu$ or 30% of the actual $sTEC$, whichever is larger, for

satellites above 10° elevation and nominal ionospheric conditions. Orus et al. (2007a) conclude that NeQuick meets this specification. Considering a high solar activity year (2000), they state an error of 30% for the latest version of the model and improvements at almost all latitudes by comparison to the previous version. They also show a large decrease of the global bias (between 60 and 80%) down to below 1 $TECu$ for NeQuick 2 and the whole year 2000.

In the present study, we use co-located GPS and ionosonde measurements during a high solar activity year to illustrate the different elements exploited within Galileo SF ICA. We first focus the analysis on the optimisation procedure, called data ingestion, constituting the core of the algorithm. We compare it with another use of the model based on ionosonde measurements to infer how it can cope with NeQuick possible inaccuracies. Then we extend the analysis towards Galileo and GPS SF ICA.

Data ingestion and assimilation techniques are usually associated but not often clearly distinguished. Both of them combine an underlying ionospheric model and actual measurements to estimate and predict ionospheric characteristics. However data assimilation formally consists in merging observed information from one or more sources into a first-principles physics model (Wilson et al., 2008). Practically it depends on three choices: the underlying model (which is sometimes empirical), a state representation (e.g. spherical harmonics) and an estimation strategy (e.g. Kalman filter). On the other hand data ingestion intend to drive an empirical model towards one specific data set (Nava et al., 2006). To this extent it computes "effective" parameters associated to the model and the data from single-criterion optimisation.

B.2 Tools and method

B.2.1 NeQuick model

NeQuick belongs to the "DGR family" of ionospheric models known as "profilers". They indeed fit analytical functions on a set of anchor points, namely the E, F_1 and F_2 layer peaks, to represent these principal ionospheric layers and compute the electron density profile. NeQuick is the simplest one and was adopted by the ITU-R recommendation for TEC modelling. The NeQuick model is divided into two regions (Radicella & Leitinger, 2001): the bottomside, up to the F_2-layer peak, consists of a sum of five semi-Epstein layers and the topside, above the F_2-layer peak, described by means of a single sixth semi-Epstein layer with a height-dependent thickness parameter. The parameters of the Epstein layers are computed on the basis of the ionosonde parameters, f_oE, f_oF_1, f_oF_2 and $M(3000)F_2$. To obtain these critical frequencies and transmission factor, models can be used such as the CCIR maps for the F_2 characteristics described in ITU-R Recommendation P.1239. A monthly

median situation is then represented. However an advantage of NeQuick consists in its ability to easily accommodate measured values for these parameters (Bidaine & Warnant, 2010).

On the basis of position, time and solar activity index (solar flux or sunspot number) provided as input, the model returns the corresponding electron density. Its first version, referred to either as version 1 or ITU-R, constitutes the current baseline for Galileo. Its FORTRAN 77 code is downloadable from the Internet[1] within a package including numerical integration subroutines allowing to compute $vTEC$ and $sTEC$.

In the recent years, a second version of NeQuick has been designed (Nava et al., 2008) and is available from the model designers. The main evolution concerns the topside representation. Topside soundings data were indeed processed to modify the formulation of the shape parameter k involved in the topside thickness parameter calculation (Coisson et al., 2006). It was previously computed on the basis of two formulas, one for months between April and September and the other for the rest of the year, which are replaced by a single one in NeQuick 2.

B.2.2 Data ingestion

Ionospheric models such as NeQuick often use solar activity indices as standard input. These indices are based on solar observation and do not necessarily account perfectly for the solar activity in EUV radiations inducing the ionisation in the Earth atmosphere. On the other hand, models involve mismodellings related to simplified representations of the various ionospheric drivers including solar activity. Hence different "effective" indices have been developed from the combination of ionospheric models and experimental data. They allow to drive a model towards measured values by adapting it to a specific data set, a reconstruction technique usually referred to as data ingestion. These indices are then strictly related to a model/data set combination and should therefore not be considered as better proxies of the solar activity.

NeQuick has often been used in this framework in combination with TEC data (Nava et al., 2006; Bidaine & Warnant, 2008b). At a given time and for a given ray path, the TEC value obtained from the integration of NeQuick electron density profile depends monotonically on its solar flux input. The latter is then usually called effective ionisation level Az and is computed by minimising the mismodelling between the model and a subset of TEC measurements. This mismodelling is defined as the Root Mean Square (RMS) difference between modelled and measured TEC

$$RMS = \sqrt{\left\langle \left(TEC_{mod}(Az) - TEC_{meas}\right)^2 \right\rangle} \tag{B.2}$$

[1] ITU-R Rec. P.531, http://www.itu.int/oth/R0A04000018/en

Figure B.1: Simulated stations of Galileo IOV phase.

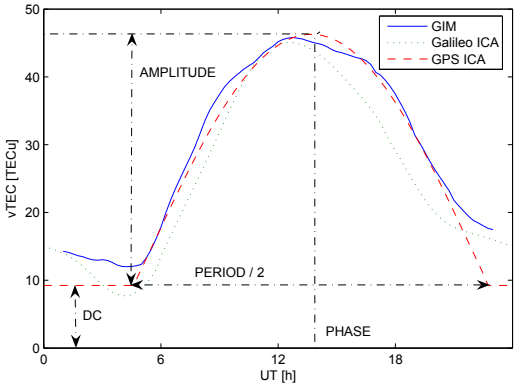

Figure B.2: Daily $vTEC$ profile at Dourbes on September 24^{th}, 2002.

where $\langle\rangle$ denotes averaging the available differences within a given period. For a given station, Az can then be inferred from $sTEC$ epoch by epoch or for longer time frames.

B.2.3 Ionospheric correction algorithms

The Galileo SF ICA will rely on daily ingestion of $sTEC$ data collected within the Ground Mission Segment (Hofmann-Wellenhof et al., 2008). Daily effective parameters will indeed be computed at each Galileo Sensor Station (GSS) in various number for the successive Galileo phases. The current experimental mission GIOVE involves 13 stations while the In-Orbit Validation (IOV) phase planned for 2011 will include 18 GSS and the Full Operation Capability (FOC) around 40. For our study, we chose to simulate the IOV network by means of IGS (Dow et al., 2009) and EUREF (Bruyninx, 2004) stations (cf. Fig. B.1).

To obtain the three coefficients broadcast in the navigation message, the Az values will then be merged through a parabolic adjustment along the modified dip latitude μ (modip). This parameter linked to the geomagnetic field reveals particularly appropriate for modelling purposes as it combines the geomagnetic dip I [°] and the geographic latitude ϕ [°] (Rawer, 1963).

$$\tan \mu = \frac{I}{\sqrt{\cos \phi}} \tag{B.3}$$

At last the user computes the solar activity input of NeQuick by means of the broadcast coefficients a_0, a_1 and a_2 generated the previous day :

$$Az = a_0 + a_1 \mu + a_2 \mu^2. \tag{B.4}$$

By comparison, the GPS SF ICA is very different. This algorithm by Klobuchar (1987) is based on the Bent model and includes many geometric approximations aiming at reducing user computational requirements. It is primarily intended to provide a $vTEC$ daily profile consisting in a cosine representation during the day and a constant (DC) during night (cf. Fig. B.2). The amplitude and the period of the cosine term are obtained each thanks to four broadcast coefficients defining a third order polynomial of the magnetic latitude. The phase of the maximum is fixed at 14:00 local time. The vertical time delay actually computed in this manner is then converted to slant by means of a dedicated mapping function.

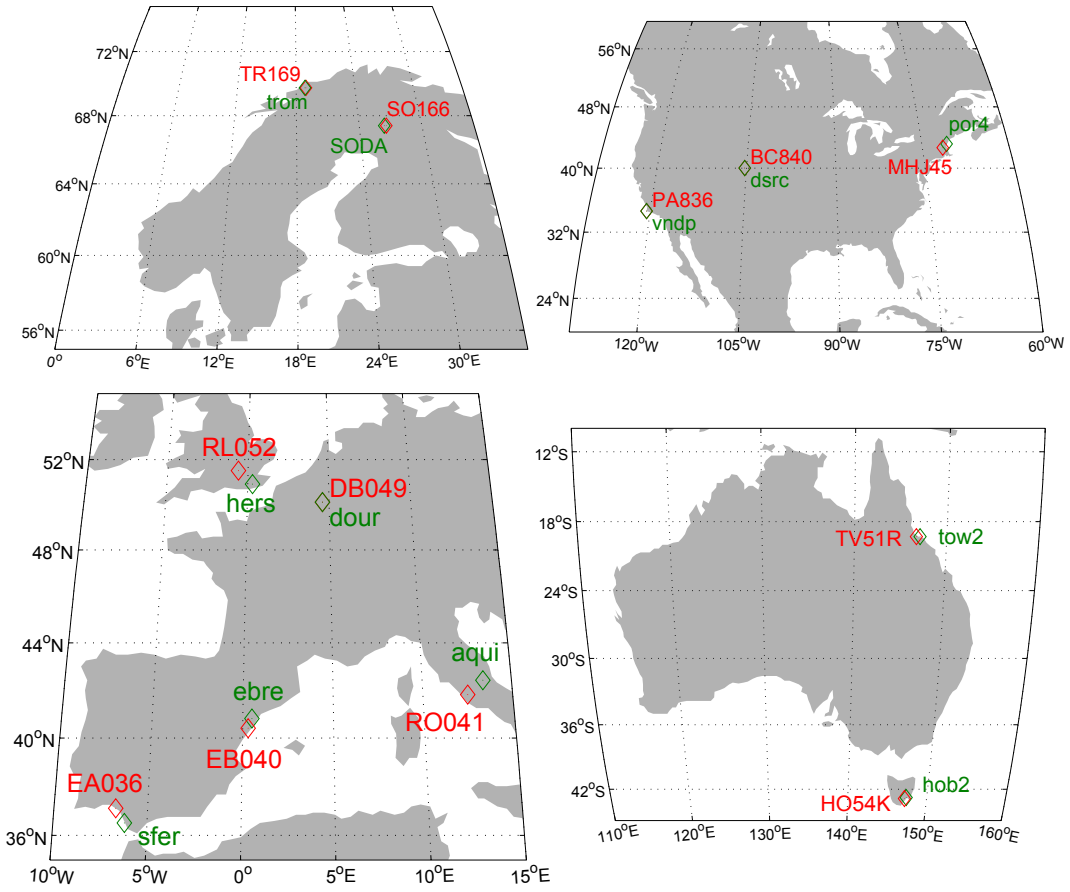

Figure B.3: Co-located ionosondes and GPS stations (top left: high-latitude Europe; bottom left: mid-latitude Europe; top right; North America; bottom right: Australia).

Table B.1: Stations identification.

Location	Ionosonde	Type	Lat. [°N]	Long. [°E]	GPS station	Network	Distance from ionosonde [km]
Tromso	TR169	DGS	69.6	19.2	trom	IGS	16
Sodankyla	SO166		67.4	26.6	soda	EUREF	9
Chilton	RL052	DGS	51.5	-0.6	hers	IGS	91
Dourbes	DB049	DGS	50.1	4.6	dour	EUREF	0
Rome	RO041		41.9	12.5	aqui	EUREF	93
Roquetes	EB040	DGS	40.8	0.5	ebre	IGS	0
El Arenosillo	EA036	DGS	37.1	-6.7	sfer	IGS	80
Millstone Hill	MHJ45	DGS	42.6	-71.5	por4	CORS	86
Boulder	BC840	DGS	40.0	-105.3	dsrc	CORS	0
Point Arguello	PA836	DGS	34.8	-120.5	vndp	IGS	24
Townsville	TV51R		-19.6	146.9	tow2	IGS	40
Hobart	HO54K		-42.9	147.3	hob2	IGS	14

B.2.4 Data sets

In this study, we use three kinds of ionospheric data: ionosonde parameters, $sTEC$ and $vTEC$. For the first, we consider manually validated measurements mainly obtained by ionosondes (Altadill et al., 2009)[2] and, for the others, GPS-derived data calibrated by means of Global Ionospheric Maps (GIM) (Hernández-Pajares et al., 2009)[3]. As explained in Bidaine & Warnant (2010), the maps provide $sTEC$ values to estimate the ambiguities of the phase geometry-free combination (Orus et al., 2007b). Finally, a subset of $sTEC$ values corresponding to high elevation angles multiplied by the appropriate mapping function are averaged every 15 min to obtain $vTEC$ at stations where ionosonde data are available (Warnant & Pottiaux, 2000).

For the sake of consistency and to enable the comparison described in next subsection, we select 12 locations with co-located ionosonde – DGS when digisonde (Galkin et al., 2006) – and GPS station belonging to IGS, EUREF and CORS (Snay & Soler, 2008) networks (cf. Fig. B.3 and Tab. B.1). We also focus on a high solar activity period (year 2002).

We give the availability levels of each kind of data and for the combined use of ionosonde parameters and $vTEC$ in Fig. B.4. We count maximum 1,051,200 GPS $sTEC$ measurements (one every 30 s corresponding to the standard sampling rate of GPS observations), 35,040 GPS $vTEC$ values (one every quarter) and 8760 sets of ionosonde parameters (soundings every hour). We explain partially the lower availabilities

- for ionosonde parameters, because no data is available for some months (Tromso: January to April; El Arenosillo: August and September; Townsville and Hobart: November and December; Dourbes and Boulder: January; Point Arguello: July)
- and for $vTEC$, because the odd-hour IONEX format for the GIM leads to a systematic gap between 23 and 1 UT[4] and because less $sTEC$ data are available at high elevation angles for high-latitude stations (Tromso and Sodankyla).

[2]Most of these measurements were downloaded from the World Data Center for Solar-Terrestrial Physics at Chilton, UK (`http://www.ukssdc.ac.uk/wdcc1/data_menu.html`).

[3]The data set used was computed at ESA using UPC GIMs.

[4]On the one hand, GIM are provided in daily files containing maps every two hours from 1 to 23 UT until November 2nd, 2002. On the other hand, two consecutive maps of a given day are used to compute TEC values at a given location and time. Hence no $vTEC$ data is available for periods outside any 2-hour interval between two maps ie before 1 and after 23 UT.

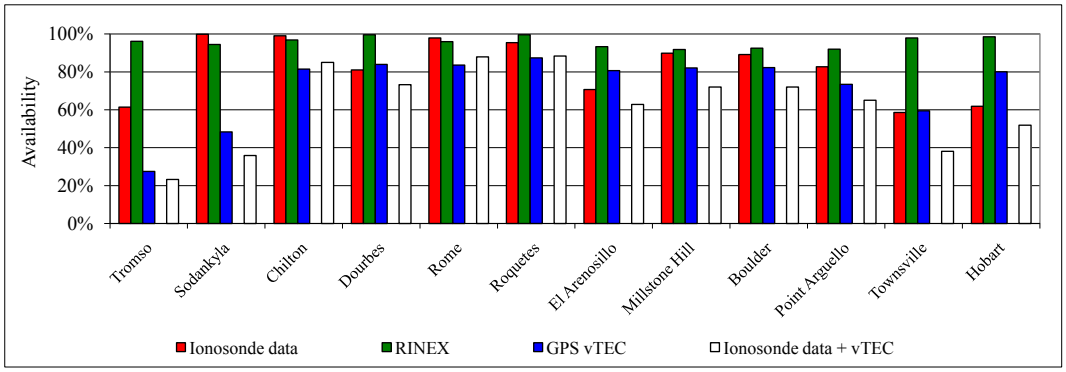

Figure B.4: Data availability.

B.2.5 Analysis method

The first step of our analysis consists in uncoupling NeQuick formulation from its underlying data. As explained in Bidaine & Warnant (2010), we use ionosonde parameters (measured values of f_oF_2 and $M(3000)F_2$) instead of the CCIR maps to obtain a daily representation of the ionosphere in place of the standard monthly median electron density.

Our following and main focus involves a data ingestion scheme similar to the one which will be run at each GSS. We generate daily Az values using the Brent optimisation method (Brent, 1973) with all available satellite-to-receiver ray paths[5]. This allows us to observe how data ingestion can cope with NeQuick intrinsic residual errors. Investigating next the use of the previous day Az will bring us even closer to the Galileo SF ICA. Hence we will quantify the impact of this pragmatic option.

Finally we consider Galileo and GPS SF ICA. It is worth noting that we simulated Galileo broadcast coefficients by means of $sTEC$ obtained from UPC GIMs at the stations of the simulated IOV ground segment (cf. Fig. B.1).

To compare the results of these different techniques, we analyse different statistics of $vTEC$ (mean, standard deviation of the difference between measured and modelled values $\sigma_{\Delta TEC}$ or relative standard deviation $\sigma_{\Delta TEC,Relative}$; cf. eqs. B.5 to B.7) and different time frames (yearly or monthly).

$$\overline{\Delta TEC} = \langle TEC_{meas} - TEC_{mod} \rangle \tag{B.5}$$

$$\sigma_{\Delta TEC} = \sqrt{\left\langle \left(TEC_{meas} - TEC_{mod} - \overline{\Delta TEC} \right)^2 \right\rangle} \tag{B.6}$$

$$\sigma_{\Delta TEC,Relative} = \frac{\sigma_{\Delta TEC}}{\langle TEC_{meas} \rangle} \tag{B.7}$$

For computing yearly statistics, we also group the stations in four regions (cf. Fig. B.3) as long as the features of the ionosphere can be considered homogeneous within these regions.

B.3 Analysis

B.3.1 Ionosonde parameters constrain

Constraining NeQuick with ionosonde parameters allows us to investigate the intrinsic behaviour of the model. The data ingestion scheme will indeed drive this initial situation towards measured TEC. In this context, we first examine

[5] To limit computation time, we actually used a 30-minute sampling rate.

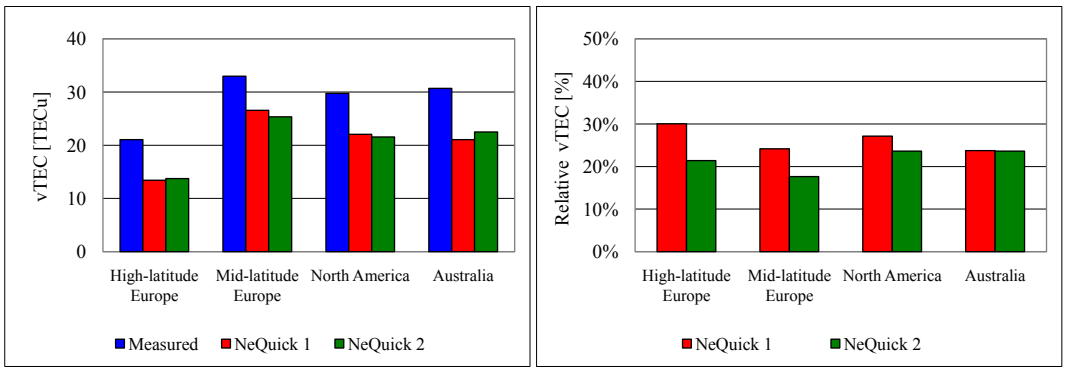

Figure B.5: Yearly $vTEC$ mean (left) and relative standard deviation (right) corresponding to ionosonde parameters constrain.

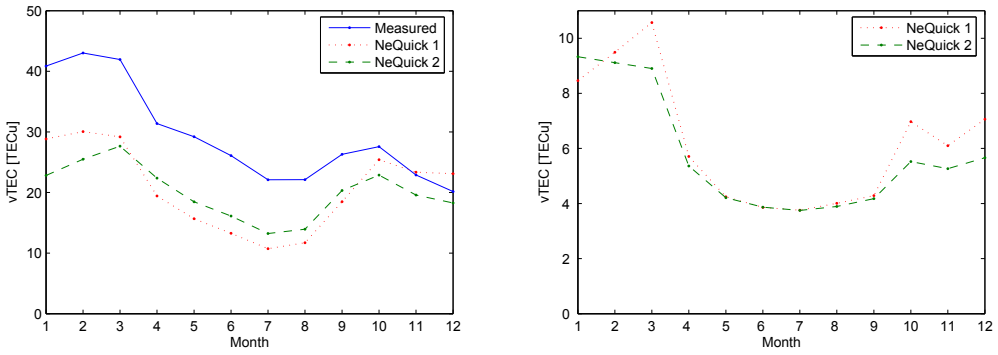

Figure B.6: Monthly $vTEC$ mean (left) and standard deviation (right) for Millstone Hill.

yearly statistics of $vTEC$. To obtain consistent statistics, we do not consider the months January to April for Sodankyla as ionosonde parameters are not available for Tromso in this period. The same statement applies to the Australian stations for November and December.

Fig. B.5 shows the influence of latitude: lower mean TEC values are observed at high latitudes (21 $TECu$ for high-latitude Europe by comparison to 33 for mid-latitude Europe, 30 for North America and 31 for Australia). We also state an average underestimation of about 25% of both versions of the model, which evolves differently between NeQuick 1 and NeQuick 2 for the different regions. It is increasing for mid-latitude Europe (by about 19%) and North America (by about 7%) and apparently decreasing for high-latitude Europe (by about 4%) and Australia (by about 15%). However we must not forget that several months of data are not included in the statistics for the last two regions. Hence the following discussion on monthly statistics will help us to clarify the situation.

The observed underestimation has to be interpreted carefully regarding the GPS TEC reconstruction technique. As outlined by previous studies (Ciraolo et al., 2007; Prieto-Cerdeira et al., 2006; Orus et al., 2007a; Bidaine & Warnant, 2009b), the latter may indeed be affected by discrepancies of several $TECu$ at least comparing it with other techniques. The levelling procedure seems here to lead to important consequences, including on the interpretation of the detected bias of the model, a part of which might have to be attributed to the measurements.

The right panel of Fig. B.5 presents the relative standard deviation which amounts about 24%. Its reduction by about 17% for NeQuick 2 indicates an improvement from the second version of the model. In particular its decrease reaches about 28% in Europe, 13% in North America and is very small in Australia where the result must be interpreted considering the missing data for this region.

To refine our analysis, we investigate monthly statistics an example of which is given in Fig. B.6 for Millstone Hill. We find the same underestimation than for yearly statistics apart from November and December for NeQuick 1. Regarding the evolution from one version of the model to the other, we note decreasing biases for April to September, increasing underestimation for the rest of the year and decreasing standard deviations for the whole year apart from January. However the improvement suggested by the lower standard deviations appears rather small for the months April to September. The latter 6-month period seems then distinct from the other in terms of bias as well as standard deviation.

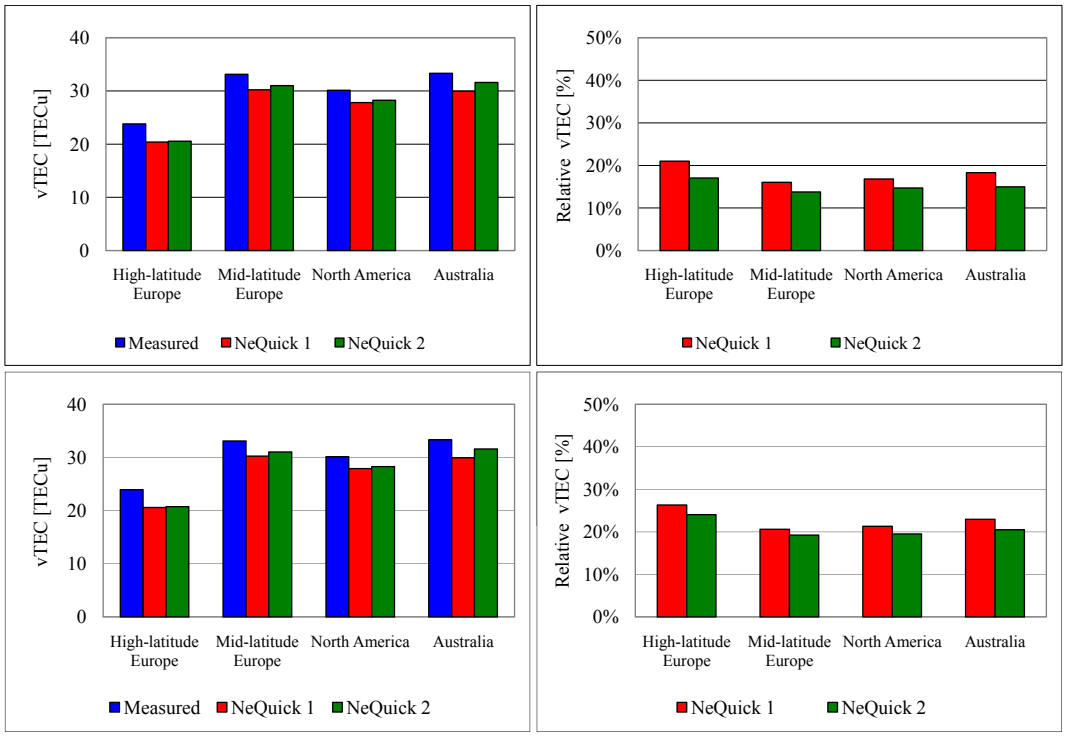

Figure B.7: Yearly $vTEC$ mean (left) and relative standard deviation (right) corresponding to $sTEC$ data ingestion using current day (top) and previous day (bottom) Az.

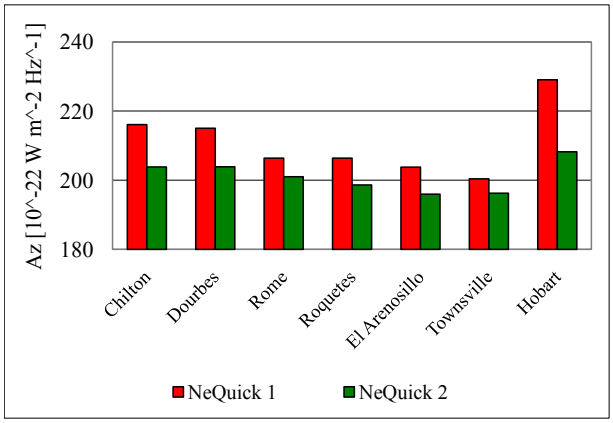

Figure B.8: Yearly Az mean.

As described in Section B.2.1, the major modification between both NeQuick versions is related to the topside. The two formulas (one for April to September and the other for October to March) for the shape parameter k in NeQuick 1 were replaced by a single one in NeQuick 2. Hence the two identified periods correspond to the k formulas in NeQuick 1, which enables to get different statistics for both of them. In the illustrated example, the bias decreases for the first period and the standard deviation for the second, leading to an homogenisation of NeQuick performances all along the year. An expected significant bias increase from November to March would then have influenced yearly statistics for high-latitude Europe and Australia in a consistent way with the other regions. A similar reasoning can be followed for November and December in the Australian region regarding the standard deviation.

Finally considering the overall scheme for this use of the model, we conclude that it provides the best results in mid-latitude Europe and that it works the worst in high-latitude Europe.

B.3.2 Slant TEC data ingestion

For this second part of the study, we do not need ionosonde parameters anymore. Hence the yearly statistics in which we are interested are not affected by missing months anymore. To perform $sTEC$ data ingestion, we generate daily Az values which minimise the RMS difference between modelled and measured $sTEC$ data of each entire day at a given station. Then we run the model with these parameters to compute $vTEC$ to be compared with GPS $vTEC$.

We still observe an underestimation for both versions of NeQuick (cf. Fig. B.7) but it drops to about 8% by comparison with the use in combination with ionosonde measurements. Unlike for that use, it is decreasing between NeQuick 1 and NeQuick 2 for all regions (about 5% for high-latitude Europe, 27% for mid-latitude Europe, 19% North America and 49% for Australia). Thus the bias is absorbed thanks to data ingestion even better with NeQuick 2.

In terms of relative standard deviation, the average is much smaller than in the first part of the analysis (about 16%). The modifications of the second version of the model reduce the standard deviation by about 15%. Therefore both indicators show better performances for NeQuick 2 and how $sTEC$ data ingestion can handle the model residual errors. They also confirm the best case for mid-latitude Europe and the worst for high-latitude Europe.

Another interesting characterisation of $sTEC$ data ingestion results concerns the effective ionisation level Az. This parameter plays the role of the solar activity input of the NeQuick model. The use of the monthly smoothed sunspot number R_{12}, the adequate index to accommodate CCIR maps and provide monthly median output, or various solar flux averages leads to biases. In our case, the absorption of the corresponding underestimation obtained when

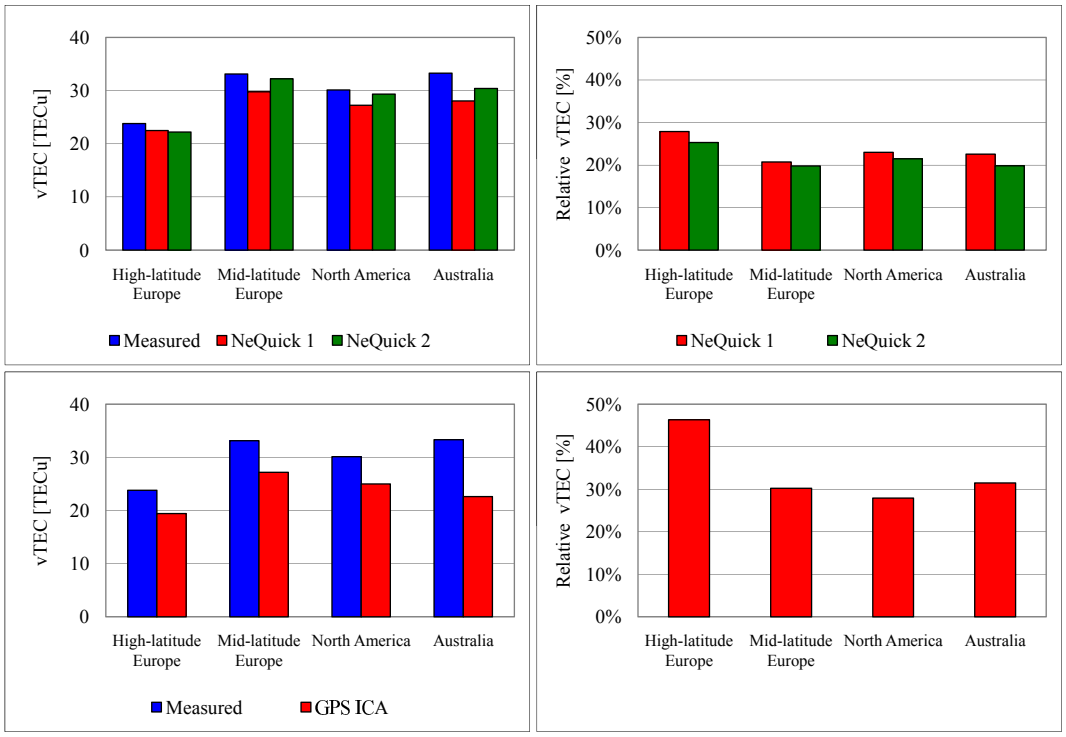

Figure B.9: Yearly $vTEC$ mean (left) and relative standard deviation (right) corresponding to the Galileo (top) and GPS (bottom) SF ICA.

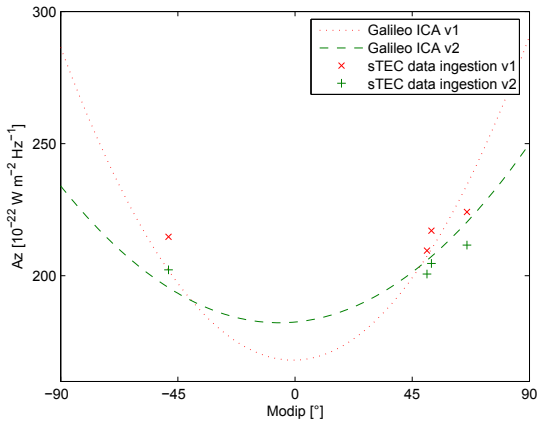

Figure B.10: Comparison between yearly Az mean obtained from Galileo broadcast coefficients and $sTEC$ data ingestion.

constraining NeQuick with ionosonde parameters induces Az values (cf. Fig. B.8) larger than the converted R_{12} (yearly mean $\simeq 147$ $[10^{-22}Wm^{-2}Hz^{-1}]$) or even than solar flux (yearly mean of daily flux $\simeq 179.5$ $[10^{-22}Wm^{-2}Hz^{-1}]$).

Even if the bias is larger for NeQuick 2, lower values of Az are computed thanks to its better topside formulation. The $vTEC$ values obtained with NeQuick 2 depend indeed more linearly on Az than those from NeQuick 1. Consequently, in many cases, a smaller increase in Az within some intermediate interval (e.g. between 140 and 240 flux units for most of the year at Dourbes) leads to the same gain in $vTEC$. The dependence of Az towards latitude – increasing towards high latitudes – justifies also the representation of the global daily Az for the Galileo algorithm as a second order polynomial of μ.

For the Galileo SF ICA, the broadcast coefficients valid for one day will be estimated from the effective parameters of the previous day. Using the latter instead of the current day Az values enables us to focus on the impact of the day-to-day variability only. On the one hand, we notice a comparable underestimation (around 8% on average) for both versions (cf. Fig. B.7). On the other hand, the relative standard deviation increases up to 21% on average. The other observations detailed for sTEC data ingestion using current day Az are similar for all regions and versions of NeQuick.

B.3.3 Ionospheric correction algorithms

The last step of our reasoning relates to the ionospheric corrections provided to single frequency users. In the case of Galileo, we calculate NeQuick daily effective parameters at our 12 test locations from the simulated broadcast coefficients of the IOV phase (cf. Section B.2.3). As in the previous subsections, we inspect yearly statistics of $vTEC$ (cf. Fig. B.9) and we compare them with the latest use of previous day Az. We still obtain an underestimation, larger for NeQuick 1 (around 10% for mid-latitude Europe and North America, about 16% for Australia) except for high-latitude Europe (dropping to 5%), and smaller for NeQuick 2 (less than 3% for mid-latitude Europe and North America, 7% for high-latitude Europe) except for Australia (9%). Considering the relative standard deviation, the only noticeable increase appears for North America. Therefore the influence of the interpolation of Az from the broadcast coefficients seems much smaller than the day-to-day variability.

The above-described evolution of $vTEC$ underestimation can be explained comparing, for the different regions of interest, yearly means of Az involved in the Galileo ionospheric correction and local one (cf. Fig. B.10; crosses for the second and corresponding points on the curves for the first). Indeed we find corresponding differences between Az values for both uses of NeQuick: negative for NeQuick 1 (inducing a larger $vTEC$ bias) except for high-latitude Europe, and positive for NeQuick 2 (leading to a smaller $vTEC$ bias) except

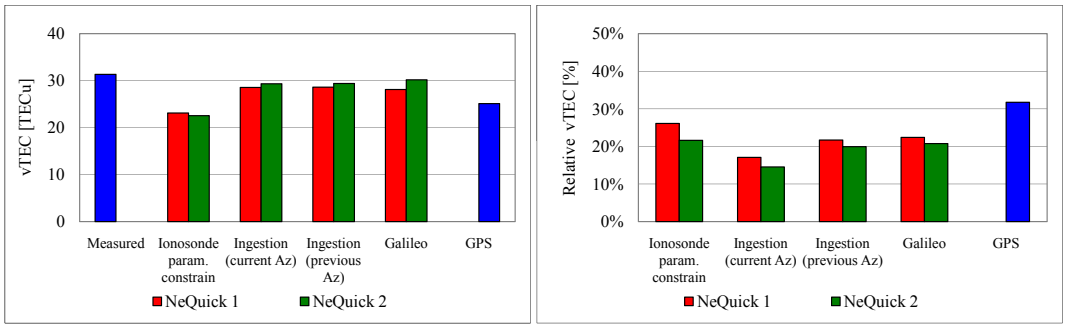

Figure B.11: Yearly $vTEC$ mean (left) and relative standard deviation (right) corresponding to analysed modelling techniques.

for Australia. Several statements related to $sTEC$ data ingestion effective parameters (cf. Fig. B.8) still hold in this case. All interpolated Az values exceed the yearly mean converted R_{12}. The improved topside formulation leads to smaller Az variations for NeQuick 2 (smaller range of values between minimum at low latitudes and maximum at high latitudes).

Finally a comparison between Galileo and GPS ionospheric corrections is of prime interest. The GPS SF ICA also underestimates $vTEC$ (by around 18% except for Australia with about 32%; cf. Fig. B.9). However the computed biases amount between about 1.8 (mid-latitude Europe and North-America for NeQuick 1) and around 6.5 (same regions for NeQuick 2) times those of the Galileo SF ICA. The ratio between GPS and Galileo standard deviations equals around 1.5 with a value of around 30% for this statistic in the case of the Klobuchar algorithm (except for high-latitude Europe with about 46%). Following its design drivers (main interest in the CONUS area), it reaches its best performances in North America.

B.3.4 Synthesis

In the current section, we have been able to differentiate the performances of the different steps of the Galileo ionospheric correction for single frequency users in terms of $vTEC$. To reach this goal, we established yearly statistics for the year 2002 at 12 locations (cf. Fig. B.11; mean $vTEC$ of 31 $TECu$).

We depicted an 8% underestimation for both versions of NeQuick in the cases involving $sTEC$ data ingestion. This value was three times larger when constraining the model with ionosonde parameters. NeQuick 2 provided better means than NeQuick 1 for cases involving ingestion (more than twice for the Galileo ICA) but worse for the first use of the model. Comparing the latter to $sTEC$ data ingestion, we observed averages decreasing by 2.5–4. Replacing the effective parameters by their values for the previous day did not imply significant modifications. On the contrary, employing the effective ionisation level deduced from simulated broadcast coefficients lead to a different evolution for NeQuick 1 (about 20% larger underestimation) and NeQuick 2 (about 40% smaller). For the same situations, the GPS ICA ended up with a 20% underestimation. If performed thus better than when NeQuick was driven with ionosonde parameters but worse than procedures involving data ingestion. Considering Galileo ionospheric correction in particular, the bias equalled twice and 5 times those obtained with NeQuick 1 and 2 respectively.

The second major statistic assessed consisted in the relative standard deviation of the difference between modelled and measured $vTEC$. Its values ranged from 15% ($sTEC$ data ingestion, NeQuick 2) to 26% (ionosonde parameters constrain, NeQuick 1). We outlined better results from NeQuick 2 in all cases (around 15% improvement for the first two techniques, less than

10% when using the previous day Az and for the Galileo ICA). $sTEC$ data ingestion presented the best figures, 34% smaller than when replacing CCIR maps by ionosonde measurements. Operating NeQuick with effective parameters of the previous day or based on broadcast coefficients instead of those of the current day raised the relative standard deviation by 27% to 43%. In any case, it remained below the level of 32% exhibited by the GPS ICA. For the latter, we stated a 1.5-ratio with respect to the Galileo ionospheric correction.

B.4 Conclusion and perspectives

As a tool allowing to exploit different ionospheric data, the NeQuick model can be used in combination with GNSS $sTEC$ data in the framework of an optimisation procedure called data ingestion. Instead of using solar flux as input, a new parameter, the "effective ionisation level" Az, is then computed in order to minimise the model mismodelling from a specific set of $sTEC$ data. This technique constitutes the basis of the Galileo SF ICA.

In order to understand how data ingestion accommodates the model residual errors, we first constrained NeQuick with ionosonde data to characterise its intrinsic mismodelling. We analysed statistically the difference between GPS-derived vertical TEC and corresponding modelled values for a dozen stations distributed in four mid-latitude and high-latitude regions for the last solar maximum in 2002. We also considered the latest version of the model in order to quantify the evolution from the current ITU baseline. We found standard deviations decreasing by around 17% to reach about 22% in relative values with NeQuick 2; biases increasing by about 8% up to around 26% on average (care must be taken about GPS TEC data regarding the bias). Examining monthly statistics, we highlighted the influence of the unification of the topside shape parameter k as the two former formulas corresponded with periods exhibiting opposite behaviours. We identified the region exhibiting the best results as mid-latitude Europe and the one with the worst as high-latitude Europe.

In a second step, we examined results of $sTEC$ data ingestion. Computing daily Az values, we reached biases of about 8% and standard deviations of about 16%. We also obtained better statistics with NeQuick 2 (decrease of 27% in bias and 15% in standard deviation). We stated that Az values are much larger than the usual solar indices as they must drive TEC to accommodate residual errors. We also noted the dependence of Az on latitude: increasing towards high latitudes. Running NeQuick with the previous day effective ionisation level, another common characteristic with the Galileo ionospheric correction, mainly impacted the relative standard deviation which enlarges then to about 21%.

Ultimately we compared the Galileo and GPS SF ICA. For the first, the parabolic formulation of Az in function of modip and the broadcast coefficients primarily induced a larger underestimation for NeQuick 1 (11%) and a smaller one for NeQuick 2 (4%). We explained this difference by a larger sensitivity to Az variations for the second version of the model. Nevertheless we concluded to a better correction for Galileo than for GPS taking into account the 20% bias and the 32% standard deviation of the Klobuchar algorithm.

To deepen our analysis, we will consider statistics of other ionospheric parameters such as $sTEC$ or maximum electron concentrations. This will allow us to investigate the interest of different data ingestion schemes based on the NeQuick model (Buresova et al., 2009) and their applicability to GNSS applications. Another important user-oriented future research direction will relate to the ionospheric corrections performances in terms of position.

(Bidaine, Lonchay et Warnant, 2012)

Galileo Single Frequency Ionospheric Correction: Performances in Terms of Position

Abstract For GPS single frequency users, the ionospheric contribution to the error budget is estimated by the well-known Klobuchar algorithm. For Galileo, it will be mitigated by a global algorithm based on the NeQuick model. This algorithm relies on the adaptation of the model to slant Total Electron Content (sTEC) measurements. Although the performance specifications of these algorithms are expressed in terms of delay and TEC, the users might be more interested in their impact on positioning. Therefore, we assessed the ability of the algorithms to improve the positioning accuracy using globally distributed permanent stations for the year 2002 marked by a high level of solar activity. We present uncorrected and corrected performances, interpret these and identify potential causes for Galileo correction discrepancies. We show vertical errors dropping by 56–64 % due to the analyzed ionospheric corrections, but horizontal errors decreasing by 27 % at most. By means of a fictitious symmetric satellite distribution, we highlight the role of TEC gradients in residual errors. We describe mechanisms permitted by the Galileo correction, which combine sTEC adaptation and topside mismodeling, and limit the horizontal accuracy. Hence, we support further investigation of potential alternative ionospheric corrections. We also provide an interesting insight into the ionospheric effects possibly experienced during the next solar maximum coinciding with Galileo Initial Operation Capability.

Keywords Galileo, positioning, ionospheric correction, single frequency, NeQuick model, data ingestion

C.1 Introduction

Since Global Navigation Satellite Systems (GNSS) signals travel through the atmosphere, GNSS receiver operation largely depends on the dynamics of the ionosphere. Most civilian receivers model the ionospheric delay to mitigate its effect on positioning. When processing single frequency measurements only, they cannot compensate for ionospheric errors by taking advantage of ionosphere dispersion causing differential effects between frequencies. They run an internal model fed with external information about the state of the ionosphere disseminated by the navigation system. Hence, the Global Positioning System (GPS) broadcasts 8 coefficients suited for the ionospheric correction algorithm (ICA) designed by Klobuchar (1987). The future Galileo system will transmit 3 coefficients a_0, a_1 and a_2 dedicated to the NeQuick model, the core of the so-called Galileo single frequency ionospheric correction algorithm (Hofmann-Wellenhof et al., 2008). For the solar activity input of the model, these coefficients define an "effective ionization level" Az as a second-order polynomial of the receiver modified dip-latitude (modip) μ,

$$Az = a_0 + a_1\mu + a_2\mu^2 \tag{C.1}$$

with

$$\tan\mu = \frac{I}{\sqrt{\cos\varphi}} \tag{C.2}$$

being a function of the geomagnetic inclination I and the geographic latitude φ (Rawer, 1963). The coefficients will be issued daily by the Galileo Mission Segment based on data adaptation via an optimization procedure to find the best input for the model to fit a specific dataset. This procedure will be performed at each Galileo Sensor Station (GSS): Each GSS will routinely measure the slant Total Electron Content (slant TEC or sTEC) toward each satellite and compute the Az value minimizing the root mean square (RMS) difference between measured and modeled sTEC,

$$\mathrm{RMS} = \sqrt{\left\langle \left(sTEC_{mod}(Az) - sTEC_{meas}\right)^2 \right\rangle} \tag{C.3}$$

Future GNSS single frequency applications will depend on the capability of the GPS and Galileo algorithms to account for the ionospheric delay but even more to reduce positioning errors. Consequently we investigated the positioning accuracy reached with ionospheric corrections supplied by these algorithms. For Galileo, we considered three different versions of the underlying NeQuick model: NeQuick 1 (Radicella & Leitinger, 2001), which is publicly available from the ITU-R website (ITU-R Rec. P.531; `http://www.itu.int/oth/R0A04000018/en`), NeQuick G, which will be implemented in Galileo and was kindly provided by the European Space Agency (ESA), and NeQuick 2 (Nava et al., 2008), furnished by the model designers at the Abdus Salam International Centre for Theoretical Physics (ICTP). We performed stand-alone

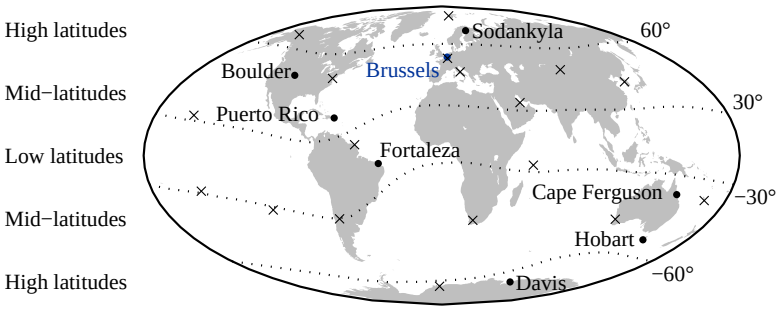

Figure C.1: Location of the GPS stations selected as test sites (dots) and representative IOV GSS (crosses). These stations cover all modip bands.

Table C.1: Characteristics of the GPS stations selected as test sites.

Station	Code	Network	Modip [°]
Sodankyla	SODA	EUREF	65.2
Brussels	BRUS	IGS/EUREF	55.3
Boulder	DSRC	CORS	53.5
Puerto Rico	PUR3	CORS	39.7
Fortaleza	FORT	IGS/CORS	–8.7
Cape Ferguson	TOW2	IGS	–40.1
Hobart	HOB2	IGS	–55.3
Davis	DAV1	IGS	–64.3

point positioning from GPS single frequency code measurements. We used the actual broadcast coefficients from GPS RINEX files to apply the Klobuchar algorithm. Regarding NeQuick, we simulated them for the In-Orbit Validation (IOV) phase of Galileo (Bidaine & Warnant, 2011). We selected 18 stations belonging mainly to the International GNSS Service (IGS) (Dow et al., 2009) to represent the GSS (Fig. C.1). At these stations, we adapted the model to sTEC values calibrated by means of IGS Global Ionospheric Maps (GIM) (Orus et al., 2007b; Hernández-Pajares et al., 2009).

We discuss the impact of several real and simulated single frequency ionospheric corrections on positioning. First we characterize the correction performances for the high solar activity year 2002. Second we propose an intuitive interpretation of these performances in particular for horizontal positioning. Third we identify different potential origins for the observed discrepancies of the Galileo correction.

C.2 Ionospheric corrections performances

We derived ionospheric correction performances studying 8 test sites. These sites cover all modip bands (Fig. C.1) and should therefore involve ionospheric conditions characteristic for low, mid- and high latitudes at solar maximum. The associated GPS stations (Table C.1) belong to the IGS, the European Reference Frame (EUREF) Permanent Network (Bruyninx, 2004) or the Continuously Operating Reference Stations (CORS) network (Snay & Soler, 2008) and provide at least 90 % RINEX data availabilities for 2002. They also lie in the vicinity of ionosondes that are potentially useful for further investigation.

This section describes the performances of the Klobuchar and NeQuick models for the chosen sites and year. First we consider their effectiveness in terms of sTEC, which is the primary parameter they are intended to provide for each satellite in view. Moreover, this parameter—the equivalent ionospheric delay for the Klobuchar algorithm—is employed for dedicated system specifications. Then we focus on the positioning errors reduction enabled by the corrections which informs about services accuracy. Finally we address the spatio-temporal variability of the observed positioning performances.

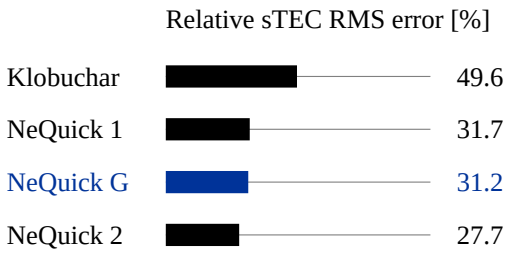

Figure C.2: Relative sTEC RMS error obtained with the ionospheric corrections in 2002. The NeQuick model exhibits better performances in terms of sTEC by comparison with the Klobuchar model.

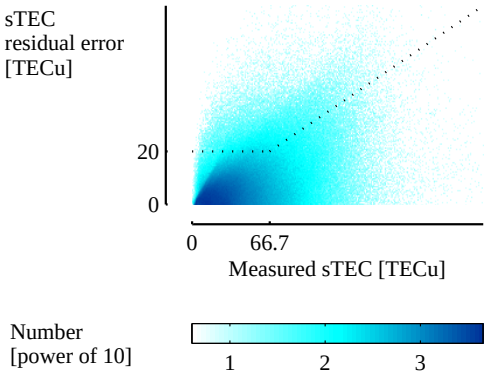

Figure C.3: sTEC residual errors from NeQuick G compared to the Galileo algorithm specifications in 2002. 93 % of the residual errors meet the specifications (below the dotted line).

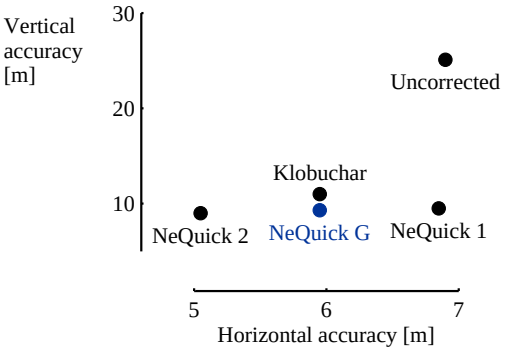

Figure C.4: Positioning accuracies obtained with and without the ionospheric corrections in 2002. The corrections improve more the vertical accuracy than the horizontal one. These numbers correspond to the 95th percentile of absolute horizontal and vertical positioning errors.

C.2.1 sTEC

In order to analyze sTEC modeling, we compared modeled values to GPS-derived data calibrated by means of GIM. The latter reference sTEC measurements were generated from the geometry-free phase combination of which the ambiguities were computed using sTEC estimates from IGS maps (Orus et al., 2007b). From all the available differences between these reference measurements and corresponding modeled values for the selected year and sites, we calculated the relative RMS errors (Fig. C.2): We divided the absolute RMS errors by the mean measured sTEC which amounts to 44 TECU (1 TECU equals $10^{16}\ m^{-2}$ and induces an error of 0.16 m on the L1 carrier).

According to the sTEC statistics, NeQuick outperforms the Klobuchar model. Even if the Klobuchar model fits the declared performance of 50 % RMS correction, it underestimates sTEC by 11 TECU and the standard deviation of its differences equals 19 TECU. NeQuick 1 and G yield biases 5 and 7 times smaller and 27 % reduced standard deviations. In agreement with other studies (Orus et al., 2007a), NeQuick 2 significantly decreases the mean sTEC difference below 1 TECU and ends up with a 12-TECU standard deviation, that is, 11 % less than the other versions.

NeQuick complies with the Galileo algorithm specifications for the stations and year of study. This algorithm has been designed to limit the residual error to 30 % of the actual sTEC or 20 TECU, whichever is larger. In our simulation using NeQuick G, 93 % of the residual errors meet this criterion (Fig. C.3). This proportion is less than 1 % smaller for NeQuick 1 and larger for NeQuick 2 and is consistent with previous results (Prieto-Cerdeira et al., 2006). By comparison with the other versions, the compliant data for NeQuick 2 include more large sTEC measurements—larger than $\frac{20TECu}{30\%} \simeq 66.7TECu$, associated to large residual errors—but less smaller sTEC measurements.

C.2.2 Positioning errors

The second performance analysis dealt with differences between the actual position of the test stations and the ones computed with and without each ionospheric correction. Thanks to the gLAB software tool suite (Hernandez-Pajares et al., 2010), we performed single-point single-epoch (SPSE) positioning characteristic of the operation of a typical mass-market single frequency receiver: We used L1 C/A pseudorange measurements, broadcast orbits, clocks and hardware biases as well as a simple nominal tropospheric model and the Niell mapping function. As such this processing corresponds to a first "uncorrected" case. Applying additional pseudorange corrections accounting for the ionospheric delay using each model renders the four other cases. To this extent, we integrated adequate NeQuick-related instructions into gLAB. We synthesized the results in terms of horizontal and vertical 95 % accuracies (Fig.

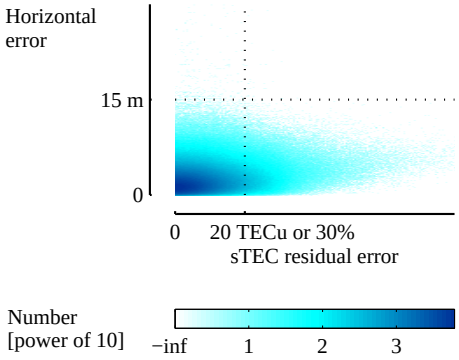

Figure C.5: Combined comparison of sTEC residual errors and horizontal residual errors from NeQuick G to the Galileo ionospheric correction algorithm and Open Service specifications in 2002. The sTEC specifications (on the left of the vertical dotted line) and the positioning requirements (below the horizontal dotted line) are met simultaneously for 93 % of the residual errors. However, sTEC and horizontal errors outside specifications do not necessarily correspond to each other. The sTEC residual error axis consists in a hybrid scale using TECU for values associated to measured sTEC smaller than 66.7 TECU and % otherwise. It enables a graphical comparison to the Galileo algorithm specifications (depicted by a straight line when aligning 20 TECU and 30 %) independently from the measured sTEC.

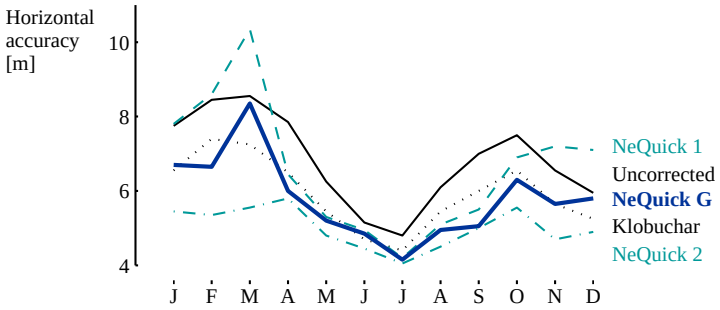

Figure C.6: Monthly variability of the horizontal accuracy obtained with and without the ionospheric corrections (continuous line for uncorrected case, dotted for Klobuchar, dashed for NeQuick 1, thick for NeQuick G and dash-dotted for NeQuick 2).

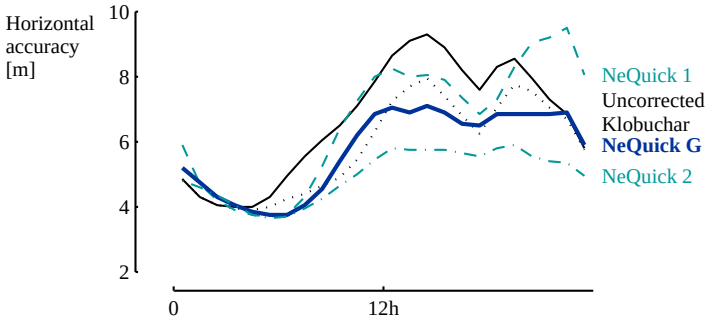

Figure C.7: Local time variability of the horizontal accuracy obtained with and without the ionospheric corrections (continuous line for uncorrected case, dotted for Klobuchar, dashed for NeQuick 1, thick for NeQuick G and dash-dotted for NeQuick 2).

C.4), as these metrics are regularly used in services specifications, for example, 15 and 35 m for the Galileo single frequency open service (Hofmann-Wellenhof et al., 2008).

All the ionospheric corrections analyzed increase the positioning accuracy with respect to the uncorrected case at different levels, however, for the horizontal and vertical components. The vertical error (25.1 m) drops significantly for the Klobuchar algorithm (–56 %) and even more with successive NeQuick versions (–62 %, –63 % and –64 %). On the other hand, the horizontal error (6.9 m) decreases much less with the Klobuchar, NeQuick G and 2 models (–14 %, –14 % and –27 %) but barely with NeQuick 1. These results easily reach the target performance specifications of the Galileo single frequency open service. However, they suggest to investigate the correlation between sTEC and positioning residual errors which is low (Fig. C.5). They bring forward the influence of the satellite sky distribution explaining partially this decorrelation as well as the generally larger vertical errors by comparison to horizontal ones. Given the chosen year, these errors likely exceed those obtained for lower solar activity periods. Furthermore, they do not correspond to ionosphere mismodeling only. They are indeed largely affected by the accuracy of the various products implemented (orbits, clocks, hardware biases and troposphere) as well as code noise and multipath which should be smaller for Galileo than for the GPS data exploited for this simulation.

C.2.3 Spatio-temporal variability

Looking for explanations for the differences between the obtained positioning performances, we inspected their variations in space and time. In particular, we examined 95th-percentile dependencies on month, local time and modip, three variables conditioning the state of the ionosphere. As the effectiveness of the ionospheric corrections appears more questionable for horizontal positioning, we focused on this component.

The monthly horizontal accuracy shows a similar trend as the TEC, having maxima around the equinoxes (Fig. C.6). It is uniformly improved by any of the ionospheric corrections considered apart by NeQuick 1, which exhibits larger values than the uncorrected case for about half of the year (November to March). It is the best with NeQuick 2 and better with NeQuick G than with Klobuchar for two-third of the year.

The intra-day variability of horizontal errors only partially resembles the TEC profile (Fig. C.7). The uncorrected positioning errors raise faster than TEC in the morning and remain large in the evening. They are partially mitigated by all the corrections except by NeQuick 1 which amplifies them at night. They are handled at best by NeQuick 2. NeQuick G competes again with Klobuchar and especially involves discrepancies at nighttime.

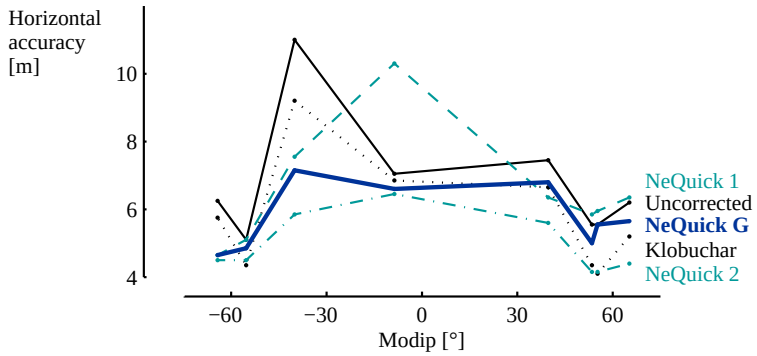

Figure C.8: Modip variability of the horizontal accuracy obtained with and without the ionospheric corrections (continuous line for uncorrected case, dotted for Klobuchar, dashed for NeQuick 1, thick for NeQuick G and dash-dotted for NeQuick 2).

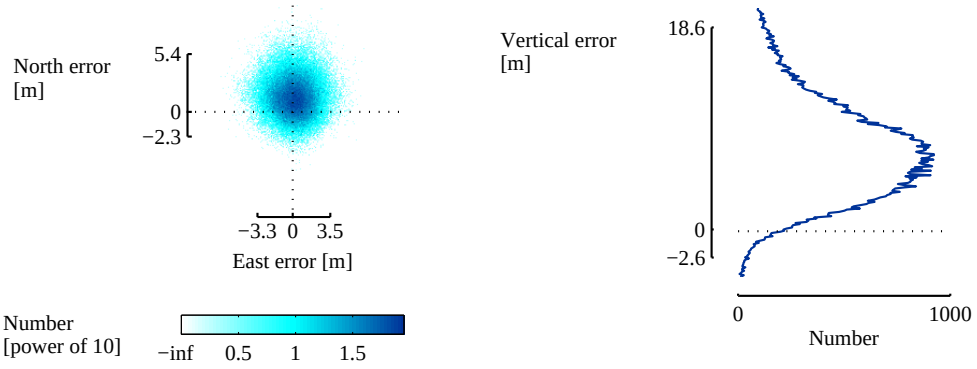

Figure C.9: Distributions of the horizontal (left plot) and vertical (right plot) uncorrected positioning errors at Brussels. The axes represent 2-σ intervals around corresponding means.

The horizontal accuracy shows comparable orders of magnitude at different modip with or without correction with the largest range within the mid-latitude region. Its largest (resp. smallest) values appear at low (resp. high) mid-latitudes unlike TEC (Fig. C.8). The models still provide a correction apart from NeQuick 1 which even adds errors at four stations including Fortaleza. Once more, NeQuick 2 is associated to the best accuracy in nearly all of the cases. NeQuick G and Klobuchar stand between the two other models. In particular, NeQuick G brings only little improvement at Brussels where NeQuick 1 worsens the horizontal accuracy. Hence, Brussels constitutes the worst of the selected sites in terms of positioning performances improvement from the Galileo correction with respect to the uncorrected case. Therefore, this station deserves the focus of the following sections interpreting the positioning performances and dealing with the Galileo correction discrepancies.

C.3 Interpretation

Interpreting the impact of the ionosphere and its modeling on SPSE positioning is not straightforward. Positioning errors do not simply follow TEC trends (Fig. C.8). They depend on the satellite sky distribution, each satellite-to-receiver link probing a different region of the ionosphere. Therefore, we assessed a single station (Brussels) below a smoother ionospheric region. We mainly covered horizontal errors for their rather small correction levels despite the good sTEC performances.

This section addresses the way the ionospheric (residual) delay translates into final coordinates. It successively explains the influence of the ionosphere on uncorrected positions and discusses the conclusions applicability to corrected solutions.

C.3.1 Ionosphere influence on positioning

The distributions of horizontal and vertical uncorrected positioning errors underlying the 95 % accuracies described in the previous section reveal systematic trends at northern mid-latitudes (Fig. C.9). They display average offsets toward the north and up directions. Yet negative heights would intuitively have ensued from ionospheric delays lengthening the pseudoranges from every satellite. The horizontal distribution is also characterized by a larger dispersion along the north axis than along the east one suggesting a larger role of the north error in horizontal accuracy.

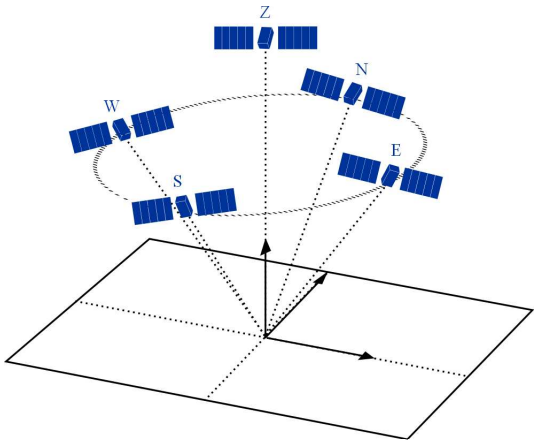

Figure C.10: Fictitious highly symmetrical distribution of 5 satellites. A satellite sky distribution involving 5 fundamental directions (northwards—N, eastwards—E, southwards—S, westwards—W—and at the zenith—Z) yields the simplest analytical expressions binding ionospheric delays to positioning errors.

We referred to the positioning mathematical problem to explain these tendencies (Hofmann-Wellenhof et al., 2008). This problem aims at determining the three coordinate differences $\mathbf{\Delta r}$ from a priori approximations and an unknown bias Δb usually assimilated to the receiver clock error, all gathered in the vector $\mathbf{\Delta x}$. These unknowns relate to the differences $\mathbf{\Delta P}$ between the measured pseudoranges to the n satellites in view of the receiver and the corresponding values computed from the a priori coordinates as follows

$$\mathbf{\Delta P} = A\ \mathbf{\Delta x} + \boldsymbol{\nu} \tag{C.4}$$

with

$$\mathbf{\Delta P} = \begin{pmatrix} \Delta P^1 \\ \vdots \\ \Delta P^n \end{pmatrix}, A = \begin{pmatrix} -\mathbf{u}^1 & 1 \\ \vdots & \vdots \\ -\mathbf{u}^n & 1 \end{pmatrix}, \mathbf{\Delta x} = \begin{pmatrix} \mathbf{\Delta r} \\ \Delta b \end{pmatrix}, \tag{C.5}$$

The corresponding system of equations is usually overdetermined ($n > 4$), with design matrix A containing the satellite unit vectors $\mathbf{u}^i$ ($i = 1$ to n) and least-squares solution (unit weight matrix)

$$\mathbf{\Delta x} = \left(A^T A\right)^{-1} A^T\ \mathbf{\Delta P} \tag{C.6}$$

We further developed our understanding of the influence of the ionosphere on positioning on a particular case of the problem. This particular case involves directly ionospheric delays I^i in place of the observations ΔP^i producing positioning errors induced only by the ionosphere (Mohino, 2008). It enables the development of the matrix $\left(A^T A\right)^{-1} A^T$ to obtain analytical expressions binding ionospheric delays to positioning errors through a fictitious highly symmetrical satellite distribution. This distribution consists of one zenithal satellite and an even number of satellites at constant elevation η uniformly distributed in azimuth. The simplest example of such a distribution comprises five satellites, one at the zenith and the others toward each cardinal direction (Fig. C.10).

This particular case yields simple formulas for horizontal errors:

$$\Delta N = \frac{1}{2\cos\eta}\left(I^S - I^N\right) \tag{C.7}$$

and

$$\Delta E = \frac{1}{2\cos\eta}\left(I^W - I^E\right) \tag{C.8}$$

Indeed the north (resp. east) component depends only on the ionospheric delays—or corresponding TEC—along the north (resp. east) axis. Furthermore, the horizontal errors relate not only on TEC but on its gradients.

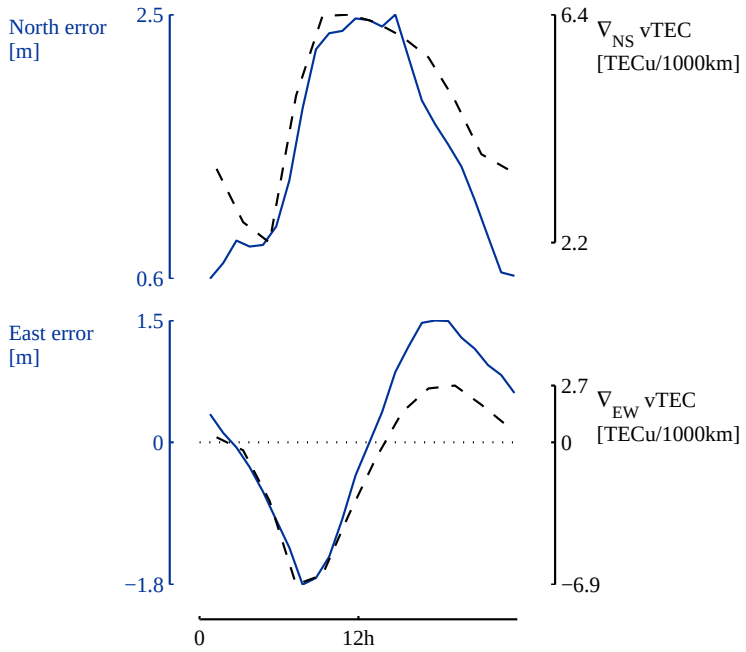

Figure C.11: Relations between the north (top plot) and east (bottom plot) uncorrected positioning errors (solid lines) and the north–south and east–west TEC gradients ∇TEC (dashed lines) at Brussels. These statistics result from the breakdown of the positioning errors dataset in 1-hour bins and the computation of TEC from 2-hour IGS GIM at ionospheric pierce points at about 666 km from the station toward each cardinal direction.

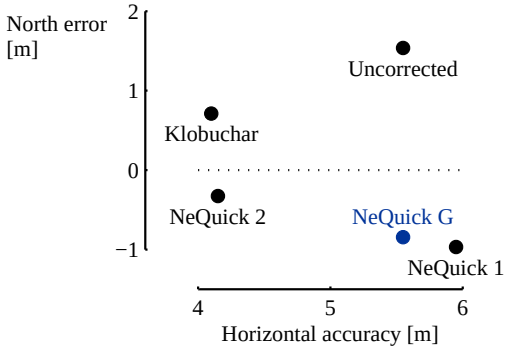

Figure C.12: Relation between the north error and the horizontal accuracy obtained with and without the ionospheric corrections at Brussels. Decreasing absolute values of the north error correspond to enhanced horizontal accuracies.

Based on this reasoning, hourly means of horizontal errors and TEC gradients supply a useful interpretation of the observed error distribution (Fig. C.11). At mid-latitudes, these statistics disclose the effect of larger TEC values toward the equator with the largest gradients around local noon, leading to a north bias without proper correction. Following sun course, their profile along the east axis corresponds to a larger TEC eastwards in the morning and westwards in the afternoon. The combination of north and east errors explains the local-time profile of the uncorrected horizontal accuracy, a concave curve from north error with modulations in the morning and evening from east error (similar to Fig. C.7). This profile is also depicted by Allain & Mitchell (2009) performing absolute positioning using precise products.

C.3.2 Horizontal discrepancies left by the corrections

As for the uncorrected horizontal accuracy, the mean north error constitutes an important driver of the corrected horizontal solutions. These solutions would indeed become significantly more accurate if the models eliminated the north bias. Unfortunately this bias persists and deteriorates the horizontal accuracy when it increases in absolute value (Fig. C.12). It is indeed insufficiently corrected with the Klobuchar algorithm but overcorrected with NeQuick with its associated negative mean north errors.

Similar conclusions prevail for the other stations included in the global performances description. The largest absolute values of the mean uncorrected north error (Fig. C.13) coincide with the worst uncorrected horizontal accuracies (Fig. C.8) at Cape Ferguson and Puerto Rico. Puerto Rico is also the only

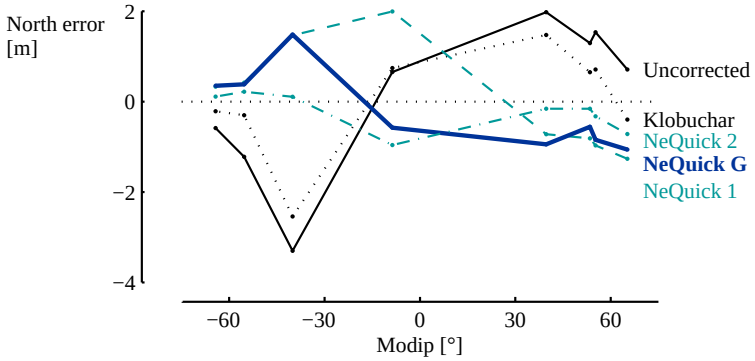

Figure C.13: Modip variability of the north error obtained with and without the ionospheric corrections. The NeQuick model (thick line for NeQuick G, dashed for NeQuick 1 and dash-dotted for NeQuick 2) overcorrects the north bias (continuous line) generally positive (resp. negative) in the northern (resp. southern) hemisphere with the exception of Fortaleza. Inversely the Klobuchar algorithm (dotted line) undercorrects it.

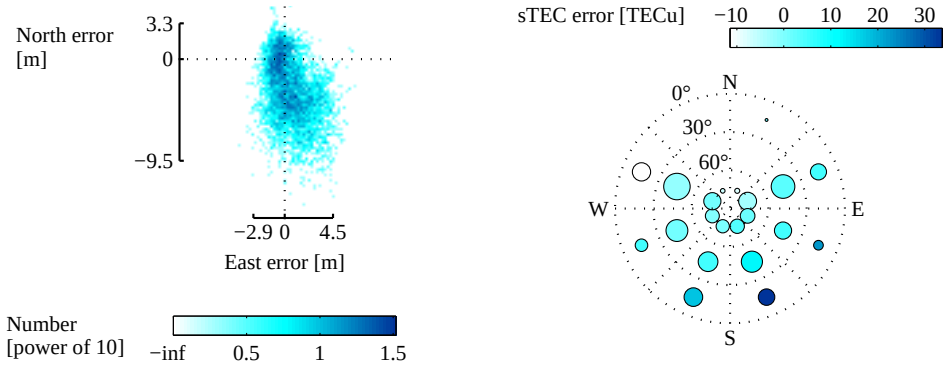

Figure C.14: Comparison between the distributions of horizontal errors (left plot) and sTEC residual errors (right plot) at Brussels in March 2002. NeQuick G induces a horizontal mean error southwards consistent with a sTEC mean overestimation in the same direction. The axes on the left plot represent 2-σ intervals around the corresponding means. The sTEC errors on the right plot correspond to mean differences with measured values for 30° elevation and 45° azimuth bins and the circle surface to the number of values in each bin.

station where NeQuick G produces worse results than NeQuick 1 both in horizontal accuracy and north error. The obtained positive (resp. negative) north bias in the northern (resp. southern) hemisphere matches the background southwards (resp. northwards) TEC gradients. It is not totally removed by the Klobuchar algorithm and, on the contrary, reversed by the NeQuick model except at Fortaleza. Noticeably NeQuick 1 amplifies the north error at this low-latitude station. There the horizontal positioning statistics for the other cases resemble more those of a north mid-latitude station. Fortaleza is indeed located under the north slope of the southern crest of the equatorial anomaly where TEC gradients point to the south.

Focusing on the horizontal discrepancies of the Galileo correction, the apparent north–south gradients mismodeling from NeQuick G should be further investigated for its key role in the limited horizontal positioning improvement despite the rather effective sTEC modeling. As an example, at Brussels for the worst month of the year 2002 (Fig. C.6), the horizontal error distribution appears skewed southwards, which influences the most the 95th percentile (Fig. C.14, left plot). Considering the original north bias, this effect highlights the mean overcorrection from NeQuick G along the north axis. It results from a mean sTEC overestimation toward south and the absence of satellites in a portion of the north sector (Fig. C.14, right plot).

C.4 Potential origins of Galileo correction discrepancies

The Galileo single frequency ionospheric correction proceeds from an algorithm in three steps, each of them potentially impacting the correction performances. The first step takes place at each GSS. It consists in measuring the sTEC and adapting the NeQuick model to measurements via a modulation of the solar activity input. Accommodating the model intrinsic weaknesses, it provides a daily effective ionization level Az for each GSS. The second step supplies the navigation message for the next day with 3 coefficients from the interpolation of all the Az values against modip (C.1). The third step is performed by the receiver: The receiver runs the NeQuick model for each satellite in view together with the Az value computed at its location from the broadcast coefficients.

This section distinguishes different effects from the combination of NeQuick intrinsic mismodeling and adapted data characteristics through the correction algorithm. It discusses the sensitivity to the effective ionization level in space and time conditioning the accessible optimization range at each GSS as well as the impact of Az interpolation errors. Then it examines the influence of the use of sTEC data for model adaptation. Finally it addresses the distortion of the electron density profile consecutive to TEC adaptation.

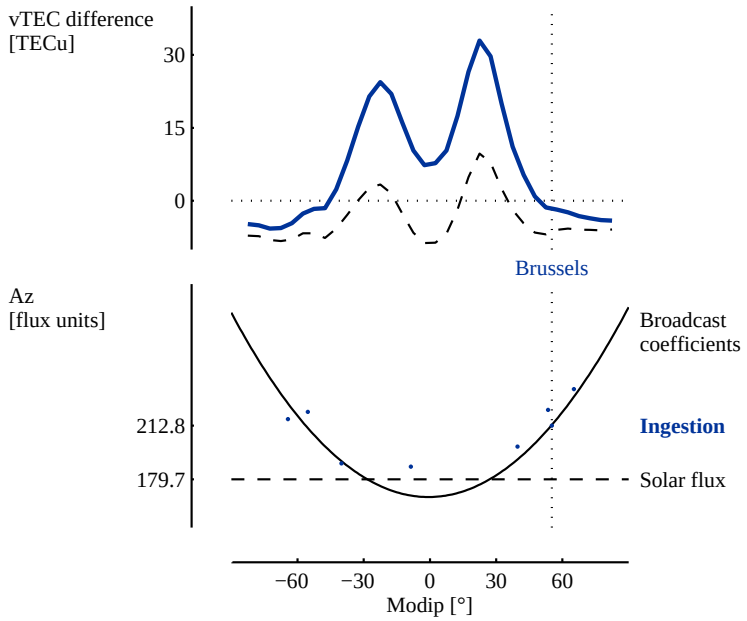

Figure C.15: Difference between IGS GIM and NeQuick G vTEC for different solar activity input parameters (top plot) and comparison between such parameters mainly obtained from sTEC adaptation (bottom plot). On the one hand, the yearly mean vTEC difference presents southwards gradients around Brussels (top plot) using the daily effective ionization level computed at Brussels from simulated broadcast coefficients or sTEC adaption (thick line). On the other hand, yearly means of daily Az values (bottom plot) obtained from sTEC adaption at the test stations (dots) are well approximated by the parabola defined by the broadcast coefficients (continuous line). The yearly mean of the daily solar flux (dashed line in bottom plot) considered as an initial value for data adaptation generally yields a vTEC underestimation apart from low latitudes (dashed line in top plot).

C.4.1 Effective ionization level sensitivity

The Galileo correction relies on the effectiveness of the data adaptation technique. In this case, this technique determines the effective ionization level that minimizes the RMS difference between a daily subset of sTEC measurements and their corresponding modeled value (Nava et al., 2006). It depends on the location and day considered.

Similar Az variations induce different TEC modifications at different locations. For a given day, the variation from an initial value–for example, the daily solar flux at 10.7 cm—providing the adequate TEC at one station possibly implies large biases at others (Fig. C.15, top plot). At Brussels modip in 2002, feeding NeQuick G with the daily solar flux leaves a yearly mean vertical TEC (vTEC) underestimation. This underestimation fades—yet not totally—thanks to sTEC adaptation at Brussels (Bidaine & Warnant, 2011). However, daily adaptation of Brussels sTEC data results in effective ionization levels imposing a large overestimation at smaller modip in absolute value. Furthermore, it reaches minimum RMS differences involving a number of modeled sTEC values on average overestimated southwards (from Brussels) and underestimated northwards. Hence, it produces excessive north–south TEC gradients.

Introduced to fit the observed Az variability in the geomagnetic north–south direction, the parabolic interpolation adjusting the broadcast coefficients renders fairly good sTEC performances in the RMS sense (Fig. C.2) but a biased representation of TEC gradients affecting horizontal positioning. At Brussels in 2002, it corresponds on average to the value obtained from sTEC adaptation (Fig. C.15, bottom plot) and delivers similar TEC results. Hence, both Az, larger than for lower latitudes, produce excessive sTEC values on average toward the equator (Fig. C.14). At Fortaleza, the mean interpolated effective ionization level differs significantly from the optimal value leading to underestimated vTEC. Yet it allows smaller TEC gradients errors and a better horizontal accuracy. The largest horizontal discrepancies occur at low mid-latitudes (Fig. C.8) where average gradients along the north axis are the most stretched.

At last, the 1-day latency in the dissemination of the broadcast coefficients—computed from sTEC measurements of the day before—has a minor effect on positioning performances, unlike TEC (Bidaine & Warnant, 2011). The yearly sTEC RMS error at Brussels in 2002 increases by 20 % when using NeQuick G with the interpolated effective ionization level instead of the current day Az value. On the contrary, the horizontal accuracy remains unchanged. Nevertheless, the intra-day variability of TEC horizontal gradients (Fig. C.11) supposes also a variable effectiveness of the TEC adaption at different hours of local time.

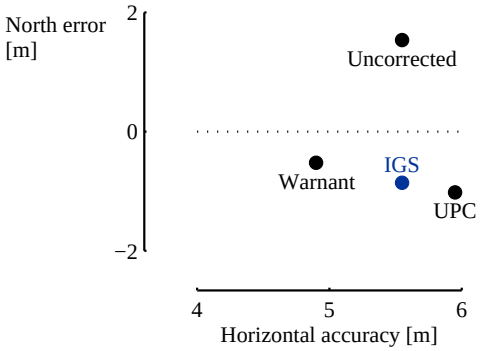

Figure C.16: Relation between the north error and the horizontal accuracy obtained with NeQuick G at Brussels from the adaptation to different sTEC data sets. The horizontal accuracy improves and the absolute mean north error decreases when using sTEC data from carrier-to-code leveling (Warnant & Pottiaux, 2000) instead of GIM calibration (Orus et al., 2007b).

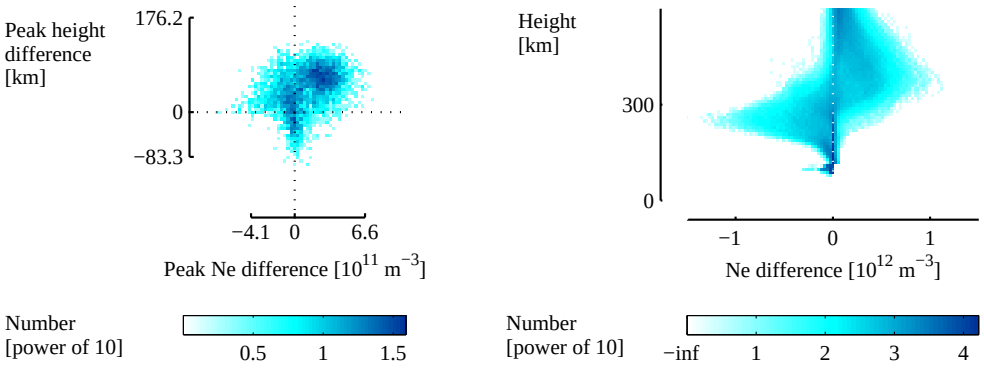

Figure C.17: Distributions of the differences of peak electron density and height (left plot) and electron density profile (right plot) between hourly manually scaled data from Dourbes digisonde and NeQuick G. sTEC data adaptation generally occasions an uplifted over-ionized peak of the electron density profile (left plot). This profile is consequently stretched with underestimated electron densities at fixed lower heights and overestimated concentrations at larger altitudes (right plot). The limited portion of the topside actually not probed but modeled by the digisonde is only shown for illustration.

C.4.2 Data characteristics

Besides the obvious influence of the elevation on sTEC adaptation, the calibration method applied to dual-frequency phase geometry-free combinations deserves more concern. This method determines the unknown numbers of cycles involved in phase measurements called ambiguities. It computes the average differences on a continuous set of epochs between these measurements and sTEC estimates from another source. In this study, it relies on GIM to collect reference sTEC (Orus et al., 2007b). More often, it uses code measurements, noisier and affected by satellite and receiver Differential Code Biases (DCB), and is then referred to as carrier-to-code leveling. According to Conte et al. (2011), this technique may cause errors of the order of 8 TECU on estimated DCB at high solar activity. Implemented following Warnant & Pottiaux (2000), it supplies sTEC data 6.8 TECU smaller on average than the first technique at Brussels in 2002 (Bidaine & Warnant, 2009b). Moreover, these data used for NeQuick G adaptation at that station in that year yield a smaller modeled sTEC, less stretched horizontal TEC gradients and better positioning performances (Fig. C.16). Hence, these performances would be further improved for more accurate TEC monitoring procedures potentially ensuing from triple-frequency combinations (Spits & Warnant, 2011).

C.4.3 Electron density profile distortion

The main advantage of the NeQuick model regarding TEC modeling lies in its 3D representation of the ionosphere. Avoiding mapping functions and associated drawbacks, this representation—often called "profiling"—renders TEC in a specific direction from the integration through vertical electron density profiles. These profiles consist in analytical functions of which the characteristics are obtained from peak parameter values. In this respect, the main peak of the profile (in the F2 layer) constitutes a strong driver of the model performances.

sTEC adaptation provokes a distortion of the electron density profile. NeQuick G profile utilizes a too simplistic suboptimal formulation for the topside, the upper part of the ionosphere, like NeQuick 1 (Bidaine & Warnant, 2010). Compensating for this intrinsic mismodeling when adapting TEC, the profile is stretched in height and electron density following its uplifted over-ionized F2 peak (Fig. C.17). Obtained from sTEC adaptation at Dourbes, located 80 km south from Brussels, in 2002 and compared to Dourbes digisonde measurements, it adopts first too weak then too strong electron densities for increasing fixed heights.

The model intrinsic modifications underpin the observed favorable evolution from one version of NeQuick to the next. By comparison to NeQuick 1, NeQuick G benefits from simplifications in the bottomside (Leitinger et al., 2005) and updated modip information. In particular, it improves low latitude performances, for example, at Fortaleza (Figs. C.8, C.13). However, it remains affected by the aforementioned topside limitation also identified by Stankov et al. (2007). This limitation relates to a twofold formula describing a coefficient shaping the topside height-dependent thickness parameter. It generates different effects during the two corresponding periods of the year, from April to September and from October to March, which become more homogeneous with NeQuick 2 (Fig. C.6). This latest version has indeed received a new topside shape parameter formula based on topside soundings (Coisson et al., 2006).

C.5 Conclusion and perspectives

Simulating the Galileo single frequency ionospheric correction, we analyzed its performances at different stations in 2002. In addition to the official Galileo version of the underlying NeQuick model, we built hypothetical counterparts on two other versions and we compared their results to the Klobuchar algorithm implemented in the GPS.

We obtained 32, 31 and 28 % sTEC RMS residual errors for successive NeQuick versions, 50 % for the Klobuchar algorithm and a 92–94 % compliance of NeQuick with the Galileo algorithm specifications (residual error smaller than 30 % of the actual sTEC or 20 TECU, whichever is larger). Looking to positioning errors, we observed a significant vertical accuracy improvement from the ionospheric corrections (95th percentiles between 9 and 11 m vs. 25 m without correction) but comparable horizontal accuracies with and without correction (between 5 and 7 m residual errors with a maximum for the uncorrected case). As reaffirmed through our spatio-temporal variability study, positioning accuracies, although influenced by similar drivers, do not simply follow sTEC performances.

Focusing on Brussels, we put these observations into perspective forming our intuition on a particular case of the positioning mathematical problem. Considering a fictitious highly symmetrical satellite distribution, we depicted the effect of TEC gradients on horizontal positioning errors, emphasizing the role of the north component. In this respect, systematic mismodeling materializing the difference between accuracy and precision should not be neglected.

Finally concentrating on Galileo correction horizontal discrepancies, we discussed how sTEC data adaptation transposes the limitations of the modeled electron density profile—mainly related to the topside representation—in other products. We associated the effective ionization level spatial sensitivity to the

detected excessive north–south TEC gradients and we addressed the sTEC measurement technique. Obviously, optimizing against one criterion may yield unpredictable effects on unconsidered features.

Benefiting from this background possibly reviewed during the In-Orbit Validation phase of Galileo, we will further address single frequency users' needs for an effective ionospheric correction. We will envisage possible alternatives to the current definition of the Galileo algorithm, among which regional procedures.

Table D.1: Main variables and units for NeQuick.

Position and geomagnetism	
Height	h $[km]$
Latitude	φ [°]
Longitude	λ [°]
Magnetic dip	I [°]
Modified dip latitude	μ [°] (Eq. 2.11)
Solar activity	
Monthly mean of $F10.7$	Φ $[10^{-22}\ W\ m^{-2}\ Hz^{-1}]$
Monthly smoothed sunspot number	R_{12}
Time and season	
Universal time	UT [hours]
Month	month
Zenith angle of the sun	χ [°]

Table D.2: Main parameters and units for NeQuick. L stands for the layer index which possible values are E, F_1 and F_2.

Electron density of layer L	N^L $[10^{11}\ el.\ m^3]$
Peak electron density of layer L	N^L_{max} $[10^{11}\ el.\ m^3]$
Global electron density at the peak height of layer L	N_mL $[10^{11}\ el.\ m^3]$
Peak height of layer L	h_mL $[km]$
Thickness parameter of layer L	B^L $[km]$
Critical frequency of layer L	f_oL $[MHz]$
Transmission factor	$M(3000)F_2$

NeQuick details

D.1 Version 1 (ITU-R)

Electron density NeQuick models the *bottomside* ionosphere electron density (Eq. D.1 when 100 $km \leq h \leq h_m F_2$) as a sum of five semi-Epstein layers (Eq. 2.12) (Di Giovanni & Radicella, 1990)[1]. The height h determines whether to use the top thickness parameter B^L_{top} or the bottom one B^L_{bot}. A fading out effect in the shape of a coefficient $\zeta(h)$ has also been added to the E and F_1 layers in the vicinity of the F_2-layer peak to avoid secondary maxima and ensure that the electron density at the F_2-layer peak corresponds exactly to $f_o F_2$ (Leitinger et al., 1999)[2].

$$\begin{aligned} N_{bot}(h) &= N^{F_2}(h) + N^{F_1}(h) + N^{E}(h) \\ &= 4\ N^{F_2}_{max}\ \frac{e^{\frac{h-h_m F_2}{B^{F_2}}}}{\left(1+e^{\frac{h-h_m F_2}{B^{F_2}}}\right)^2} + 4\ N^{F_1}_{max}\ \frac{e^{\zeta(h)\frac{h-h_m F_1}{B^{F_1}}}}{\left(1+e^{\zeta(h)\frac{h-h_m F_1}{B^{F_1}}}\right)^2} \\ &\quad + 4\ N^{E}_{max}\ \frac{e^{\zeta(h)\frac{h-h_m E}{B^{E}}}}{\left(1+e^{\zeta(h)\frac{h-h_m E}{B^{E}}}\right)^2} \end{aligned} \tag{D.1}$$

$$\zeta(h) = e^{\frac{10}{1+2|h-h_m F_2|}}$$

[1] The latest publication including most of NeQuick equations is (Leitinger et al., 2005).

[2] The second and third terms corresponding to the F_1 and E layers are equalled to 0 if $|\zeta(h)\frac{h-h_m L}{B^L}| > 25$.

The *topside* ($h > h_m F_2$) corresponds to a sixth semi-Epstein layer with a height-dependent thickness parameter H.

$$N_{top}(h) = 4\ N_{max}^{F_2}\ \frac{e^{\frac{h-h_m F_2}{H}}}{\left(1+e^{\frac{h-h_m F_2}{H}}\right)^2} \tag{D.2}$$

For the *lowest part* of the ionosphere ($h < 100\ km$), a Chapman formulation (equation D.3) is used to avoid unrealistically high electron densities below 90 km from very thick lower F_1 layer in lower latitudes (Leitinger et al., 1999). The equation for b is translated from the code[3].

$$N_{low}(h) = N_{bot}(100)\ e^{1-\ b\frac{h-100}{10}\ -\ e^{-\frac{h-100}{10}}} \tag{D.3}$$

$$\begin{aligned} b &= 1 - \left[\frac{1}{N_{bot}(h)}\frac{dN_{bot}}{dh}(h)\right]_{h=100} \\ &= 1 - \frac{10}{N_{bot}(100)}\left[\frac{4\ N_{max}^{F_2}\ \left(1-e^{\frac{100-h_m F_2}{B_{bot}^{F_2}}}\right)\ e^{\frac{100-h_m F_2}{B_{bot}^{F_2}}}}{B_{bot}^{F_2}\ \left(1+e^{\frac{100-h_m F_2}{B_{bot}^{F_2}}}\right)^3}\right. \\ &\quad + \frac{4\ N_{max}^{F_1}\ \left(1-e^{\zeta(100)\frac{100-h_m F_1}{B_{bot}^{F_1}}}\right)\ e^{\zeta(100)\frac{100-h_m F_1}{B_{bot}^{F_1}}}}{B_{bot}^{F_1}\ \left(1+e^{\zeta(100)\frac{100-h_m F_1}{B_{bot}^{F_1}}}\right)^3} \\ &\quad \left. + \frac{4\ N_{max}^{E}\ \left(1-e^{\zeta(100)\frac{100-h_m E}{B_{bot}^{E}}}\right)\ e^{\zeta(100)\frac{100-h_m E}{B_{bot}^{E}}}}{B_{bot}^{E}\ \left(1+e^{\zeta(100)\frac{100-h_m E}{B_{bot}^{E}}}\right)^3}\right] \end{aligned}$$

$$\zeta(100) = e^{\frac{10}{1+2|100-h_m F_2|}}$$

[3]The second and third terms in the parenthesis corresponding to the F_1 and E layers are equalled to 0 if $|\zeta(100)\frac{100-h_m L}{B^L}| > 25$.

Peak electron densities

The following equation (Radicella & Zhang, 1995) was derived

- taking into account the fading out effect of E and F_1 layers near the F_2-layer peak to explain equation D.4,
- neglecting the E layer when considering the F_1 layer,
- but using original Epstein layers to compute their values at the other peaks in the following equations[4].

$$N_{max}^{F_2} = N(h_m F_2) = N_m F_2 \tag{D.4}$$

$$\begin{aligned} N_{max}^{F_1} &= N(h_m F_1) - N^E(h_m F_1) - N^{F_2}(h_m F_1) \\ &= N_m F_1 - N^{F_2}(h_m F_1) \\ N_{max}^{E} &= N(h_m E) - N^{F_1}(h_m E) - N^{F_2}(h_m E) \\ &= N_m E - N^{F_1}(h_m E) - N^{F_2}(h_m E) \end{aligned} \tag{D.5, D.6}$$

The *global electron densities* at the peak height of layer L $N_m L$ are calculated from the critical frequencies $f_o L$ by means of equation 2.26 repeated here under with the appropriate units.

$$N_m L = 0.124\ f_o L^2 \tag{D.7}$$

Peak heights The following equations (Radicella & Zhang, 1995) are based on Dudeney's form (Dudeney, 1983) of the Bradley and Dudeney formula (Bradley & Dudeney, 1973)[5].

$$\begin{aligned} h_m F_2 &= \frac{1490\ MF}{M + DM} - 176 \\ DM &= \frac{0.253}{f_o F_2 / f_o E - 1.215} - 0.012 \\ MF &= M\sqrt{\frac{0.0196 M^2 + 1}{1.2967 M^2 - 1}} \\ M &= M(3000) F_2 \end{aligned} \tag{D.8}$$

[4] $N_{max}^{F_1}$ and N_{max}^{E} are limited at a minimum value of 0.05. The transition is computed by means of equation D.34 with $\alpha = 60$.

[5] The ratio $f_o F_2 / f_o E$ is limited at a minimum value of 1.75. The transition is computed by means of equation D.34 with $\alpha = 20$.

The following equation[6] can be found into (Radicella & Zhang, 1995) or (Leitinger et al., 2005) for a correct version.

$$h_m F_1 = 108.8 + 14\ N_m F_1 + 0.71\ |I| \tag{D.9}$$

$$h_m E = 120 km \tag{D.10}$$

Thickness parameters

The following equations can be found into (Radicella & Zhang, 1995).

$$\begin{aligned} B_{bot}^{F_2} &= \frac{0.385\ N_m F_2}{0.01\ (dN/dh)_{max}} \\ \ln\left((dN/dh)_{max}\right) &= -3.467 + 0.857 \ln\left(f_o F_2\right)^2 \\ &\quad + 2.02 \ln\left(M(3000) F_2\right) \end{aligned} \tag{D.11}$$

$(dN/dh)_{max}$ $[10^9\ el.\ m^{-3}\ km^{-1}]$ is the gradient of $N(h)$ at the characteristic point at the base of the F_2 layer i.e. the first derivative of equation 2.12 for F_2 layer at the inflection point.

The following equations can be found into (Radicella & Zhang, 1995) and (Radicella & Leitinger, 2001) ((Leitinger et al., 2005) for a correct version of H)[7].

$$H = B_{top}^{F_2} \left(1 + \frac{12.5(h - h_m F_2)}{100 B_{top}^{F_2} + 0.125(h - h_m F_2)}\right) \tag{D.12}$$

$$B_{top}^{F_2} = \frac{k\ B_{bot}^{F_2}}{\nu}$$

$$k = \begin{cases} -7.77 + 0.097 \left(\frac{h_m F_2}{B_{bot}^{F_2}}\right)^2 + 0.153\ N_m F_2 & \text{from October to March} \\ 6.705 - 0.014\ R_{12} - 0.008\ h_m F_2 & \text{from April to September} \end{cases} \tag{D.13}$$

$$2 \le k \le 8$$

$$\nu = (0.041163\ x - 0.183981)\ x + 1.424472$$

$$x = \frac{k\ B_{bot}^{F_2} - 150}{100}$$

[6] The transition at $I = 0$ is computed by means of equation D.34 with $\alpha = 12$.

[7] The transitions at $k = 2$ and $k = 8$ are computed by means of equation D.34 with $\alpha = 1$.

The formula for $B_{top}^{F_1}$ (Radicella & Zhang, 1995) is obtained from a simplification of the top F_1 semi-Epstein layer without fading out effect (equation 2.12 adapted to F_1), the shape of F_1 peak amplitude from equation D.1 and assuming the value of NF_1 at the F_2-layer peak[8].

$$\begin{aligned} NF_1(h_mF_2) &\approx 4\ N_{max}^{F_1}\ e^{-\frac{h_mF_2-h_mF_1}{B_{top}^{F_1}}} \\ &\approx 4\ \left(N_mF_1 - N^{F_2}(h_mF_1)\right)\ e^{-\frac{h_mF_2-h_mF_1}{B_{top}^{F_1}}} \\ &\approx 0.1\ N_mF_1 \end{aligned} \tag{D.14}$$

$$B_{top}^{F_1} = \frac{h_mF_2 - h_mF_1}{\ln\left(4\ \frac{N_mF_1 - N^{F_2}(h_mF_1)}{0.1\ N_mF_1}\right)} \tag{D.15}$$

The following equations can be found into (Radicella & Zhang, 1995).

$$B_{bot}^{F_1} = 0.7\ B_{top}^{F_1} \tag{D.16}$$

$$B_{top}^{E} = \begin{cases} 0.5\ B_{top}^{F_1} & \text{if } F_1 \text{ is present} \\ 7km & \text{if not} \end{cases} \tag{D.17}$$

$$B_{bot}^{E} = 5km \tag{D.18}$$

Critical frequencies and transmission factor The following equations (Leitinger et al., 1999) allow to compute the effective critical frequencies for the E and F_1 layers[9].

$$\begin{aligned} (f_oE)^2 &= a_E^2\ \sqrt{\Phi}\ \cos^{0.6}\chi_{eff} + 0.49 \\ a_E &= 1.112 - 0.019\ s_E\ \frac{e^{0.3\phi}-1}{e^{0.3\phi}+1} \\ s_E &= \begin{cases} -1 & \text{for "Winter" (November to February)} \\ 0 & \text{for "Equinox" (March, April, September and October)} \\ 1 & \text{for "Summer" (May to August)} \end{cases} \end{aligned} \tag{D.19}$$

[8] The ratio $4\frac{N_mF_1 - N^{F_2}(h_mF_1)}{0.1\ N_mF_1}$ is limited at a minimum value of 1.5. The transition is computed by means of equation D.34 with $\alpha = 20$.
$B_{top}^{F_1}$ is limited at a maximum value of $B_{bot}^{F_2} + 50$. The transition is computed by means of equation D.34 with $\alpha = 20$.

[9] The transitions between day and night for χ_{eff} and f_oF_1 at $\chi = \chi_0$ are computed by means of equation D.34 with $\alpha = 12$.

$$\chi_{eff} = \begin{cases} \chi & \text{for daytime } (\chi < \chi_0) \\ 90 - 0.24\ e^{20-0.2\chi} & \text{for nighttime } (\chi > \chi_0) \end{cases}$$

$\chi_0 = 86.23°$ denotes the limit between day and night.

$$f_oF_1 = \begin{cases} 1.4\ f_oE & \text{for daytime } (\chi < \chi_0) \\ 0 & \text{for nighttime } (\chi > \chi_0) \end{cases} \tag{D.20}$$

The following equation can be found into (ITU, 2009b). This general form of the *numerical map* function Ω providing the evaluation of the monthly median of f_oF_2 or $M(3000)F_2$ has the shape of a Fourier time series.

$$\Omega(\phi, \lambda, T) = \sum_{k=0}^{K} U_{0,k} G_k(\phi, \lambda) + \sum_{j=1}^{H} \sum_{k=0}^{K} \left[U_{2j,k} \cos(jT) + U_{2j-1,k} \sin(jT) \right] G_k(\phi, \lambda) \tag{D.21}$$

T denotes the universal time UT expressed as an angle ($-180° \leq T \leq 180°$).

H denotes the maximum number of harmonics used to represent the diurnal variation (6 for f_oF_2 and 4 for $M(3000)F_2$).

The coefficients $U_{i,k}$ are calculated from the CCIR files by linear combination with R_{12} as weighting coefficient (low solar activity: $R_{12} = 0$, $U^-_{i,k}$; high solar activity: $R_{12} = 100$, $U^+_{i,k}$).

$$U_{i,k} = U^-_{i,k} \left(1 - \frac{R_{12}}{100} \right) + U^+_{i,k} \frac{R_{12}}{100} \tag{D.22}$$

The geographic coordinate functions G_k are composed of three trigonometric functions in the following way.

$$G_k(\phi, \lambda) = \sin^{q(k)} \mu\ \cos^{m(k)} \phi \begin{Bmatrix} \cos \\ \sin \end{Bmatrix} (m(k)\lambda) \tag{D.23}$$

$q(k)$, the order in modified dip latitude, and $m(k)$, the order in longitude, are linked to the order of current harmonic.

The following formulation allows to *understand the code more easily.*

$$\Omega(\mu,\phi,\lambda,UT) = \sum_{L=1}^{q(1)+1} C_{i(1,L)}(UT)\ \sin^{L-1}\mu + \sum_{j=2}^{k_1}\sum_{L=1}^{q(j)+1}\left[C_{i(j,L)}(UT)\ \cos\left((j-1)\lambda\right) + C_{i(j,L)+1}(UT)\ \sin\left((j-1)\lambda\right)\right] \cos^{j-1}\phi\ \sin^{L-1}\mu \quad \text{(D.24)}$$

The first term could be included in the sum noticing that, for $j = 1$, $\cos^{j-1}\phi = 1$, $\cos\left((j-1)\lambda\right) = 1$ and $\sin\left((j-1)\lambda\right) = 0$.

$q(j)$ denotes the maximum order in modified dip latitude for current order in longitude.

k_1 denotes the maximum order in longitude.

$$i(j,L) = \begin{cases} L & \text{if } j = 1 \\ q(1) + 2\left(\sum_{l=2}^{j-1} q(l) + j + L\right) - 4 & \text{else} \end{cases}$$

$$C_i(UT) = U_{1,i} + \sum_{j=1}^{H} U_{2j,i}\sin\left(j\left(\frac{\pi}{12}UT - \pi\right)\right) + U_{2j+1,i}\cos\left(j\left(\frac{\pi}{12}UT - \pi\right)\right) \quad \text{(D.25)}$$

D

D.2 Version G

Epstein parameters The first modifications related to the *peak electron densities* are translated from the code as they are not published yet.

As a consequence of the modified formulation of f_oF_1 (cf. equation D.31), $N_{max}^{F_1}$ is equalled to 0 if $f_oF_1 \leq 0.5$ and N_{max}^{E} is obtained from equation D.6 taking into account the disappearing of the F_1 layer. In the other case, $N_{max}^{F_1}$ and N_{max}^{E} are calculated by means of five successive iterations of equations D.26 and D.6[10].

$$N_{max}^{F_1} = N_mF_1 - N^{F_2}(h_mF_1) - N^{E}(h_mF_1) \tag{D.26}$$

The equations of the F_1 *peak height* and the *thickness parameters* from section D.1 were also updated as follows (Leitinger et al., 2005).

$$h_mF_1 = \frac{h_mF_2 + h_mE}{2} \tag{D.27}$$

$$B_{top}^{F_1} = 0.3\ (h_mF_2 - h_mF_1) \tag{D.28}$$

$$B_{bot}^{F_1} = 0.5\ (h_mF_1 - h_mE) \tag{D.29}$$

$$B_{top}^{E} = \max \left\{ \begin{array}{c} 0.5\ (h_mF_1 - h_mE) \\ 7km \end{array} \right\} \tag{D.30}$$

Ionosonde parameters The following modifications to equation D.20 are described into (Leitinger et al., 2005).

$$f_oF_1 = \left\{ \begin{array}{ll} 1.4\ f_oE & f_oE \geq 2 \\ 0 & f_oE < 2 \\ 0.85\ 1.4\ f_oE & 1.4\ f_oE > 0.85\ f_oF_2 \end{array} \right. \tag{D.31}$$

The last condition corresponds a 15% reduction when f_oE is too close to f_oF_2.

[10] N_{max}^{E} is still limited at a minimum value of 0.05 and the transition is still computed by means of equation D.34 with $\alpha = 60$.
At each iteration, $N_{max}^{F_1}$ is limited at a minimum value of 0.2 N_mF_1. The transition is computed by means of equation D.34 with $\alpha = 1$.

D.3 Version 2

The latest and major revision concerns the topside shape parameter k (Coisson et al., 2006).

$$B_{top}^{F_2} = k\ B_{bot}^{F_2}$$
$$k = 3.22 - 0.0538\ f_o F_2 - 0.00664\ h_m F_2 + 0.113 \frac{h_m F_2}{B_{bot}^{F_2}} + 0.00257\ R_{12} \quad \text{(D.32)}$$
$$k \geq 1$$

D.4 Implementation tools

To represent the *piecewise function* $f(x)$ (Eq. D.33), NeQuick uses an exponential transition (cf. equation D.34) depending on the (steepness) parameter α related to steepness of the transition between the two pieces $f_+(x)$ and $f_-(x)$. An interesting interpretation of this formulation is obtained considering the limits for $x \to \pm\infty$.

$$f(x) = \begin{cases} f_+(x) & \text{if } x > 0 \\ f_-(x) & \text{if } x < 0 \end{cases} \quad \text{(D.33)}$$

The following equation is translated from the code.

$$f(x) = \frac{f_+(x)\ e^{\alpha x} + f_-(x)}{e^{\alpha x} + 1} \quad \text{(D.34)}$$

Finally it is important to mention that NeQuick *restricts the argument of exponential functions* within the interval $[-80, 80]$ to avoid extreme values which could result (cf. equation D.35).

$$e_*^x = \begin{cases} e^{80} \approx 5.5406\ 10^{34} & \text{if } x > 80 \\ e^x & \text{if } -80 \leq x \leq 80 \\ e^{-80} \approx 1.8049\ 10^{-35} & \text{if } x < -80 \end{cases} \quad \text{(D.35)}$$

List of Figures

List of Tables

Bibliography

Allain, D., & Mitchell, C. (2009). Ionospheric delay corrections for single-frequency GPS receivers over Europe using tomographic mapping. *GPS Solutions*, 13 (2), 141–151. doi:10.1007/s10291-008-0107-y.

Altadill, D., Boska, J., Cander, L. R., Gulyaeva, T., Reinisch, B. W., Romano, V., Krankowski, A., Bremer, J., Belehaki, A., Stanislawska, I., Jakowski, N., & Scotto, C. (2009). Near Earth space plasma monitoring under COST 296. *Annals of Geophysics*, 52 (3-4), 221–234. Available at http://www.annalsofgeophysics.eu/index.php/annals/article/view/4562.

Arbesser-Rastburg, B. (2006). The Galileo Single Frequency Ionospheric Correction Algorithm. In *3rd European Space Weather Week*, Brussels (Belgium), November 13th to 17th, 2006. Available at http://sidc.oma.be/esww3/presentations/Session4/Arbesser.pdf.

Arbesser-Rastburg, B., & Jakowski, N. (2007). Effects on satellite navigation. In V. Bothmer, & I. A. Daglis (Eds.), *Space Weather - Physics and Effects*, pp. 383–402. New York (USA): Springer Berlin Heidelberg. doi:10.1007/978-3-540-34578-7_13. ISBN 978-3-540-23907-9.

Belabbas, B., Schlueter, S., & Sadeque, M. Z. (2005). Impact of NeQuick Correction Model to Positioning and Timing Accuracy using the Instantaneous Pseudo Range Error of Single Frequency Absolute Positioning Receivers. In *Proceedings of the 18th International Technical Meeting of the Satellite Division of The Institute of Navigation (ION GNSS 2005)*, pp. 712–722.

Bidaine, B. (2006). *Ionosphere Crossing of GALILEO Signals*. M. Sc. thesis, University of Liège. Available at http://orbi.ulg.ac.be/handle/2268/682.

Bidaine, B. (2008). *Combining Ionosonde and GPS TEC Data to Assess NeQuick Formulation*. Short Term Scientific Mission report. COST Action 296. Available at http://orbi.ulg.ac.be/handle/2268/1548.

Bidaine, B., Lonchay, M., & Warnant, R. (2012). Galileo Single Frequency Ionospheric Correction: Performances in Terms of Position. *GPS Solutions*,

published online. doi:10.1007/s10291-012-0261-0. Available at http://orbi.ulg.ac.be/handle/2268/117284.

Bidaine, B., Nava, B., Stankov, S., & Warnant, R. (2010). M-Ingestion: Simultaneous Ingestion of Ionosonde and GNSS Data into the NeQuick Model. In P. Doherty, M. Hernández-Pajares, J.-M. Juan, J. Sanz, & A. Aragon-Angel (Eds.), *Proceedings of the International Beacon Satellite Symposium 2010 (BSS 2010)*. Barcelona (Spain): CIMNE. Available at http://orbi.ulg.ac.be/handle/2268/40738.

Bidaine, B., Prieto-Cerdeira, R., & Orus, R. (2006). NeQuick: In-Depth Analysis and New Developments. In *Proceedings of the 3rd ESA Workshop on Satellite Navigation User Equipment Technologies NAVITEC 2006*. Available at http://orbi.ulg.ac.be/handle/2268/1556.

Bidaine, B., & Warnant, R. (2007). Assessment of the NeQuick Model at Mid-latitudes using GPS TEC and Ionosonde Data. In *Proceedings of the First Colloquium Scientific and Fundamental Aspects of the Galileo Programme*. Available at http://orbi.ulg.ac.be/handle/2268/1561.

Bidaine, B., & Warnant, R. (2008a). Modelling the Ionosphere over Europe: Investigation of NeQuick Formulation. In *5th European Space Weather Week*, Brussels (Belgium), November 17th to 21st, 2008. Poster. Available at http://orbi.ulg.ac.be/handle/2268/1564.

Bidaine, B., & Warnant, R. (2008b). Towards an Improved Single-Frequency Ionospheric Correction: Focus on Mid-Latitudes. In *Proceedings of the 4th ESA Workshop on Satellite Navigation User Equipment Technologies NAVITEC 2008*. Available at http://orbi.ulg.ac.be/handle/2268/1551.

Bidaine, B., & Warnant, R. (2009a). Ionosphere Modelling Based on the NeQuick Model and GNSS Data Ingestion. In *Proceedings of the Second International Colloquium - Scientific and Fundamental Aspects of the Galileo Programme*. Available at http://orbi.ulg.ac.be/handle/2268/19132.

Bidaine, B., & Warnant, R. (2009b). Measuring Total Electron Content with GNSS: Investigation of Two Different Techniques. In *Proceedings of the 11th International Conference on Ionospheric Radio Systems and Techniques (IRST 2009)*, pp. 201–206. London (UK): Institution of Engineering and Technology - IET. doi:10.1049/cp.2009.0063. ISBN 0781849191234. Available at http://orbi.ulg.ac.be/handle/2268/1553.

Bidaine, B., & Warnant, R. (2010). Assessment of the NeQuick model at mid-latitudes using GNSS TEC and ionosonde data. *Advances in Space Research*, 45 (9), 1122–1128. doi:10.1016/j.asr.2009.10.010. Available at http://orbi.ulg.ac.be/handle/2268/26082.

Bidaine, B., & Warnant, R. (2011). Ionosphere modelling for Galileo single frequency users: illustration of the combination of the NeQuick model and GNSS data ingestion. *Advances in Space Research*, 47 (2), 312–322. doi:10.1016/j.asr.2010.09.001. Available at http://orbi.ulg.ac.be/handle/2268/72765.

Béniguel, Y., & Hamel, P. (2011). A Global Ionosphere Scintillation Propagation Model for Equatorial Regions. *Journal of Space Weather and Space Climate*, 1 (1). doi:10.1051/swsc/2011004.

Bourdillon, A., Cander, L. R., & Zolesi, B. (2009). COST 296 MIERS: Mitigation of Ionospheric Effects on Radio Systems. *Annals of Geophysics*, 52 (3-4). Available at http://www.annalsofgeophysics.eu/index.php/annals/article/view/14.

Bradley, P. A. (1995). *PRIME (Prediction Regional Ionospheric Modelling over 253 Europe)*. Final Report COST Action 238. Brussels (Belgium): Commission of the European Communities.

Bradley, P. A., & Dudeney, J. R. (1973). A simple model of the vertical distribution of electron concentration in the ionosphere. *Journal of Atmospheric and Terrestrial Physics*, 35 (12), 2131–2146. doi:10.1016/0021-9169(73)90132-3.

Brent, R. P. (1973). *Algorithms for minimization without derivatives*. Englewood Cliffs: Prentice-Hall. ISBN 0-13-022335-2. Available at http://isbndb.com/d/book/algorithms_for_minimization_without_derivatives_a01.html.

Bruyninx, C. (2004). The EUREF Permanent Network: a multi-disciplinary network serving surveyors as well as scientists. *GeoInformatics*, 7, 32–35.

Buresova, D., Nava, B., Galkin, I., Angling, M., Stankov, S. M., & Coisson, P. (2009). Data ingestion and assimilation in ionospheric models. *Annals of Geophysics*, 52 (3-4), 235–253. Available at http://www.annalsofgeophysics.eu/index.php/annals/article/view/4575.

Ciraolo, L., Azpilicueta, F. J., Brunini, C., Meza, A., & Radicella, S. M. (2007). Calibration errors on experimental slant total electron content (TEC) determined with GPS. *Journal of Geodesy*, 81 (2), 111–120. doi:10.1007/s00190-006-0093-1.

Coisson, P., Radicella, S. M., Leitinger, R., & Ciraolo, L. (2004). Are models predicting a realistic picture of vertical total electron content? *Radio Science*, 39 (1). doi:10.1029/2002rs002823.

Coisson, P., Radicella, S. M., Leitinger, R., & Nava, B. (2006). Topside electron density in IRI and NeQuick: Features and limitations. *Advances in Space Research*, 37 (5), 937–942. doi:10.1016/j.asr.2005.09.015.

Conte, J., Azpilicueta, F., & Brunini, C. (2011). Accuracy assessment of the GPS-TEC calibration constants by means of a simulation technique. *Journal of Geodesy*, , pp. 1–8. doi:10.1007/s00190-011-0477-8.

Cueto, M., Coisson, P., Radicella, S. M., Herraiz, M., Ciraolo, L., & Brunini, C. (2007). Topside ionosphere and plasmasphere: Use of NeQuick in connection with Gallagher plasmasphere model. *Advances in Space Research*, 39 (5), 739–743. doi:10.1016/j.asr.2007.01.073.

Davies, K. (1990). *Ionospheric Radio*. London (UK): Peter Peregrinus. ISBN 0-86341-186X.

Di Giovanni, G., & Radicella, S. M. (1990). An analytical model of the electron density profile in the ionosphere. *Advances in Space Research*, 10 (11), 27–30. doi:10.1016/0273-1177(90)90301-f.

van Diggelen, F. (2009). *A-GPS: Assisted GPS, GNSS, and SBAS*. Artech House Publishers. ISBN 978-1-59693-374-3.

Dow, J. M., Neilan, R. E., & Rizos, C. (2009). The International GNSS Service in a changing landscape of Global Navigation Satellite Systems. *Journal of Geodesy*, 83 (3-4), 191–198. doi:10.1007/s00190-008-0300-3.

Dudeney, J. R. (1983). The accuracy of simple methods for determining the height of the maximum electron concentration of the F2-layer from scaled ionospheric characteristics. *Journal of Atmospheric and Terrestrial Physics*, 45 (8-9), 629–640. doi:10.1016/S0021-9169(83)80080-4.

Epstein, P. S. (1930). Reflection of waves in an inhomogeneous absorbing medium. *Proceedings of the National Academy of Sciences*, 16 (10), 627–637.

European Union (2010). European GNSS (Galileo) Open Service Signal In Space Interface Control Document. OS SIS ICD Issue 1.1. Available at `http://ec.europa.eu/enterprise/policies/satnav/galileo/files/galileo-os-sis-icd-issue1-revision1_en.pdf`.

Feess, W. A., & Stephens, S. G. (1987). Evaluation of GPS Ionospheric Time-Delay Model. *IEEE Transactions on Aerospace and Electronic Systems*, AES-23 (3), 332–338. doi:10.1109/TAES.1987.310830.

Galkin, I. A., Khmyrov, G. M., Kozlov, A., Reinisch, B. W., Huang, X., & Kitrosser, D. F. (2006). Ionosonde networking, databasing, and Web serving. *Radio Science*, 41 (5), 8 pp.–8 pp. doi:10.1029/2005rs003384.

García-Rigo, A., Monte, E., Hernández-Pajares, M., Juan, J. M., Sanz, J., Aragón-Angel, A., & Salazar, D. (2011). Global prediction of the vertical total electron content of the ionosphere based on GPS data. *Radio Science*, 46 (4), RS0D25. doi:10.1029/2010rs004643.

GPS Wing (2010). Navstar GPS Space Segment/Navigation User Interfaces. IS-GPS-200E. Available at http://www.gps.gov/technical/icwg/IS-GPS-200E.pdf.

GSA (2012). *GNSS Market Report*. Issue 2. Available at http://gsa.europa.eu/sites/default/files/uploads/MarketReportMEP72012WEB.PDF.

Hanbaba, R. (1999). *Improved Quality of Service in Ionospheric Telecommunication Systems Planning and Operation*. Final Report COST Action 251. Warsaw (Poland): Space Research Centre.

Hernandez-Pajares, M., Juan, J. M., Sanz, J., Ramos-Bosch, P., Rovira-Garcia, A., Salazar, D., Ventura-Traveset, J., Lopez-Echazarreta, C., & Hein, G. (2010). The ESA/UPC GNSS-Lab tool (gLAB): an advanced multipurpose package to process and analyse GNSS data. In *Proceedings of the 5th ESA Workshop on Satellite Navigation User*. Available at http://gage6.upc.es/gAGE_WEB/papers/2010/gLAB_paper_Navitech-1.pdf.

Hernandez-Pajares, M., Zornoza, J. M. J., & Subirana, J. S. (2008). *GPS data processing: code and phase - Algorithms, Techniques and Recipes*. ISBN 84-932230-5-0. Available at http://gage6.upc.es/sites/default/files/TEACHING_MATERIAL/GPS_BOOK/ENGLISH/PDGPS/BOOK_PDGPS_gAGE_NAV_08.pdf.

Hernández-Pajares, M., Juan, J. M., Sanz, J., Orus, R., Garcia-Rigo, A., Feltens, J., Komjathy, A., Schaer, S. C., & Krankowski, A. (2009). The IGS VTEC maps: a reliable source of ionospheric information since 1998. *Journal of Geodesy*, 83 (3-4), 263–275. doi:10.1007/s00190-008-0266-1. Available at http://gage6.upc.es/gAGE_WEB/papers/2009/igs-maps_jog09.pdf.

Hidalgo, I., Rodríguez, D., Cueto, M., Prieto-Cerdeira, R., & Binda, S. (2009). GIOVE Mission Experimentation: Ionospheric and Interfrequency Bias Analysis and Results. In *Proceedings of the Second International Colloquium - Scientific and Fundamental Aspects of the Galileo Programme*.

Hochegger, G., Nava, B., Radicella, S., & Leitinger, R. (2000). A family of ionospheric models for different uses. *Physics and Chemistry of the Earth, Part C: Solar, Terrestial and Planetary Science*, 25 (4), 307–310. doi:10.1016/S1464-1917(00)00022-2.

Hofmann-Wellenhof, B., Lichtenegger, H., & Wasle, E. (2008). *GNSS - Global Navigation Satellite Systems - GPS, GLONASS, Galileo, and more*. Vienna

(Austria): Springer. doi:10.1007/978-3-211-73017-1. ISBN 978-3-211-73012-6.

ITU (2009a). Ionospheric propagation data and prediction methods required for the design of satellite services and systems. Rec. ITU-R P.531-10. Available at http://www.itu.int/rec/R-REC-P.531/.

ITU (2009b). ITU-R reference ionospheric characteristics. ITU-R P.1239-2. Available at http://www.itu.int/rec/R-REC-P.1239/.

Kintner, P. M., & Ledvina, B. M. (2005). The ionosphere, radio navigation, and global navigation satellite systems. *Advances in Space Research*, 35 (5), 788–811. doi:10.1016/j.asr.2004.12.076.

Klobuchar, J. A. (1987). Ionospheric Time-Delay Algorithm for Single-Frequency GPS Users. *IEEE Transactions on Aerospace and Electronic Systems*, AES-23 (3), 325–331. doi:10.1109/TAES.1987.310829.

Klobuchar, J. A., & Kunches, J. M. (2000a). Eye on the Ionosphere: Correcting for Ionospheric Range Delay on GPS - Temporal Decorrelation. *GPS Solutions*, 4 (2), 78–82. doi:10.1007/pl00012846.

Klobuchar, J. A., & Kunches, J. M. (2000b). Eye on the Ionosphere: The Spatial Variability of Ionospheric Range Delay. *GPS Solutions*, 3 (3), 70–74. doi:10.1007/pl00012808.

Knezevich, M., & Radicella, S. M. (2004). Development of an ionospheric NeQuick model algorithm for GNSS receivers. In *Proceedings of the 2nd ESA Workshop on Satellite Navigation User Equipment Technologies NAVITEC 2004*. Available at ftp://ftp.estec.esa.nl/pub3/tos-ett/navitec2004/papers/P21-Knezevich.pdf.

Leitinger, R., Radicella, S., Hochegger, G., & Nava, B. (2002). Diffusive equilibrium models for the height region above the F2 peak. *Advances in Space Research*, 29 (6), 809–814. doi:10.1016/s0273-1177(02)00036-4.

Leitinger, R., Radicella, S. M., Nava, B., Hochegger, G., & Hafher, J. (1999). NeQuick - COSTprof - NeUoG-plas, a family of 3D electron density models. In *Proceedings of the COST 251 Madeira Workshop*, pp. 75–89.

Leitinger, R., Zhang, M. L., & Radicella, S. M. (2005). An improved bottomside for the ionospheric electron density model NeQuick. *Annals of Geophysics*, 48 (3), 525–534. Available at http://www.annalsofgeophysics.eu/index.php/annals/article/view/3217.

Lonchay, M. (2009). *Précision du positionnement par satellites : influence de la géométrie de la constellation [Precision of satellite positioning: impact of satellite geometry]*. M. Sc. thesis, University of Liège. Available at http://orbi.ulg.ac.be/handle/2268/33666.

Mohino, E. (2008). Understanding the role of the ionospheric delay in single-point single-epoch GPS coordinates. *Journal of Geodesy*, 82 (1), 31–45. doi:10.1007/s00190-007-0155-z.

Nava, B., Coisson, P., Amarante, G. M., Azpilicueta, F., & Radicella, S. M. (2005). A model assisted ionospheric electron density reconstruction method based on vertical TEC data ingestion. *Annals of Geophysics*, 48 (2), 313–320. Available at http://www.annalsofgeophysics.eu/index.php/annals/article/view/3203.

Nava, B., Coisson, P., & Radicella, S. M. (2008). A new version of the NeQuick ionosphere electron density model. *Journal of Atmospheric and Solar-Terrestrial Physics*, 70 (15), 1856–1862. doi:10.1016/j.jastp.2008.01.015.

Nava, B., Radicella, S. M., Leitinger, R., & Coisson, P. (2006). A near-real-time model-assisted ionosphere electron density retrieval method. *Radio Science*, 41 (6), RS6S16. doi:10.1029/2005rs003386.

Odijk, D. (2002). *Fast precise GPS positioning in the presence of ionospheric delays*. Ph.D. thesis, TU Delft. ISBN 90 6132 278 2. Available at http://www.ncg.knaw.nl/Publicaties/Geodesy/pdf/52Odijk.pdf.

Orus, R. (2005). *Contributions on the improvement, assessment and application of the Global Ionospheric VTEC Maps computed with GPS data*. Ph.D. thesis, Universitat Politècnica de Catalunya. Available at http://gage6.upc.es/gAGE_WEB/PhD/Thesis_Raul_Orus.pdf.

Orus, R., Arbesser-Rastburg, B., Prieto-Cerdeira, R., Hernandez-Pajares, M., Juan, J. M., & Sanz, J. (2007a). Performance of Different Ionospheric Models for Single Frequency Navigation Receivers. In *2007 Beacon Satellite Symposium*, Boston (USA). Oral communication.

Orus, R., Cander, L. R., & Hernandez-Pajares, M. (2007b). Testing regional vertical total electron content maps over Europe during the 17-21 January 2005 sudden space weather event. *Radio Science*, 42 (3), RS3004. doi:10.1029/2006rs003515. Available at http://gage6.upc.es/gAGE_WEB/papers/2007/2006RS003515.pdf.

Orus, R., Hernandez-Pajares, M., Juan, J. M., Sanz, J., & Garcia-Fernandez, M. (2002). Performance of different TEC models to provide GPS ionospheric corrections. *Journal of Atmospheric and Solar-Terrestrial Physics*, 64 (18), 2055–2062. doi:10.1016/S1364-6826(02)00224-9. Available at http://gage6.upc.es/gAGE_WEB/papers/2003/sdarticle.pdf.

Orus, R., & Prieto-Cerdeira, R. (2008). GIOVE-A Experimentation Campaign: Ionospheric Related Data Analysis. In *Proceedings of the 4th ESA Workshop on Satellite Navigation User Equipment Technologies NAVITEC 2008*.

Prieto-Cerdeira, R., Orus, R., & Arbesser-Rastburg, B. (2006). Assessment of the Ionospheric correction algorithm for GALILEO Single Frequency Receivers. In *Proceedings of the 3rd ESA Workshop on Satellite Navigation User Equipment Technologies NAVITEC 2006*.

Radicella, S. M. (2009). The NeQuick model genesis, uses and evolution. *Annals of Geophysics*, 52 (3-4), 417–422. Available at http://www.annalsofgeophysics.eu/index.php/annals/article/view/4597.

Radicella, S. M., & Leitinger, R. (2001). The evolution of the DGR approach to model electron density profiles. *Advances in Space Research*, 27 (1), 35–40. doi:10.1016/S0273-1177(00)00138-1.

Radicella, S. M., Nava, B., & Coïsson, P. (2008). Ionospheric models for GNSS single frequency range delay corrections. *Física de la Tierra*, 20. Available at http://revistas.ucm.es/index.php/FITE/article/view/FITE0808110027A/11464.

Radicella, S. M., & Zhang, M.-L. (1995). The improved DGR analytical model of electron density height profile and total electron content in the ionosphere. *Annali di Geofisica*, XXXVIII (1), 35–41. Available at http://www.annalsofgeophysics.eu/index.php/annals/article/view/4130.

Rawer, K. (1963). Propagation of Decameter Waves (HF-Band). In B. Landmark (Ed.), *Meteorological and Astronomical Influences on Radio Wave Propagation*, pp. 221–250. New York (USA): Academic Press.

Rawer, K. (1982). Replacement of the present sub-peak plasma density profile by a unique expression. *Advances in Space Research*, 2 (10), 183–190. doi:10.1016/0273-1177(82)90387-8.

Schaer, S. (2001). *Generating Klobuchar-Style Ionospheric Coefficients for Single-Frequency Real-Time and Post-Processing Users*. Astronomical Institute, University of Berne.

Seynat, C., Kealy, A., & Zhang, K. (2004). A Performance Analysis of Future Global Navigation Satellite Systems. *Journal of Global Positioning Systems*, 3 (1-2), 232–241. Available at http://www.gnss.com.au/JoGPS/v3n12/v3n12p29.pdf.

Snay, R. A., & Soler, T. (2008). Continuously Operating Reference Station (CORS): History, Applications, and Future Enhancements. *Journal of Surveying Engineering-ASCE*, 134 (4), 95–104. doi:10.1061/(Asce)0733-9453(2008)134:4(95).

Spits, J., & Warnant, R. (2011). Total electron content monitoring using triple frequency GNSS: Results with Giove-A/-B data. *Advances in Space Research*, 47 (2), 296–303. doi:10.1016/j.asr.2010.08.027. Available at http://orbi.ulg.ac.be/handle/2268/84597.

Stankov, S. M., Marinov, P., & Kutiev, I. (2007). Comparison of NeQuick, PIM, and TSM model results for the topside ionospheric plasma scale and transition heights. *Advances in Space Research*, 39 (5), 767–773. doi:DOI 10.1016/j.asr.2006.10.023.

Stankov, S. M., Stegen, K., Muhtarov, P., Marinov, P., & Warnant, R. (2011). On the real time reconstruction of the ionospheric electron density profile based on concurrent measurements from collocated digital ionosonde and GNSS receiver. In *Proceedings of the 13th International Ionospheric Effects Symposium IES2011*. Available at http://orbi.ulg.ac.be/handle/2268/89407.

Ventura-Traveset, J., & Flament, D. (2006). *EGNOS: the European Geostationary Navigation Overlay System : a cornerstone of Galileo*. ESA. ISBN 978-9290924531.

Warnant, R. (1996). *Etude du comportement du Contenu Electronique Total et de ses irrégularités dans une station de latitude moyenne. Application aux calculs de positions relatives par le GPS. [Study of Total Electron Content behaviour and irregularities at a mid-latitude station. Application to the calculation of relative positions with the GPS.]*. Ph.D. thesis, Catholic University of Louvain.

Warnant, R., Foelsche, U., Aquino, M., Bidaine, B., Gherm, V., Hoque, M. M., Kutiev, I., Lejeune, S., Luntama, J. P., Spits, J., Strangeways, H. J., Wautelet, G., Zernov, N., & Jakowski, N. (2009). Mitigation of ionospheric effects on GNSS. *Annals of Geophysics*, 52 (3-4), 373–390. Available at http://orbi.ulg.ac.be/handle/2268/1924.

Warnant, R., & Pottiaux, E. (2000). The increase of the ionospheric activity as measured by GPS. *Earth Planets and Space*, 52 (11), 1055–1060. Available at http://www.terrapub.co.jp/journals/EPS/pdf/5211/52111055.pdf.

Wilson, B. D., Akopian, V., Komjathy, A., Pi, X., Dumett, M., Hajj, G., Wang, C., & Mannucci, A. (2008). Ionospheric Data Assimilation: Techniques and Performance. In *XXIXth URSI General Assembly 2008*, Chicago (USA), August 7th to 16th, 2008. Tutorial. Available at http://ursi-test.intec.ugent.be/files/URSIGA08/papers/GTp1.pdf.

Zolesi, B., & Cander, L. R. (2004). COST 271 Action - Effects of the upper atmosphere on terrestrial and Earth-space communications. *Annals of Geophysics*, 47 (2-3). Available at http://www.annalsofgeophysics.eu/index.php/annals/article/view/14.

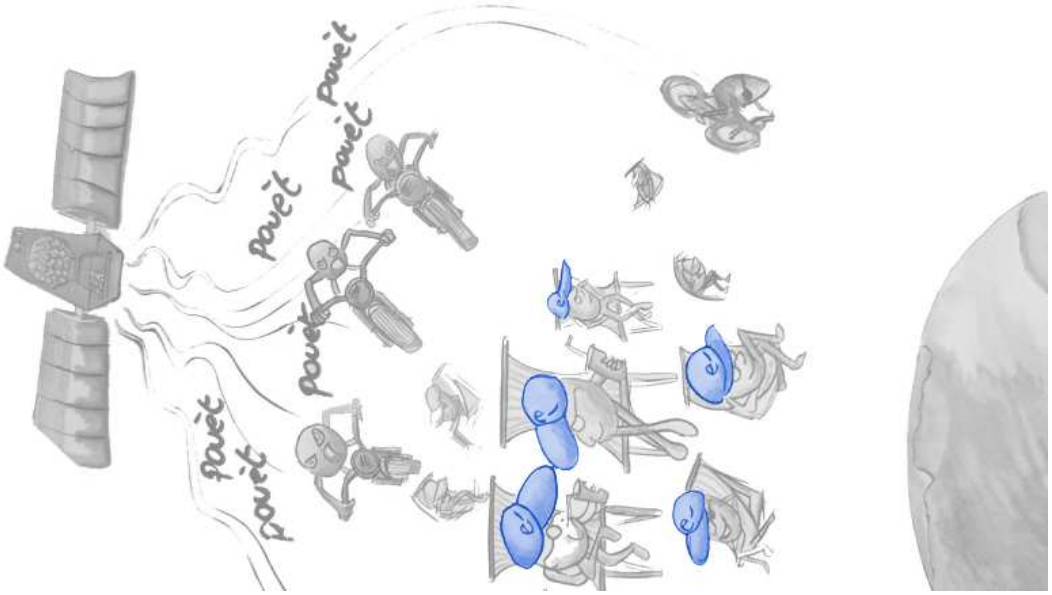

Benoît Bidaine fullfilled this PhD thesis as a F.R.S.-FNRS Research Fellow at the University of Liège (Belgium). He undertook this research within the Geomatics Unit after an internship at the European Space Agency (ESA) in 2006, at the end of his physics engineering master awarded by the University of Liège. At the Geomatics Unit, he contributed to the training of future surveyors and geomaticians in the field of least-squares adjustments, geodesy and GNSS. His hobby? The violin.

fnrs
LA LIBERTÉ DE CHERCHER

Unité de Géomatique
Geomatics Unit

Université
de Liège